

THE MECHANISM OF LYSIS-LYSOGENY DECISION-MAKING OF
BACTERIOPHAGE P1

A Dissertation

by

KAILUN ZHANG

Submitted to the Office of Graduate and Professional Studies of
Texas A&M University
in partial fulfillment of the requirements for the degree of

DOCTOR OF PHILOSOPHY

| | |
|---------------------|--------------|
| Chair of Committee, | Ryland Young |
| Committee Members, | Lanying Zeng |
| | Jason Gill |
| | Craig Kaplan |
| Head of Department, | Josh Wand |

May 2021

Major Subject: Biochemistry

Copyright 2021 Kailun Zhang

ABSTRACT

Recently, more attention has been raised in regard to the study of bacteria-infecting viruses or bacteriophages for a number of reasons. First, they serve as new weapons against antibiotic-resistant pathogens. In addition, a number of phages, especially temperate phages, have been identified that could help shape bacterial evolution and community composition in the mammalian microbiome, and may influence human health. In virology, *temperate* refers to the ability of some viruses to choose between alternative modes of propagation, lysis or lysogeny. In the lytic pathway, host cells are killed and new phages are produced; while, in the lysogenic pathway, the virus remains dormant until induction. Coliphage P1 lysogenizes host cells as a low-copy plasmid, and P1-like plasmids have been identified to be prevalent in animal and human pathogens. In order to unveil the role of phage decision-making in virulence dissemination, we investigate the mechanisms underlying P1 lysogenization in comparison with the established paradigm phage λ , using single-cell and single-virus techniques.

First, we examined the influence of early steps in the P1 infection cycle. We found that recognizing the core region of lipopolysaccharides gave P1 the potential of adsorbing at any location on the bacterial cell surface, which ensured a high probability of successful infection in a variety of host bacteria and hence promoted pathogenic spread. Further, it has been reported that P1 exhibits a constant probability of lysogeny regardless of multiplicity of infection (MOI, or the number of phages infecting a cell),

which could benefit P1-carried virulent genes maintaining in bacterial hosts. To explore the underlying mechanism, we investigated the expression of P1 regulatory proteins and the interaction between phages infecting the same host. We demonstrated that the constant repression activity of lytic genes for each infecting phage and the ensemble decision made by all infecting phages led to the MOI-independent lysogenic response. Finally, though the probability of an infected cell undergoes lysogeny is consistent over MOIs, factors that bias the final cell outcome is still obscure. In our work, we found that the bacterial cell growth state and different patterns of viral DNA replication exhibited associations with P1 lysis-lysogeny decision-making.

ACKNOWLEDGEMENTS

I would like to thank my advisor, Dr. Lanying Zeng, for her role in my graduate career at Texas A&M. She offered me her guidance, encouragement, and trust as I developed myself over the years in graduate study. Several times when I was struggling in the research process, she was patient and helped me conquer those difficulties. Without her help and suggestions, I wouldn't have become as confident and independent as I am now. I also greatly appreciate the opportunities that she provided for scientific training, collaborations, and intellectual freedom. My committee members, Dr. Ryland Young, Dr. Craig Kaplan, and Dr. Jason Gill have also contributed immensely towards my growth and success, through their encouragement and constructively critical suggestions. I give a lot of credit to Dr. Kaplan for helping me culture my creative and analytical perspectives, speaking skills, as well as ambition and passion in my research. I want to specifically thank Dr. Young for sharing his seemingly infinite knowledge and insights and providing great suggestions on my project developments. He is always encouraging and his enthusiasm for science will continue to motivate me in the future. I also greatly appreciate Dr. Gill who did not only give me guidance during my initial working system establishment but also gave me valuable suggestions from different perspectives, which broadened my horizons and inspired me to explore more in my studies.

I wish to thank the current and former members of the Zeng lab for their help and informative discussions. In particular, I want to thank Dr. Qiuyan Shao, Dr. Jimmy Trinh

and Dr. Jingwen Guan for their helpful discussion and critiques. Jingwen helped me quickly get familiar with the lab environment and provided good companionship both during work and in daily life. I feel thankful for other members, namely Laith Harb, Matthew Theodore and Zihao Yu for their patience and advice. It's an honor to work with them. I also want to thank the members of the Gill Laboratory, especially Dr. Denish Piya and Dr. Justin Leavitt for their collaboration and assistance on my projects, specifically sharing protocols and helping me with troubleshooting. I am also thankful to the members of the Young Laboratory, especially Dr. Karthik Chamakura and Dr. Jesse Cahill for providing reagents, bacterial strains and a lot of helpful suggestions. I want to acknowledge the undergraduates of our lab as a whole, who help with many aspects of research every day. Mentoring them has been a valuable experience. Thanks also to the students and staff here in the Department of Biochemistry and Biophysics at Texas A&M for their support and assistance with the varied sides of my graduate life.

Finally, I want to extend my gratitude to my parents for everything that they have done. Their selfless love and support have guided me to this point in my life and helped me face difficulties. For that, I feel eternally grateful and hope to continue making them proud.

CONTRIBUTORS AND FUNDING SOURCES

Contributors

This work was supervised by a dissertation committee consisting of Dr. Lanying Zeng, Ryland Young, and Craig Kaplan of the Department of Biochemistry and Biophysics, and Dr. Jason Gill of the Department of Animal Science.

In chapter II, the original phage stains (WT) were provided by the Gill lab. The EM images of phage P1 were taken by Dr. Denish Piya from the Gill lab.

In chapter III, Kiara Pankratz contributed to the strain construction, single-cell infection experiments and data analysis for decision-making in Lxc overexpression cells. Hau Duong contributed to the strain construction, single-cell infection experiments and data analysis for decision-making in cells with extra C1 operators. Jingwen Guan performed the DNA FISH experiments. Dr. Anxiao Jiang from Department of Computer Science and Engineering provided the program for automatic cell recognition. Zihao Yu assisted on deep machine learning steps for cell recognition model construction. The plasmid for λ Kil expression was constructed by Dr. Karthik Chamakura from Young lab.

All other work performed for the dissertation was completed independently by the student.

Funding Sources

This work was made possible by Texas A&M AgriLife Research and the NIH grant R01GM107597 and NSF grant MCB-2013762 to the Zeng Laboratory. This content is solely the responsibility of the authors and does not necessarily represent the

official views of Texas A&M AgriLife Research, the National Institutes of Health or the National Science Foundation.

TABLE OF CONTENTS

| | Page |
|--|------|
| ABSTRACT | ii |
| ACKNOWLEDGEMENTS | iv |
| CONTRIBUTORS AND FUNDING SOURCES..... | vi |
| TABLE OF CONTENTS | viii |
| LIST OF FIGURES..... | xi |
| LIST OF TABLES | xiv |
| CHAPTER I INTRODUCTION | 1 |
| P1 Morphology and Genomic Information | 4 |
| The Initial Steps of P1 Life Cycle..... | 6 |
| Phage Adsorption and Host Specificity..... | 6 |
| Phage DNA Injection and Circularization..... | 9 |
| P1 Gene Regulatory Network | 13 |
| The Mechanism of Prophage Maintenance | 18 |
| Maintenance of Lysogeny | 19 |
| Maintenance of Prophage as Low Copy Plasmids | 20 |
| P1 Lytic Growth..... | 26 |
| Activation of Late Transcription | 26 |
| Phage Particle Morphogenesis | 27 |
| The Comparison with Decision-Making Paradigm Phage λ | 27 |
| Decision-Making in Different Biological Systems | 31 |
| Roles of Temperate Phages in Eukaryotic Systems | 36 |
| Dissertation Overview..... | 41 |
| CHAPTER II BACTERIOPHAGE P1 DOES NOT SHOW SPATIAL PREFERENCE WHEN INFECTING ESCHERICHIA COLI..... | 43 |
| Introduction | 43 |
| Results | 46 |
| Fluorescent Capsid Labeling of P1 Particles..... | 46 |
| P1 Adsorption Shows No Preference on the Cell Surface | 50 |
| Localization of Phage P1 DNA Shows No Preference in the Cytoplasm | 53 |

| | |
|--|-----|
| Assaying the Post-Infection Lysis-Lysogeny Decision with Single-Cell Resolution..... | 56 |
| The Successful Infection and Decision-Making of P1 Are Independent of the Phage Adsorption Location | 60 |
| Discussion | 63 |
| Methods..... | 67 |
| Media..... | 67 |
| Bacterial Strains, Phages, Plasmids and Primers | 67 |
| Bacteriophage Assays..... | 72 |
| Single-cell Infection Assay | 75 |
| Microscopy Imaging..... | 76 |
| Data Analysis | 77 |
| | |
| CHAPTER III INTERACTIONS BETWEEN VIRAL REGULATORY PROTEINS ENSURE A CONSTANT PROBABILITY OF HOST OUTCOME DURING INFECTION..... | 81 |
| Introduction | 81 |
| Results | 86 |
| The Probability of Lysogeny Is Independent of the Number of Infecting Phages at the Single-Cell Level..... | 86 |
| Build A Simple Genetic Model to Elucidate MOI-Independent Decision-Making . | 90 |
| Imposition of the MOI-Dependency | 97 |
| Discussion | 103 |
| Methods..... | 108 |
| Rich Defined Media | 108 |
| Bacterial Strains, Phages, Plasmids and Primers | 108 |
| Bulk Lysogenization Assay..... | 114 |
| Single-Cell Infection Assay..... | 114 |
| RNA FISH..... | 117 |
| DNA FISH..... | 123 |
| qPCR | 125 |
| Data Analysis | 126 |
| | |
| CHAPTER IV STUDYING THE PARAMETERS THAT INFLUENCE LYSIS-LYSOGENY DECISIONS OF BACTERIOPHAGE P1 | 130 |
| Introduction | 130 |
| Results | 132 |
| The Growth State of Host Cells Influences P1 Decision-Making..... | 132 |
| The Replication of Viral DNAs Shows Distinctive Patterns in Lytic and Lysogenic Cells | 139 |
| Mixed Infection from Phages with Different Lysogenization Capabilities..... | 146 |
| Discussion | 152 |

| | |
|---|-----|
| Methods | 155 |
| Bulk Lysogenization Assay | 155 |
| RNA FISH | 156 |
| Monitoring Phage DNA Movement and Replication | 159 |
| Co-Infection Experiments | 160 |
| Linear-Tracking Analysis of Injected Phage DNA | 162 |
| Analysis of Co-Infection Movies | 162 |
| CHAPTER V SUMMARY AND CONCLUSION..... | 164 |
| The Spatial Distribution of Phage P1 During Infection | 164 |
| MOI-Independent Lysogenization | 165 |
| More Deterministic Factors for P1 Decision-Making | 166 |
| REFERENCES | 168 |

LIST OF FIGURES

| | Page |
|---|------|
| Figure I.1 The infection cycle of bacteriophage P1. | 3 |
| Figure I.2 The morphology of bacteriophage P1. | 5 |
| Figure I.3 Organization of the DNA inversion system of bacteriophage P1 ¹⁹ | 8 |
| Figure I.4 Viral DNA is packaged into proheads by a headful mechanism. | 12 |
| Figure I.5 Organization of P1 Immunity region C (ImmC). | 14 |
| Figure I.6 Organization of P1 Immunity region I (ImmI). | 16 |
| Figure I.7 Organization of P1 replication region. | 22 |
| Figure I.8 The model of P1 partition system. | 25 |
| Figure I.9 The comparison of phage P1 with λ in different aspects. | 29 |
| Figure I.10 Gene regulatory networks in different cell types show similar structures. ... | 35 |
| Figure I.11 Temperate phages can be used as tools for therapeutic treatment of pathogenic bacteria and affect human health. | 40 |
| Figure II.1 The percentage of phage adsorption in bulk with different calcium concentrations in the solution. | 44 |
| Figure II.2 Labeled phage P1 through fluorescent capsid fusion. | 48 |
| Figure II.3 Fluorescent phages lysogenize like WT phage in bulk. | 49 |
| Figure II.4 The percentage of phage adsorption in bulk at different MOIs. | 51 |
| Figure II.5 Phage P1 adsorption shows no preference on the cell surface. | 51 |
| Figure II.6 The adsorption of phage P1 follows the Poisson distribution. | 52 |
| Figure II.7 Phage P1 DNA injection shows no preference for cellular positions. | 54 |
| Figure II.8 Data analysis of injected viral DNA. | 55 |
| Figure II.9 Assaying the post-infection decision with single-cell resolution. | 58 |

| | |
|--|-----|
| Figure II.10 <i>cI</i> -labeled phages lysogenize like unlabeled phages in bulk. | 59 |
| Figure II.11 The percentage of nongrowing cells increases with MOA. | 60 |
| Figure II.12 The failed infection and decision-making do not depend on the initial adsorption locations on the cell surface. | 61 |
| Figure II.13 Expression level of C1-mVenus of cells infected at different locations. | 62 |
| Figure II.14 Phage bands after ultracentrifugation through CsCl equilibrium gradients. | 73 |
| Figure III.1 A schematic of P1 lysis-lysogeny regulatory network. | 83 |
| Figure III.2 The probability of lysogeny is independent of the number of infecting phages at the single-cell level. | 87 |
| Figure III.3 The injected DNA copy number correlates with prediction very well. | 89 |
| Figure III.4 Influence of C1 activity on P1 lysogenization. | 91 |
| Figure III.5 P1 DNA replication during infection. | 92 |
| Figure III.6 The interaction of C1, Coi and Lxc leads to MOI-independence of P1 lysogenization. | 95 |
| Figure III.7 Percentage of infected cells over total cells using smFISH assay. | 96 |
| Figure III.8 P1 virions infecting the same host cell make an ensemble lysis-lysogeny decision. | 98 |
| Figure III.9 P1 DNA behaviors during infection on different host strains. | 99 |
| Figure III.10 P1 shows MOI-dependent lysogenization tested at the bulk level. | 101 |
| Figure III.11 The MOI-dependent lysogenization is gained by enhancing the distance between infecting phages. | 102 |
| Figure III.12 The model of P1 lysis-lysogeny decision-making mechanism. | 105 |
| Figure III.13 Test the effect of <i>tetO</i> insertions in viral DNA on P1 lysogen growth and induction. | 110 |
| Figure III.14 Comparison of average <i>cI</i> and <i>coi</i> mRNA level by qRT-PCR and smFISH. | 122 |

| | |
|---|-----|
| Figure IV.1 The probability of lysogeny at different growth states. | 134 |
| Figure IV.2 The length of cells entering the lytic or lysogenic pathway. | 134 |
| Figure IV.3 Cell size acts as a deterministic factor of P1 decision-making. | 136 |
| Figure IV.4 Different infection characteristics as a function of cell length. | 136 |
| Figure IV.5 The role of Lxc in cell length effect on P1 decision-making. | 138 |
| Figure IV.6 Consider both cell length and MOI on P1 lysogenization. | 138 |
| Figure IV.7 Replication patterns of viral DNAs during P1 infection. | 141 |
| Figure IV.8 Monitoring phage DNA movement during P1 infection. | 143 |
| Figure IV.9 DNA replication over time after phage infection. | 145 |
| Figure IV.10 Representative images of the co-infection system. | 147 |
| Figure IV.11 The localization and infection rate of CFP and mCherry phages. | 148 |
| Figure IV.12 CFP and mCherry phages show different probabilities of lysogeny. | 148 |
| Figure IV.13 A quantitative analysis of C1 expression in infected cells adsorbed by different phages. | 151 |
| Figure IV.14 Representative images showing mRNA expression. | 156 |

LIST OF TABLES

| | Page |
|---|------|
| Table II.1 Bacterial Strains, Phages and Plasmids used in this work..... | 70 |
| Table II.2 Primers (5' – 3') used in this work. | 71 |
| Table III.1 Titer of P1 <i>tetO</i> phages..... | 110 |
| Table III.2 Bacterial Strains, Phages and Plasmids used in this work. | 111 |
| Table III.3 Primers (5' – 3') used in this work..... | 113 |
| Table III.4 smFISH RNA probes. | 119 |
| Table IV.1 Probabilities of lysogeny over infected cells for WT, CFP and mCherry phages tested separately in bulk assays. | 149 |
| Table IV.2 smFISH RNA probes. | 157 |
| Table IV.3 Phage Strains for Co-infection Experiments..... | 161 |

CHAPTER I

INTRODUCTION

The identification of bacteriophage P1 was reported by G. Bertani in 1951^{1,2}, the same year as discovery of phage λ . P1 belongs to a small genus *P1virus* within family *Myoviridae* and order *Caudovirales*, which also includes *Aeromonas* phage 43. When P1 was first isolated, it showed very small plaques on the slightly pathogenic *Shigella* strain. Since plaque size was an important feature for early studies on bacteriophages, P1 was ignored at the beginning and might have been completely forgotten if not for Lennox, who discovered its capability for generalized transduction³. During P1 transduction, about 100 kb fragments of the bacterial DNA are packaged into the phage head and mobilized to a recipient bacterial strain, then occasionally integrate into the host genome by recombination. As a result, the transduced bacterium does not lyse or suffer toxicity from virus infection. It thus provided an invaluable method in the fine mapping of the bacterial genome in times when no sequencing efforts were available. Even at the time of this writing, P1 continues to serve as a workhorse of genetic manipulations in bacteria⁴⁻⁶. Except as a genetic tool, P1 has not been drafted for any functions in therapy, as P1 prophage does not confer toxigenicity on harmless bacteria, as do the prophages have given us, such as diphtheria, cholera, toxic shock syndrome and botulism⁷⁻¹⁰; nor subvert antibiotic treatments, despite its capacity of transducing multidrug resistance (MDR) genes. However, recent metagenomic studies highlighted that bacteriophages, including P1, and phage-like plasmids could play prominent roles in

the dissemination of accessory adaptive traits, allowing for stable colonization and persistence of pathogenic bacteria¹¹.

Like other temperate phages, P1 can adopt lytic or lysogenic lifestyles during infection (Fig. I.1). The decision depends upon the host environment and the expression of genes that regulate P1 immunity functions. Genes promoting lysogeny establishment, by which phage-carried MDR “resides” in the host cell, are highly similar between P1 and P1 phage-like plasmids. We believe that our studies on P1 infection lifecycle and lysis-lysogeny decision-making can give a better understanding of the contribution made by temperate phages to the spread and adaptation of pathogenicity. Here we review previous studies of P1 morphology, lifecycle and gene regulatory network of decision-making in comparison with other temperate phages, especially the paradigmatic model phage λ . We also review and discuss recent discoveries of the impact of temperate phages on eukaryotic kingdoms, in the hope of presenting a more advanced picture of the tripartite phage-bacterium-host interplay with the phage fostering host-microbe symbiosis.

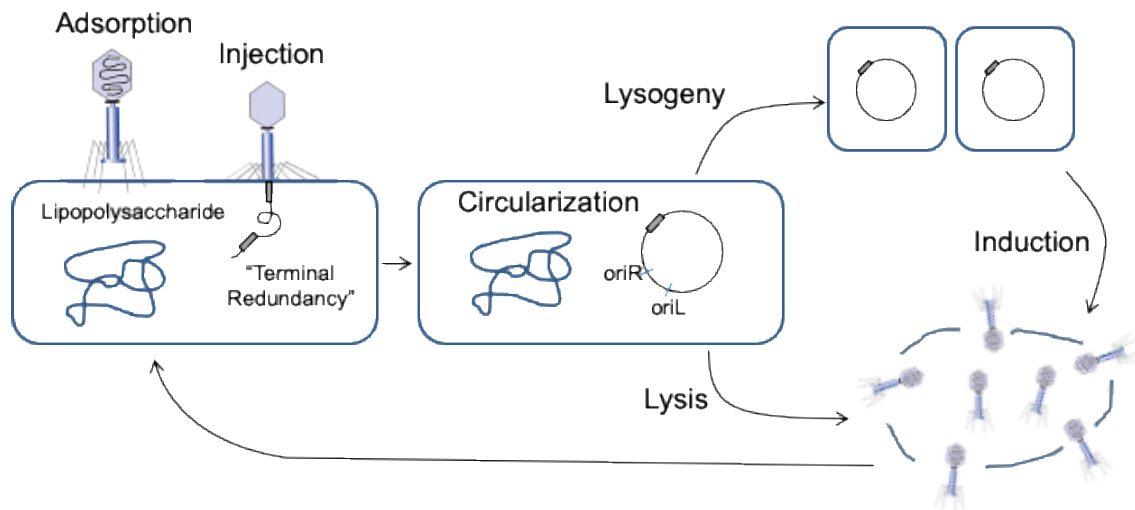


Figure I.1 The infection cycle of bacteriophage P1.

Phage P1 recognizes lipopolysaccharide (LPS) molecules on the bacterial surface to start the infection cycle. Linear viral DNA is transmitted from phage capsid into cellular cytoplasm and then circularizes by recombination between redundant ends. Following that, phage genes are expressed and ultimately commit the phage to lysis or lysogeny. During lysis, P1 produces new virions and bursts the host cell so that release these progenies to start another infection cycle. During lysogeny, P1 stays as a low-copy plasmid and replicates during cell division.

P1 Morphology and Genomic Information

The infectious P1 virion has an icosahedral head of approximately 85 nm diameter, attached to a long tail of 220 nm length (Fig. I.2A). There is a contractile sheath surrounding the rigid tail tube (Fig. I.2B). The tail ends in a baseplate linked with six kinked tail fibers. A linear dsDNA, with a terminal redundancy of 10 to 15 kb, is encompassed in the infectious phage head. A complete P1 genome sequence is around 94 kb, encoding at least 117 genes. The GC content of P1 DNA is 47.3%¹², slightly less than that of its *E. coli* host (50.8%)¹³. Protein-coding genes occupy 92% of the genome and are organized in 45 operons, of which 4 are crucial for the decision-making between lysis and lysogeny, 4 others ensure prophage maintenance and the remaining 37 operons are involved in lytic development¹².

In addition to the aforementioned normal infectious particles with big heads (P1B), P1 also produces small (P1S) and minute (P1M) particles whose head diameters are around 65 nm and 47 nm, respectively¹⁴ (Fig. I.2B). Since having similar tails with P1B, P1S and possibly the much rarer P1M can adsorb and inject their DNA into host cells normally. However, because of lacking the capacity to hold a complete P1 genome (< 45% of full-length DNA)^{15,16}, they are not productive during infection. Thus, the presence of P1B and P1M may misguide the single-cell observations in decision-making studies. The relative abundance of P1 head size variants in the lysate is influenced by both host and viral genotype. Normally, P1S particles constitute ~20% of the yield^{16,17}, but depending on the host strain, the proportion of P1S can vary extensively. The basis for this variation remains to be studied. Previous work has shown that the deletion of

entire *darA* operon (*dar* standing for defense against restriction), or transposon insertions within *lydA* and *darA*, would result in the overproduction of P1S virions, a phenotype denoted Vad⁻ (viral architecture determinant)¹⁸. Based on a more recent study of P1 Dar system, the Vad⁻ phenotype can be assigned to two adjacent genes, *hdf* and *darA*, within *darA* operon¹⁷, indicating their important roles in determining head size during P1 morphogenesis.

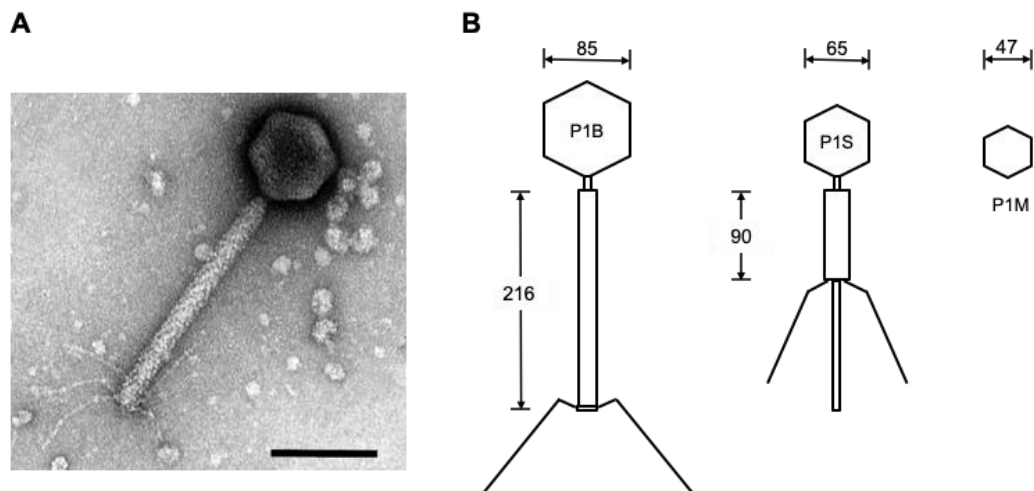


Figure I.2 The morphology of bacteriophage P1.

(A) Electron micrograph of an infectious phage P1 particle¹⁹. The scale bar represents 100 nm. (B) The diagrammatic scale drawings of P1B and P1S particles with extended and contracted tail sheaths, respectively, and a P1M head.

The Initial Steps of P1 Life Cycle

Phage Adsorption and Host Specificity

To begin its infection, a bacteriophage needs to adsorb onto the host and inject its DNA into host cytoplasm (Fig. I.3). In terms of the ability to inject its DNA, P1 has the broadest host range, spanning a variety of Gram-negative bacteria. The host specificity is governed by an inversion system denoted C-segment^{20,21}. As shown in Fig. I.2, the inversion of C-segment will lead to the expression of alternative tail fiber proteins (RSU or RS'U'). Specifically, phages carrying RSU fibers (C+) are able to infect *E. coli* K12, *E. coli* B and *E. coli* C, whereas phages carrying RS'U' fibers (C-) do not normally infect these strains. Comparisons of gpS and gpS' proteins and gpU and gpU' proteins reveal that the main differences reside within C-terminal regions¹². Further analysis of the sequence differences will help identify subregions that are essential for the recognition of P1 to its particular hosts.

C-segment inversion is an infrequent process during P1 infection and the lytic progeny will have the same host range with the infecting parent phage, while an induced lysogen is likely to produce a burst of phages with mixed genotypes^{20,22}. Since the phage particles we used for infection study were produced from P1 lysogen induction and the host strain was an *E. coli* K12 derivative, it is necessary to remove C- phage particles to avoid disturbing the single-cell analysis. It has been shown that the inversions are accomplished by the Cin site-specific recombinase^{22,23}. Cin acts on a pair of imperfect inverted 26-bp sites, *cixL* and *cixR*, flanking the C-segment^{24,25} (Fig. I.2). Unlike the tail fiber operon that is controlled under a late promoter, *cin* operon is expressed from a σ^{70}

promoter, allowing inversions of the C-segment to occur in lysogens. In addition to *cix-cin* system, the host architectural protein Fis (factor for inversion stimulation) and a 72-bp palindromic recombinational enhancer sequence, *sis*, located within the *cin* gene (Fig. I.2), appear to be required for the efficient C-segment inversion^{23,26-29}. Fis binds to and bends the enhancer sequence, stimulating the recombination between *cix* sites by more than 500-fold^{23,27,28,30} and simultaneously preventing the formation of deletions²³. Moreover, the host protein, IHF (integration host factor), probably also influences the rate of C-segment inversion¹². There is a putative IHF binding site overlapping the σ^{70} promoter for *cin* operon, suggesting a negative effect of IHF on Cin transcription. Interestingly, the expression levels of both IHF and Fis proteins are dependent on bacteria growth phase. IHF level is three times and two times more abundant in early and late stationary phase than in exponential phase³¹; whereas Fis level is drastically decreased in stationary phase. These differences suggest that C-segment inversion will be especially uncommon during stationary phase given the proposed IHF-mediated down-regulation of Cin expression and the lack of Fis-mediated enhancer function during this growth state.

Moreover, researchers have found that the tail fiber variation according to the invertible DNA segment is not a unique feature of phage P1. The associated systems include *gin* of phage Mu³², *pin* of the defective lambdoid prophage element e14 in *E. coli* genome³³, *min* of the phage-like plasmid p15B³⁴⁻³⁶ and *ein* of the phage-tail-like bacteriocin Carotovoricin Er³⁷. Furthermore, bacterium *Salmonella typhimurium* comprises an analogous *hin* system that controls the composition of surface antigens³⁸.

These tail fiber genes from unrelated phages or elements of bacteria exhibit a mosaic of homologous segments, suggesting an extensive horizontal gene transfer³⁹. Moreover, the respective recombinases show high degrees of similarity and are functionally exchangeable, implying that the independent divergence from a common ancestor plays a major role in tail fiber evolution⁴⁰.

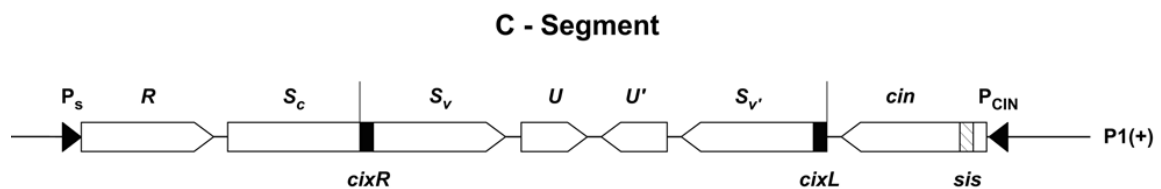


Figure I.3 Organization of the DNA inversion system of bacteriophage P1¹⁹.

Two *cix* recombination sites flanking the invertible C-segment are shown as black boxes. Two promoters, P_s , expressing the tail fiber operon and P_{CIN} , expressing the *cin* gene are shown as black arrows. Genes are shown as open boxes with arrowheads indicating the direction of transcription. In the depicted orientation, the three tail fiber proteins R, S and U are produced (C+), while a single inversion event would fuse S_c with S_v' , resulting in the expression of the three proteins R, S' and U' (C-).

Phage DNA Injection and Circularization

A success of injecting and maintaining the viral DNA within bacterial host is important for the phage infection cycle. During P1 adsorption, phage tail fibers bind to a specific host receptor that is the terminal glucose moiety on the lipopolysaccharide (LPS) core of the outer bacterial membrane⁴¹, during which Ca²⁺ ions are required⁴²⁻⁴⁴. The interaction of at least three tail fibers with the receptor molecules is assumed to be sufficient to stimulate viral DNA injection⁴⁵. To be more specific, the attachment of P1 tail fibers triggers the tail sheath to contract (Fig. I.2B), and the tail tube is pushed through the baseplate, puncturing the cell outer membrane into the periplasm. A lytic transglycosylase (Sit) on the phage tail facilitates the penetration and the passage of phage DNA through bacterial cell wall by introducing small gaps into the peptidoglycan layer, as does the soluble lytic transglycosylase of *E. coli*⁴⁶. However, the uptake of P1 DNA from the periplasmic space into the cytoplasm is mediated by an as yet uncharacterized mechanism. It is speculated that, in analogy to phage T7^{47,48}, a large internal head protein of P1, probably DarB^{12,49}, might form an inner-membrane pore allowing the DNA transmission. Another hypothesis is that the tail tube penetration induces the fusion between the cell inner and outer membrane, which allows a direct translocation of the DNA from the phage head into the host cytoplasm⁵⁰.

Another mechanism connected to the DNA injection process of P1 is the *sim* superinfection exclusion system. The Sim protein is immediately expressed after the infection and the mature protein, processed by the SecA system, is located in the periplasmic space, similarly to the SieA protein of P22⁵¹ and the Imm protein of T4⁵².

The mechanism of superimmunity is still unknown. A plausible hypothesis is that inter-membrane Sim proteins trap superinfecting P1 DNAs in the periplasm, preventing them interfering with an ongoing infection cycle. Notably, cells carrying low copy-number *sim* plasmids do not display superinfection exclusion phenotype^{53,54}. It suggests that the main function of Sim proteins is to protect the cells from superinfection, when lytic development has been initiated where the increased copy number of the *sim* gene results in a higher dosage of Sim functions.

Upon entry into a host cell, the linear P1 DNA undergoes rapid circularization. The importance of the circularization event is highlighted by the increased failed rate of P1 infections in the absence of recombination systems that are necessary for the circularization reaction⁵⁵. For example, the probability of lysogeny is reduced by 10-fold and the burst size of P1 is reduced by 20-fold upon the infection of a recombination-deficient *E. coli* strain (*recA* or *recBC*)^{56,57}. Presumably, if the injected P1 DNA is not circularized, it will be quickly degraded from its ends by host nucleases, such as RecBCD⁵⁸⁻⁶². To deal with this degradation problem, some phages, including phage λ and T4, will produce inhibitors to inactivate RecBCD⁶³. However, the RecBCD nuclease remains active during P1 infection, at least during the initial stages, which probably serves to initiate the RecA-dependent homologous recombination between two P1 redundant ends. In addition to the host-encoded recombinase system, the circularization of P1 DNAs can be mediated by a phage driven site-specific *lox-cre* recombination system. It is supposed that one of every three or four infectious P1 virions contains *lox* sites in both terminal redundant regions found in the productive burst, which are

specifically recognized by the recombinase Cre. During P1 phage assembly, P1 encoded pacase recognizes the packaging site (*pac*) on each phage DNA concatemer and cuts the DNA. The resulted double-strand end is inserted into a phage head and the DNA continues to be pushed inside the head until the head is full, known as headful packing. Once the first phage head is filled, another packaging starts. Since the amount of DNA that can be packaged into a P1 head is about 100 kb and the size of the P1 genome DNA is only ~90 kb, the encompassed DNA will have a 10-kb terminal redundancy. The processivity of packaging appears limited to three or four headfuls from each concatemer⁶⁴, generating a corresponding number of classes of viral DNAs with different redundant sequences (Fig. I.4). The *pac* site is about 5 kb from *lox*, and the direction of packaging is from *pac* toward *lox*⁶⁴⁻⁶⁶. Therefore, only class I DNA, the first headful, will have two *lox* sites. This feature may be important to the phage, because it permits the circularization of some portion of P1 DNAs packaged without consideration for the recombination potential of the host cell to which P1 infects. Furthermore, one of the four putative *cre* promoters, P4*cre*, predicted to be the strongest, is partially overlapped by the C1 operator, O*cre*, indicating that the promoter is inactive in the P1 prophage¹² and the *cre* gene is expressed most efficiently in initial steps of phage infection and during lytic development.

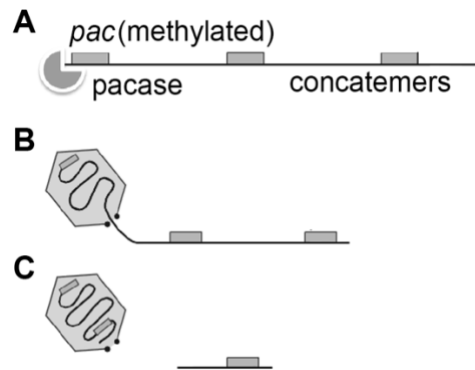


Figure I.4 Viral DNA is packaged into proheads by a headful mechanism.

P1 encoded *pacase* recognizes the *pac* site on the concatemers of phage DNA and cuts the DNA. The resulted double-strand end is inserted into a phage head and the DNA continues to be pushed inside the head until the head is full, which leads to ~10% redundancy. Once the first phage head is filled, another packaging starts. While each phage particle contains the same genes, the gene order changes, known as circular permutation of the genome.

P1 Gene Regulatory Network

At the molecular level, the decision between lysis and lysogeny is regulated by the components of the tripartite immunity circuitry or regulatory network, located in ImmC, ImmI and ImmT regions. As Heinz Schuster said, “among the temperate phages, P1 and P7 encode the most complex immunity system”⁶⁷. It is regrettable that the studies of P1 immunity halted prematurely with the death of this prime mover.

In ImmC, there are the *cI* major repressor and a C1 inactivator, *coi*. Gene *cI* is transcribed from the promoter *P_{cI}*, whose activity is controlled by a few repressor-binding sites *O_{cIab}*, *O_{cIc}* and *O_{coi}*, encompassing an autoregulatory network. *In vitro* studies showed that all operators could participate in C1-mediated DNA looping, and the loops between *O_{cIab}* and *O_{coi}* occurred predominantly⁶⁸ (Fig. I.5). The *cI* gene of phage P1 is an analog of the unrelated *cI* of phage λ . But different from λ CI, which is late expressed and functions as a dimer, C1 protein of P1 is expressed immediately after the DNA injection and acts as a monomer, binding to the operator sites scattered throughout the phage genome. The 17-bp operator consensus sequence (ATTGCTCTAATAAATTT) is found to be asymmetric and hence has directionality. The transcription of *coi* can be repressed by C1, whereas Coi protein forms a 1:1 complex with C1 and blocks its activity. The antagonistic action of C1 and Coi is crucial for a choice between lysis and lysogeny. If C1 synthesis prevails in P1-infected cells, Coi synthesis is shut down, leading to the establishment of lysogeny; on the other hand, if Coi synthesis predominates, C1 is inactivated, leading to the lytic growth.

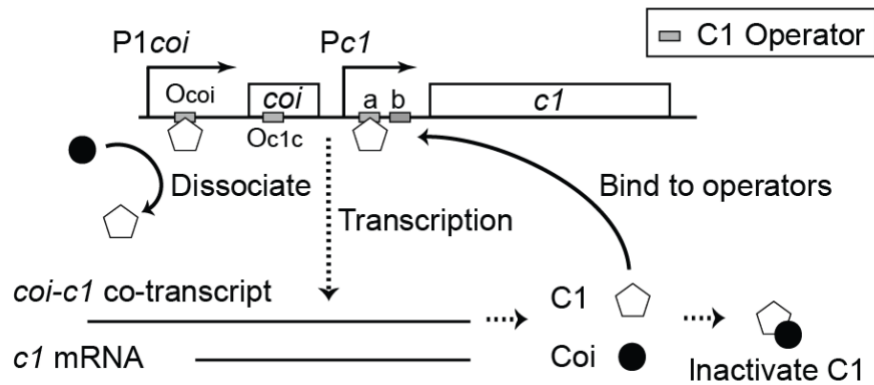


Figure I.5 Organization of P1 Immunity region C (ImmC).

White boxes represent genes inside the operon without drawing in scale. Gray boxes indicate C1 binding sites. Both $c1$ and coi can be expressed from promoter $P1_{coi}$ and $c1$ can be expressed from another promoter P_{c1} . O_{c1a} and O_{c1b} operators that control P_{c1} activity locate on different DNA strands with opposite directions. O_{c1b} is supposed to have the weakest binding affinity with C1. There is a C1 operator adjacent to $P1_{coi}$ (O_{coi}) so that C1 can inhibit the transcription of gene coi . On the other hand, the product of gene coi can inactivate C1 by directed binding and dissociate C1 from operator sites. The antagonized function of C1 and Coi creates a sensitive regulatory network that is crucial for the choice between lysis and lysogeny.

ImmI contains genes that code for another anti-repressor Ant1/2, an inhibitor for cell division (Icd), and a trans-acting RNA (C4). The message of *c4* gene is processed by RNase P (71), resulting in a 77 bp antisense RNA that folds into a cloverleaf structure. C4 RNA interaction with the complementary regions on *icd-ant* mRNA blocks the binding of the ribosome to the Shine-Dalgarno sequence of the *icd* gene⁶⁷. As *ant1* is transcriptionally coupled with *icd*, C4 binding will interrupt Ant protein translation. Besides translation, C4 also interferes the transcription of *icd* and *ant*. When C4 targets the growing message of *icd-ant*, RNA polymerase will pause at the ρ -dependent terminator within *icd*. In the absence of C4, the binding of ribosome alters the structure of the mRNA chain and thereby allows RNA polymerase to complete the transcription of the whole operon⁶⁹.

The expression of ImmI operon is dually controlled by a constitutive promoter $P1c4$ and a C1 controlled promoter $P2c4$, which indicates a 'communication' between ImmC and ImmI (Fig. I.6). Reasons why C1 repressor participates in the control of the expression of ImmI has not yet been understood. Unexpectedly, in the absence of an active C4 RNA, the synthesis of Ant proteins is stimulated when $Oc4$ is bound with C1⁶⁷. Therefore, the C1 control should not be simply inferred as a second repression function superimposed over the negative control from C4 RNA.

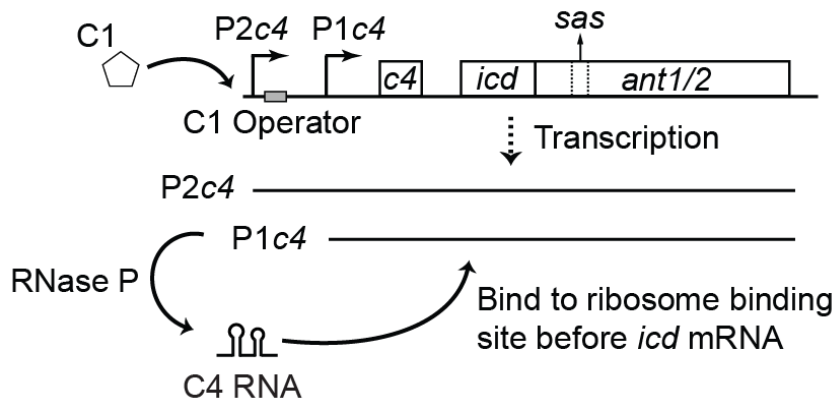


Figure I.6 Organization of P1 Immunity region I (ImmI).

ImmI contains *c4*, *icd* and *ant1/2*. These genes are expressed from a constitutive promoter P1*c4* and a C1 regulated promoter P2*c4*. Transcripts are processed by RNase P so that generate the C4 antisense RNA that is folded into a secondary structure with three loops and three stems (not shown in detail). Targeting of C4 to the complementary regions on *icd-ant* mRNA will block the binding of ribosome to the Shine-Dalgarno sequence of the *icd* gene. Since *ant* gene is translationally coupled with *icd*, this RNA-RNA interaction will also inhibit Ant expression. Icd acts as a cell division inhibitor. Ant1 and Ant2 together form heterodimer acting as an anti-repressor of C1. Both of the subunits are expressed from a single gene with the second protein translating from an inframe start codon.

In a P1 lysogen, both ImmC and ImmI regions contribute to the maintenance of host cell immunity. For example, C1 repressor alone does not render a lysogen immunity to the superinfection by P1 unless the *c4* gene is also expressed⁷⁰. In addition, ImmI may offer a flexibility of immune specificity excluded at ImmC. It is tempting to speculate that the ability to alter the immunity specificity would confer a selective advantage to the phage, similar to the ability of changing the host range through the invertible tail fiber genes. The rigid function of ImmC is due to the multiplicity of C1 binding operators - it is not possible to change the immune specificity by mutations in *c1* gene, unless C1 binding sequences are changed in the meanwhile. In contrast, mutations can happen in C4 and its target at the same time with relative ease. Phage P1 and P7 share about 90% sequence homology with respect to the genome size of P1⁷¹, however, they can plate on the lysogens of each other despite the functional interchangeability of their C1 repressors. This heteroimmunity is attributed to only four-base changes in ImmI, located in C4 antisense RNA and its target^{67,72}. A further immune specificity difference of P1 and P7 has been mapped to a small region, *sas* (site of ant specificity), within *ant* genes which are nearly identical of these two phages. It was suggested that Ant proteins normally loaded onto their phage-specific *sas* sites to perform their anti-repressor function. Therefore, the alterations in *sas* sites will affect Ant proteins and their targets simultaneously^{67,73} (Fig. I.6).

Temperate phages typically contain one (e.g. λ) or two (e.g. P22) immunity regions that encode two regulators with antagonized functions during decision-making. Phage P1 is an exception given the addition of the third region, ImmT. ImmT encodes a

small protein, Lxc, that modulates C1 repression activity by increasing its affinity to repressor binding sites and thus promotes lysogenic growth. As a consequence of C1 autoregulation, the presence of Lxc will down-regulate the synthesis of *cI* gene products⁷⁴⁻⁷⁷. Moreover, it was found that Lxc formed a ternary complex with DNA-bound C1 so as to protect the repressor from C_{oi} dissociation⁷⁸. The start codon of *lxc* overlaps with the stop codon of the preceding gene *ulx*, indicating the transcriptional and translational coupling of these genes. Therefore, *lxc* transcription can be driven from its own promoters, as well as *PdarB*, the promoter of *ulx*¹². None of these promoters are under the control of the C1 repressor suggesting that Lxc can exert its functions in both lysogeny establishment and maintenance. Schwartz⁷⁷ showed that, although the absence of Lxc in the *cI*-100 temperature-sensitive prophage lowered the temperature threshold (30°C) of the thermal induction compared to 42°C described by Rosner⁵⁶, it did not significantly affect the lytic growth and the establishment and maintenance of lysogeny for WT C1. Therefore, the question is, what are the benefits for the phage of having this small protein during phage decision-making? Based on our work, we find that Lxc is essential for P1 constant lysogenic response against different virus-to-microbe host ratios discussed in a later chapter.

The Mechanism of Prophage Maintenance

What separates P1 from the majority of characterized temperate phages is the format of its prophage. Instead of integrating the viral DNA into host chromosome, P1 lysogenizes as a plasmid of low copy number, 0.7 to 1.4 per bacterial origin⁷⁹. Thus, it is important to develop different strategies for the prophage maintenance during cell

growth. Accordingly, the loss frequency of a P1 plasmid is as low as 10^{-5} per generation⁵⁶, demonstrating that P1 lysogens are very stable. Of note, these strategies will also benefit the phage-carried virulent genes stabilizing in the bacterial host.

Maintenance of Lysogeny

First, in order to maintain the lysogeny state, the intracellular concentration of the lytic repressor has to be buffered against the fluctuant conditions during growth. An efficient solution to this problem is the autoregulatory loop (Fig. I.5). *PcI* is one of the promoters expressing *cI* but lacks a typical -35 region¹², suggesting that the activation of *PcI* might depend on a transcriptional activator. Taken together with the adjacent C1 binding operators to *PcI*, it is highly possible that C1 proteins act in both capacities and the particular activated or autorepressed functions depend on the site to which the C1 protein binds⁸⁰. *OcIab* is a bivalent operator that consists of two overlapping repressor-binding sites oriented in opposite directions (Fig. I.5). *OcIab* locates just upstream of *PcI* -35 region, which conforms the expectation of autoregulation. *OcIb* is likely to be the weakest repressor-binding site found in the entire P1 DNA, as its DNA sequence contains less conserved nucleotides compared with other binding site sequences¹². Therefore, it is assumed that C1 binds first to *OcIa* site and this binding activates the transcription of the promoter *PcI*. As the concentration of C1 protein in the lysogen cell increases, the *OcIb* site is also bound with C1 protein following all other operators. Filling of both sites forms a complex that represses *cI* transcription. Alternatively, the activation and autorepression processes can be accomplished by different proteins. In this model, both *OcIa* and b are served for autorepression and the possible activator

needs further investigations. Furthermore, given the aforementioned regulatory functions, the corepressor would play an important role of C1 autoregulation. In the presence of Lxc, moderate or even low concentrations of C1 proteins are sufficient to occupy *PcIb* binding site, thus switch off C1 expression. On the other hand, once C1 concentration drops below a certain threshold level, *OcIb* site will be the first to be clear of repression, allowing *de novo* synthesis of C1 proteins and replenish the repressor pool before any other C1-controlled promoters get derepressed. I propose that Lxc regulation narrows down the range of C1 concentration for lysogen maintenance. The advantages of this regulation are: first, to avoid any unnecessary accumulation of C1 and reduce the metabolic burden of the P1 prophage to its host; second, to permit a P1 prophage to react quickly to the stimuli that trigger lytic growth, as a low level of anti-repressor is sufficient for the inactivation of the low amount of C1 in the equilibrium condition.

Maintenance of Prophage as Low Copy Plasmids

Besides cushioned repressor level, P1 also develops various approaches to increase plasmid stability, including copy-number control, replication initiation control, active partition, dimer resolution and plasmid addiction. I will mainly focus on discussing DNA replication initiation and partition mechanisms.

Replication Control

P1 prophage replicates in the host cytoplasm as a circular plasmid. It starts from an origin (*oriR*), which is different from the one for lytic growth. As shown in Fig. I.7, the *repA* gene, encoding phage replication initiator protein, is flanked by 14 iterons, representing the binding sites of RepA. These iterons constitute two types of

incompatibility control loci, *incC* and *incA*. Saturated binding of RepA to the iterons in *incC* is required for the replication initiation. The synthesis of RepA is autoregulated as the *repA* promoter is located in *incC*. On the other hand, iterons in *incA* are involved in the initiation regulation and the control of plasmid copy number by simply titrating RepA concentration⁸¹. In the absence of *incA*, P1 plasmid copy number increases about 10-fold⁸¹.

Several host factors contribute to the replication initiation. Four GATC sites within the origin need to be methylated for replication^{82,83}, which is negatively regulated by host function. The SeqA protein of *E. coli* binds to the hemi-methylated GATC sites and sequesters them from the methylase^{84,85}. Moreover, the melting of the phage DNA double strand at *oriR* occurs through the concerted action of RepA and the host factors, DnaA and HU, thus providing the access for the host replication machinery. Furthermore, studies of iteron-based plasmids found that RepA proteins exist in both monomer and dimer forms. Chaperones such as DnaK, DnaJ and GrepE, can recognize both forms of RepA proteins as substrates and catalyze conformational changes⁸⁶⁻⁹⁰. RepA in monomeric form can bind with iterons specifically and serving as initiators⁹¹⁻⁹⁴, whereas RepA dimers participate in later replication regulation by blocking the origin through handcuffing⁹⁵ (Fig. I.7B). In summary, at the beginning of replication, the number of P1 prophages appears to be controlled by the availability of RepA initiator proteins⁹⁶, but continued increase in DNA copy number is disallowed by handcuffing⁸¹, the pairing of origins via RepA dimers (Fig. I.7).

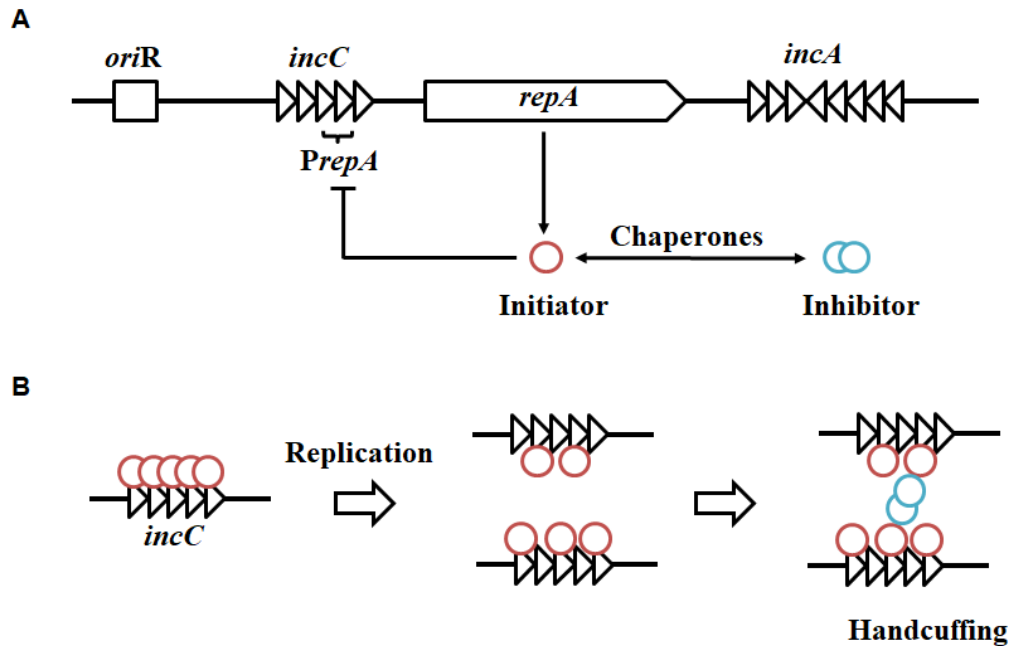


Figure I.7 Organization of P1 replication region.

(A) Schematic diagram of the P1 replication region. Small triangles indicate the organization and directionality of 19-bp iterons. In P1 prophage, the initiator promoter (*PrepA*) maps within *incC* iterons and the monomer binding serves the dual role of promoter repression (autorepression) and replication initiation. RepA dimers are inactive as initiators and participate in handcuffing, thereby serving as inhibitors of replication. (B) Following initiation, the protein is titrated by being distributed to the daughter origins so that none are saturated. This ought to prevent the initiation of further replication, which requires saturation of initiator-monomer binding to iterons. The probability of replication initiation is further inhibited by pairing of origins mediated by RepA monomers and dimers that lead to origin inactivation (handcuffing).

Plasmid Partition

Replication control without active plasmid partition can contribute little to the stability of the low copy plasmid. The partition module of P1 sits downstream of *repA*, indicating that replication might act to drive the partition of sibling plasmids. However, some studies also demonstrated the presence of active partitioning of some unreplicated plasmids⁹⁷. P1 partition module consists of an operon of two genes, *parA* and *parB*, and a centromere-like site *parS*⁹⁸. Both ATP and ADP promote the formation of ParA dimer (Fig I.8A). By binding with ADP, ParA exerts negative autoregulatory control of the partition operon^{99,100} (Fig. I.8B). In a complex with ATP, ParA joins the partition complex at *parS* via protein-protein interaction with ParB and plays an important role in plasmid partition^{101,102} (Fig. I.8C). Both repressor and ATPase activity of ParA are stimulated by ParB^{100,103}. The *parS* site contains two kinds of ParB recognition sites, heptameric and hexameric boxes, and a binding site for the host protein IHF^{12,104}. ParB, associated with IHF, forms a high affinity protein-DNA complex at *parS*^{101,102,105} (Fig. I.8C). Additionally, binding of ParB at *parS* can spread ParB proteins to the flanking DNA and silence the transcription of genes as far as several kilobases away¹⁰⁶. There is no additional sequence similar to *parS* in P1 DNA that could serve as a ParB binding site. It suggests that, in P1, the function of ParB is limited to partition, dissimilar with it in other plasmids, such as RK2, F, and N15, where the homologous proteins appear to have additional functions¹⁰⁷⁻¹⁰⁹.

Furthermore, the mechanism of ParA and ParB translocating plasmid molecules to their target positions within a cell during partitioning is still obscure. It can depend on

ParA proteins to form metastable assemblies that push or drag the partition complex attached plasmids towards each cell pole (Fig. I.8D) or depend on the attachment of the partition machinery to unknown host components (Fig. I.8E). Since the expression of the *par* operon is autoregulated, it can function during both lytic and lysogenic developments. It is possible that the partition system can help to separate the replicated phage DNAs into different clusters, forming the centers for the phage assembly during lytic growth, which will be shown in the later chapters. Thus, the study of the P1 partition system may allow us to explore more about the spatial organization of viral components during phage infection.

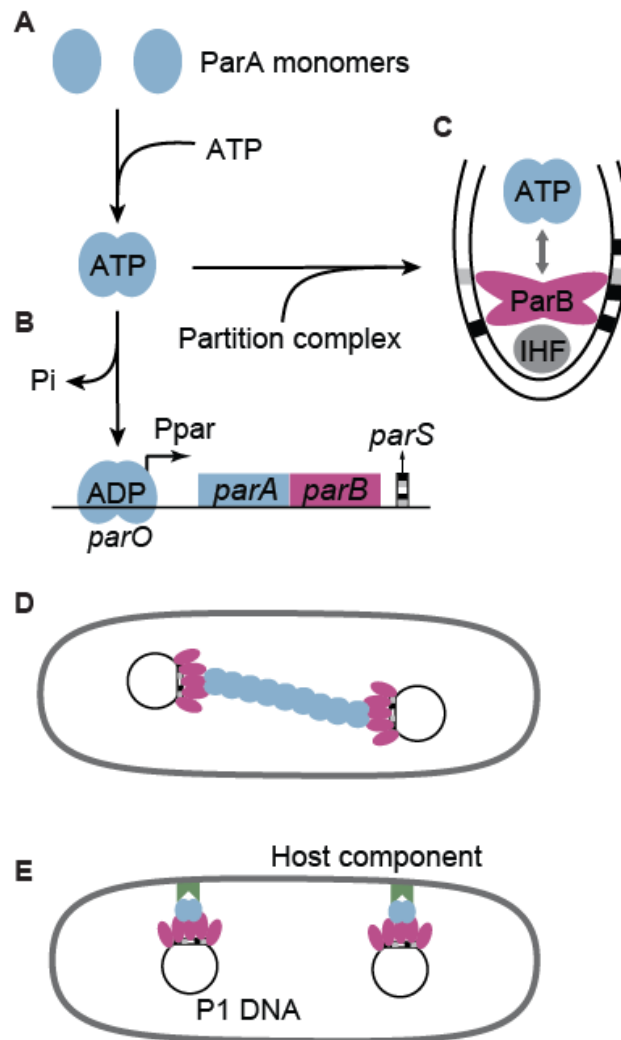


Figure I.8 The model of P1 partition system.

(A) Both ATP and ADP promote formation of the ParA dimer. (B) ATP hydrolysis converts ParA to its repressor form, ADP-ParA. It exerts negative autoregulation on *par* operon by binding to *parO* site. (C) ATP binding on ParA promotes the interaction with the partition complex formed by ParB and IHF at *parS*. Specifically, IHF binds centrally within *parS* and introduces a strong bend. ParB is able to interact with both hexamer (gray boxes) and heptamer (black boxes) sequences, located in both arms of *parS*. (D-E) Once recruited by ParB, ParA participates in as yet obscure steps in the partition process likely requiring ATP hydrolysis. The current two models are: (C) ParA protein is shown as migrating *en masse* through the cell, then briefly polymerizing to push plasmid replicas apart before dissociation; (D) The whole partition complexes are attached to host components distributing along the cell length.

P1 Lytic Growth

Learning about the genes or mechanisms that contribute to phage lytic growth and morphogenesis does not only allow us to manipulate the phages genome for scientific studies but also benefit the phage engineering which generates phage variants with specific properties for prophylactic and therapeutic applications. Here, I review the studies of P1 genes that I worked with during the construction of different fluorescent systems for the single-cell infection assay.

Activation of Late Transcription

For many phages such as λ ¹¹⁰, T4¹¹¹, Mu^{112,113}, P2¹¹⁴ and P4¹¹⁵, their gene expression cascades have been subdivided into early, middle and late stages. However, in P1, the early transcription switches directly to late, without a well-defined intermediate stage^{116,117}. C1 binding sequences act as a switch of early genes, whereas Lpa (late promoter activator) binding sequences, which enable RNA polymerase to initiate the transcription of late genes upon binding of Lpa, act as a switch of late genes. P1 late promoters resemble typical *E. coli* σ^{70} promoters in their -10 regions but lack the -35 regions¹¹⁷. Instead, they have a conserved 9-bp inverted repeat located at -22 from the transcription start site, responsible for interacting with Lpa^{118,119}. Binding of RNA polymerase to late promoter sequences requires the presence of Lpa¹¹⁹ and the *E. coli* RNA polymerase-associated protein SspA¹²⁰, tested both *in vivo* and *in vitro*^{119,121}. However, details of how Lpa and SspA cooperate to redirect the host RNA polymerase towards P1 late promoters need further investigation.



Phage Particle Morphogenesis

In common with other tailed phages, heads and tails of P1 have independent assembly pathways¹⁴ during the morphogenesis. Phage DNAs are packaged into proheads from concatemers¹²² by a headful mechanism (Fig. I.4), similar to T4, though T4 starts from an initial cut at a specific site for the packaging of each concatemer^{65,66,123}. The major head component (gp23) is a 44-kDa protein, presenting in different stoichiometric amounts in the head of P1B and P1S particles¹²⁴. The product of *gene23* undergoes protein processing during phage head assembly. The full-length gene product is 62.2 kDa, separated by SDS-PAGE. Based on bioinformatical studies, gp23 has no homologies to the well-known capsid proteins of other phages. It is possible that its evolutionary distance with other head proteins is so great that only similarities at the structural level can be retained or gp23 is the representative of a separate class of phage head proteins that can be seen as a characteristic of P1.

The Comparison with Decision-Making Paradigm Phage λ

Due to biological and historical reasons, phage λ has been served as a paradigmatic system of cell-fate studies. Although P1 and λ are both temperate phages, they differ in a number of fundamental and interesting ways (Fig. I.9): 1) Phage λ can only infect a subclass of *E. coli* strains, perhaps the ultimate ‘specialist’, however, P1 can be regarded as a ‘generalist’, with the ability to inject its DNA into a very broad range of bacterial hosts¹². Indeed, P1 can even infect *Myxococcus xanthus*, a member of the Delta Proteobacteria^{125,126}. 2) P1 uses widely distributed LPS as its receptor while λ uses a specific outer membrane protein LamB that shows helical or ring-like patterns on

cell surface¹²⁷. This contributes to the non-specific and polar adsorption to the cell surface for P1 and λ , respectively^{128,129}. 3) P1 forms a lysogen as a self-replicating plasmid while λ integrates its DNA into the host chromosome and replicates passively with the host. 4) Very intriguingly, unlike λ , which shows a strong MOI dependency on its lysogenization, P1 reaches a lysis-lysogeny decision in an MOI independent manner and in general is more biased towards lysogeny^{56,130}. This may reflect P1's real world experience, in having to deal with diverse cytoplasmic environments where the outcome of the lytic pathway may be problematic and less attractive in terms of fitness than the establishment of a stable lysogen.

| | Phage λ | Phage P1 |
|---------------------------|---|--|
| |  |  |
| Genome size | 48.5 Kbp | 93.6 Kbp |
| Adsorption | LamB as receptor Only infect <i>E. coli</i> Locate preferentially at cell poles | LPS as receptor Broad host range, e.g., <i>E. coli</i> , <i>Shigella dysenteriae</i> , <i>Salmonella typhimurium</i> , <i>Pseudomonas aeruginosa</i> , <i>Acetobacter suboxydans</i> , <i>Myxococcus xanthus</i> No location preference |
| DNA cyclization | Depends on specific "sticky ends", <i>cos</i> site | Depends on recombination of end redundancy (~10% of host DNA) |
| Regulatory network | Eight genes are located in one region Express in time cascade | Seven genes are located in three separate regions All express after injection |
| Lysogenization | Increases with MOI | Independent of MOI |
| Prophage | Integrate into host DNA | Low copy plasmid |

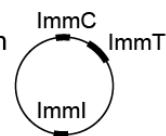


Figure I.9 The comparison of phage P1 with λ in different aspects.

The schematic of λ and P1 particles are drawn in scale. The schematic plasmid shows P1 prophage with three immunity regions at different locations in P1 genome.

Over the past decade, high-resolution studies have revealed paradigm-shifting discoveries in λ lysis-lysogeny decision-making^{129,131-135}. First, a 2-color decision-making reporter system was constructed to resolve phage λ decisions at the single-cell level, inaccessible by conventional bulk-level experiments¹²⁹. This work shows that a choice between lysis and lysogeny is first made at the level of individual phages and only unanimous lysogenic decisions by all phages lead to cell lysogeny, referring as phage “voting.” Following that, a 4-color system was constructed to unveil phage interactions during the phage voting process of λ ¹³². It indicates that with multiple phages infecting a single host cell, phages compete against each other for the host resources in producing their own progenies during the lytic development, whereas they cooperate in integrating their DNA into the host during the lysogenic development^{132,134}. These different subcellular interactions suggest a complex strategy for λ to seek optimal survival in different environmental conditions. A more recent study shows that injected DNAs of phage λ establish separate subcellular compartments in order to sustain the heterogeneous viral development in single cells¹³¹. Taken together, previous studies have demonstrated that phage λ behaves as individual entities and interact with each other inside the cell to reach a final cell fate.

Compared with the individuality of phage λ for decision-making, the independence of MOI for phage P1 strongly signals that the infecting phages make an ensemble decision. In this regard, P1 and λ serve as “opposite” paradigms in the spectrum of decision-making processes. Therefore, the study of P1 lysis-lysogeny decision-making will expand our understanding of temperate phages beyond λ and

generalize our knowledge of decision-making processes in terms of gene regulatory circuits.

Decision-Making in Different Biological Systems

Decision-making is a universal and diverse process for all organisms. Generally, it is studied as the outcome based on a careful evaluation of alternative options regarding the likelihood and the pros and cons associated with these options¹³⁶. For instance, two possible options that an animal can have when stress is encountered are fight or flight^{137,138}. A central principle of rational decision-making is the consistency across decisions, irrespective of how the available choices are presented. However, human beings are known to make “variant” decisions based on their emotions and cognitive biases. This deviation from the rational decision-making is called “framing effect”¹³⁹, during which people are inclined to avoid risk when a positive frame is presented but pursue risks in the negative frame. For example, there are two yogurt pots with the same content, but one says “10% fat” and another says “90% fat free”. The framing effect will lead us to pick the latter one that seems like “healthier.” The underlying neurobiological bases showed a specific association with the amygdala activity², representing the motivational value of studying chemical stimuli in the decision-making circuit. At its most basic interpretation, decision-making circuit is a program that senses different stimuli and produces varying responses accordingly. In animals, researchers have identified three different neural circuits involved in decision-making and each associate with a different region within the animal brain. One circuit was stimulated when a rat made a “good” choice that has a reward, another circuit was activated for a “bad”

decision with no reward and a third circuit was activated for the memory storage served as future decision reference¹⁴⁰.

The decision-making process also occur at the (sub)cellular level, where genetic circuits are instructed to sense environmental changes and then undergo different responses depending on alternative gene expressions. For example, one particular *B. subtilis* cell fate decision is the transition to competence, during which cells take up extracellular DNA for nutrient recourses or integrate it into the genome^{141,142}. During starvation, only a limited proportion of the clonal *B. subtilis* cells becomes competent and this decision is regulated by the master regulator ComK¹⁴³. In the gene regulatory circuit, ComK activates the downstream genes for developmental program, including itself, forming a positive loop. ComK levels are controlled by protease complex MecA/ClpC/ClpP that also binds to ComS. Hence ComS is able to prevent ComK degradation through competitive binding with host protease. Since *comS* expression is inhibited during competence, it forms a negative feedback loop around *comK*¹⁴⁴ (Fig. I.10A).

During embryonic stem cell (ESC) differentiation in mammals, homeobox protein NANOG acts as a transcriptional factor that assists ESCs to maintain pluripotency^{145,146}. NANOG has been found that shows a high expression level in cancer stem cells and may function as an oncogene to promote carcinogenesis^{147,148}. Analyzing its gene regulatory network found that the expression of NANOG relies on a similar structure with competence initiation network in *B. subtilis*, including both nested

positive and negative feedback loops, such as mutual *Oct4* and *Nanog* activation, *Oct4* and *Nanog* autoregulation, and *Nanog* repression by *Oct4* (Fig. I.10B).

Additionally, some recent studies have worked on regulatory circuits controlling the decision-making of temperate phages, especially when they are related with human diseases, such as Pf phages. Pf phages belong to *Inoviruses*, a genus of non-enveloped filamentous viruses. One unique feature of Inoviruses is their ability to establish a chronic infection cycle where newly produced virions are continuously extruded from the bacterial envelope instead of lysing the cell¹⁴⁹. The infection of Pf phages initiates with adsorbing to the tip of type IV pili of *Pseudomonas aeruginosa* (Pa) and then the ssDNA is transmitted into cell cytoplasm. At this point, phages make decisions between a chronic or a lysogenic lifecycle. A few players involved in Pf decision-making have been characterized in recent studies. The repressor Pf4r contributes to lysogenic development and maintenance by repressing the excisionase XisF4 expression. XisF4 promotes the transcription of replication initiation protein PA0727 and integrase IntF. Two nucleosome-like transcriptional regulators MvaT and MvaU suppress *xisF4* while transcriptional regulator OxyR suppresses *pf4r* expression^{150,151} (Fig. I.10C). Considering the roles of Pf phages during *Pa* biofilm formation and pathogenesis¹⁵²⁻¹⁵⁴, it is important to examine more factors that influence the decision-making and progeny phage production.

Comparing these examples, and with phage P1, we find that lysis-lysogeny decision involves multiple feedback loops, competing regulators and posttranscriptional control, similar to decision-making in other cell types with different levels of biological

complexity. Therefore, studies on phage decision-making will have broader implications.

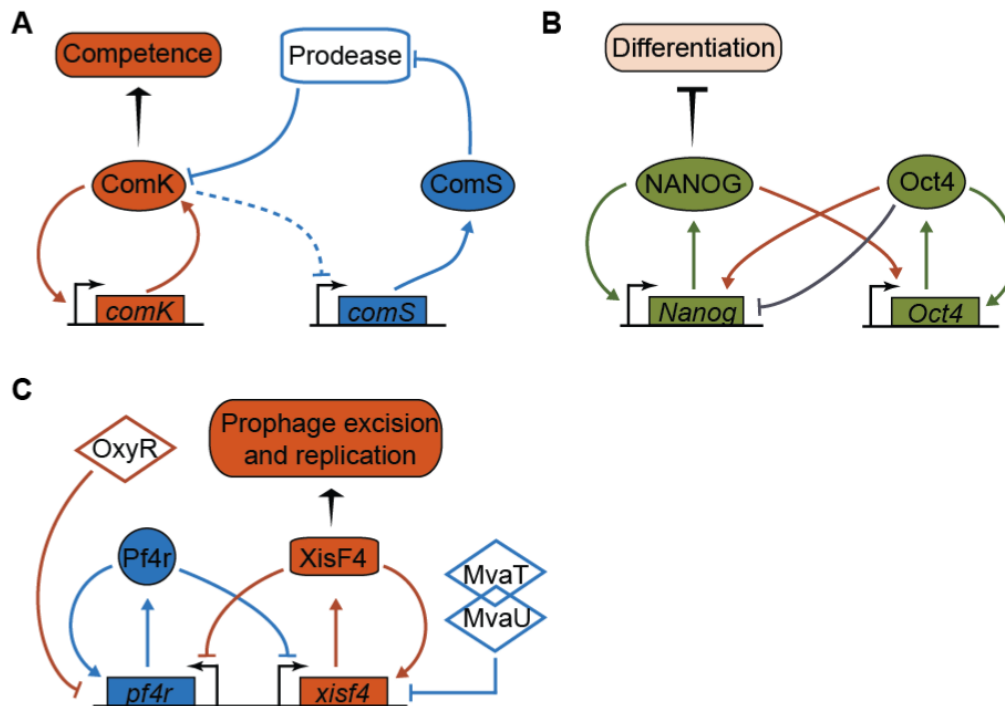


Figure I.10 Gene regulatory networks in different cell types show similar structures.

(A) The decision of becoming competence in *B. subtilis* is dictated by the master regulator ComK that activates the genes involved in this developmental program including itself. ComK levels are controlled by the protease complex. Its indirect activator, ComS, can prevent ComK degradation through the competitive interaction to the protease. ComS is downregulated during competence. These result in a structure of nested positive (red) and negative (blue) feedback loops. (B) During EMC differentiation, NANOG is a critical pluripotency marker and the low state of NANOG promotes the differentiation process. Oct4 acts as a gatekeeper for ESC pluripotency. The Nanog-Oct4 regulatory network primes ESC decision-making. It involves nested positive and negative feedback loops: mutual NANOG and Oct4 activation (red), NANOG and Oct4 autoactivation (green) and NANOG repression by Oct4 (dark grey). (C) Regulation of Pf phage decisions between lysogeny and chronic life cycle. The repressor Pf4r leads to and maintains lysogeny. The excisionase XisF4 promotes transcription of a phage operon encoding both the replication initiation protein and the integrase. Pf4r and XisF4 not only autoactivate their own expression but also repress each other. The transcriptional regulator OxyR suppresses *pf4r* when suffering oxidative stresses while the global histone-nucleosome-like transcriptional regulators MvaT and MvaU suppress *xisF4*. In all gene regulatory networks, arrowheads indicate activation; blunt arrows indicate repression.

Roles of Temperate Phages in Eukaryotic Systems

Temperate phages have been commonly identified in microbiome and human body system^{8,155-160}. Functionally, temperate phages are able to alter the biology of their bacterial hosts, such as enhancing host adaptation and survival under adverse conditions, and in turn, influence the community structures of host and non-host cells¹⁶¹⁻¹⁶⁶. Specifically, lysogenized prophages can be “domesticated” by either losing genes (e.g., for virion production) or acquiring cargo genes (e.g., MDR and virulence). The resulting prophage-derived genomic elements can be selectively maintained and confer advantages to the host cells, such as contribution to the pathogenicity of their bacterial hosts primarily via the production of phage-encoded virulence factors¹⁶⁷. For example, researchers have long known that many toxins produced by bacteria, including Shiga and cholera toxins, secreted by pathogenic *E. coli* and *Vibrio cholerae*, are in fact encoded by viral genes carried by bacterial chromosomes.

Advanced deep sequencing studies revealed the prevalence of P1 phage-like elements in animal and human pathogens and emphasized the hidden roles in spreading the antibiotic resistance¹⁶⁸⁻¹⁷². Some of these P1-like plasmids are carrying both phage properties and unique modifications that may associate with pathogen adaptations. For example, in pTZ20_1P, a core P1-like genome is associated with the insertion of plasmid modules encoding MDR¹⁷¹. Although this element was not able to transfer by conjugation, it was able to lysogenize a commensal *E. coli* strain with consequent transfer of MDR. When contemplating the process of MDR dissemination on a P1 backbone, there are many properties of P1 that potentially make it serve as an optimal

carrier of cargo genes. First, it can be transferred to a variety of gram-negative bacteria due to P1's broad host range^{42,80,173-177}. Then, the injected phage DNA will be protected from host Type I Restriction-Modification (RM) system by phage anti-restriction proteins^{17,18,49,178}. Following that, the establishment of prophage is guaranteed by the constant probability of cell lysogeny regardless of virus-cell ratio^{56,130}, regulated by the P1 immunity network. After lysogeny establishment, this regulatory network also enhances the stability of P1 phage-like elements through providing protection from the infection of foreign DNAs and competing phages¹². In addition, the prophage can be further stabilized and maintained using P1's own RM system¹⁷⁹⁻¹⁸¹, autonomous replication system^{79,182} and toxin-antitoxin system^{183,184}. We believe that a thorough elucidation of each step of these processes will help us to inhibit the dissemination of antibiotic resistance driven by P1 phage-like elements.

Expert for antimicrobial resistance, there is increasing interest of studying the influence of phages on human immunology. This trend parallels the resurgence of the efforts to develop phage therapies against pathogenic bacterial infections^{185,186} which will be discussed later, as well as the finding of endogenous phages residing on and within the human body^{187,188}. It has been reported that some temperate phages can help a pathogen host escape from the human immune system. A typical example happens during *Listeria monocytogenes*, the pathogenic bacteria that causes listeriosis, escaping mammalian cell phagosomes^{162,189,190}. An infective A118-like prophage is inserted within *L. monocytogenes comK* thereby blocking its expression. ComK encodes the master transcriptional activator of the late *com* genes required for cellular

competence^{143,191,192}. Upon *L. monocytogenes* invasion into mammalian cells, the prophage excises from the host genome. The resulting intact *comK* gene produces functional ComK proteins, which in turn activate the expression of the competence system to allow efficient bacterial phagosome escape through an unknown mechanism. Notably, throughout the excision process, the phage cannot undergo lytic production, and the phage DNA eventually reintegrates into *comK* during bacterial growth in the cytosol of the mammalian cell.

In addition to influencing bacterial gene expression, some phages can regularly modulate immune responses and directly impact human immune functions. Recent studies of *Pa* phages (Pf) have shown that, after the intracellular taken up by human immune cells, Pf increases the production of IL-12 and type 1 interferon and negatively regulated tumor necrosis factor (TNF) production^{153,154}. TNF, an inflammatory cytokine, is critical to bacterial clearance via phagocytes¹⁹³⁻¹⁹⁵. Thus, these data indicate that Pf phages trigger the production of anti-viral pattern recognition receptors that antagonize antibacterial immune functions.

In summary, unlike the traditional predator-prey relationships in other kingdoms of life, temperate phages can incorporate with their hosts by inserting their genomes into the bacterial chromosome, or stay as an intracellular plasmid, which adds complexity to the relationship between phages, bacteria and the environments they reside in. Given the contributions to antibiotic tolerance and immune evasion of their bacteria host, temperate phages are an exciting frontier in microbiology, immunology, and human

health. Further investigations are likely to yield additional insights into both pathogenesis and novel therapeutic development (Fig. I.11).

On the other hand, as I mentioned above, phage has been successfully used to treat patients with the previously “untreatable” multidrug resistance infection (phage therapy)¹⁹⁶⁻¹⁹⁸. In general phage therapeutics depend on the lytic pathway of infection. However very few obligatorily lytic phages have been identified in current biological systems, leaving temperate phages as the only choice for therapeutic applications. Therefore, phage therapy might need to largely rely on engineered temperate phages¹⁹⁸. Additionally, to hobble dangerous bacteria, temperate phages can carry pathogenicity-reducing genes during infection or disrupt the normal expression of the bacterial chromosome through insertion. For example, using a phage belonging to *Siphoviridae*, researchers found that infected *Bordetella bronchiseptica*, a bacterium that often causes respiratory diseases in livestock, were substantially less virulent in mice, probability due to the viral DNA inserted in the middle of a gene functioning during bacterium infection. What’s more, mice with pre-injected phages seemed to be protected from the infection by *B. bronchiseptica*, hinting at the possibility of utilizing temperate phages as vaccines against microbes¹⁹⁹ (Fig. I.11).

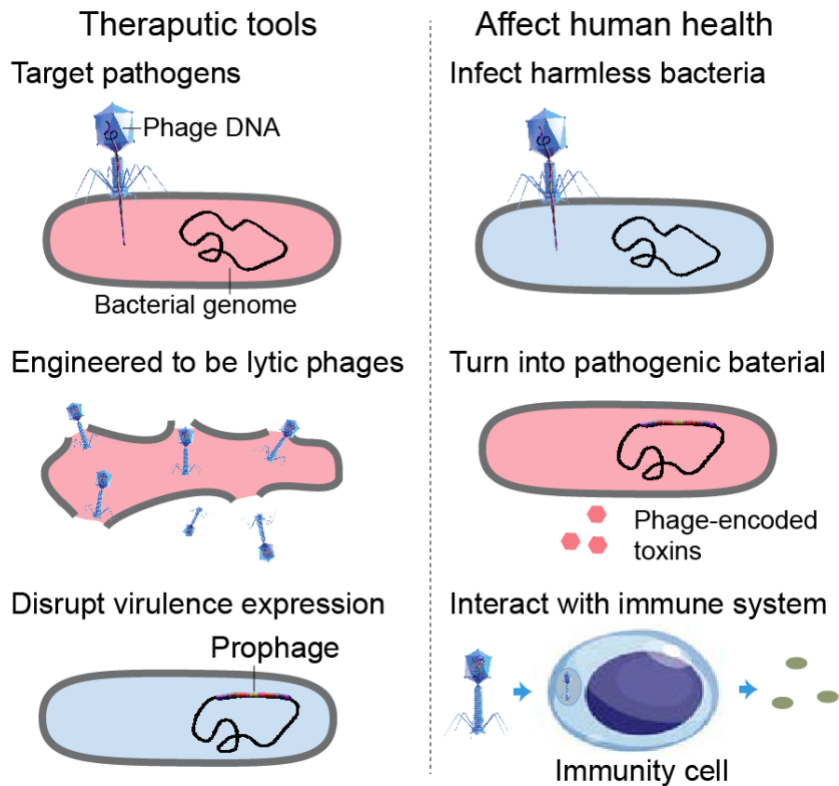


Figure I.11 Temperate phages can be used as tools for therapeutic treatment of pathogenic bacteria and affect human health.

Bacteriophages' ability to selectively target and kill bacterial strains has been used as possible weapons against pathogenic bacteria, as "the enemy of my enemy is my friend." General phage therapeutics depends on the lytic pathway of infection. However, very few obligatorily lytic phages have been identified in biological systems, leaving engineered temperate phages as the only choice for therapeutic applications. Moreover, temperate phages' ability to insert themselves into bacterial genomes has applications in novel antibacterial approaches as well. The insertion of pathogenicity-reducing genes or disrupt the normal expression of bacterial chromosome can be used to hobble dangerous bacteria. Besides therapeutic tools, temperate phages are able to influence microbial communities in the mammalian gut in different ways, and perhaps influence human biology. Through predation, phages can affect the abundance of specific bacterial taxa so that indirect influence the rest of the community. It also can drive the evolution of specific bacterial phenotypes via the incorporation their genomes into bacterial chromosomes. Moreover, researchers have found that phages interact directly with mammalian cells in the gut. The intracellular uptake of phages into immunity cell endosomes can trigger anti-viral pattern recognition receptors that antagonize antibacterial immunity or phage-specific antibodies that worsen inflammatory diseases.

Dissertation Overview

This project is to enclose novel decision-making behaviors of fundamental life using high-resolution approaches. The biological system used for the study is phage P1. The experimental methods went beyond single cells and single viruses, to look at single molecules during phage DNA replications and regulatory gene expressions within single cells. A more completed and unifying picture is presented here based on literature reviews, including the unique features of P1's morphology, initial infection stages, prophage maintenance and the key players involved in decision-making between lysis and lysogeny. Moreover, decision-making circuits of various temperate phages and organisms are also introduced for comparisons. The interactions between phages with mammalian systems are mentioned in awe at the end, contemplating the abundance and "intelligence" of these simplest creatures. In the next few chapters, the research systems conducted for P1 decision-making studies as well as the new findings will be discussed.

In chapter II, evidence is obtained for the uniform distribution of absorbing localization of phage P1 on the *E. coli* cell surface. The success rate of DNA injection and lysis-lysogeny outcomes are also detected with different single-cell systems, in order to study the influence of infection locations. Our findings in P1 differs from phage λ in varied ways, suggesting that these two temperate phages show significant diversity in important functional aspects.

In chapter III, the mechanism of MOI-independent lysogenization of P1 is examined, regarding the expression of viral regulatory proteins and the interactions between co-infecting phages. At the molecular level, the constant repressor activity for

each infecting phage is the key that leads to the MOI-independent decisions. Moreover, a DNA visualization system is constructed to detect viral DNA interactions and the efficient communication between phages infecting the same cell is discovered.

In chapter IV, I investigate more factors that influence P1 lysis-lysogeny decision-making. It shows that the P1 lysogenic response is associated with cell growth state and host cells with smaller growth rate show higher probabilities for lysogeny. Evidence for different DNA replication patterns in lytic and lysogenic cells are also observed. More novel methods for single-cell studies on phage decision-making are discussed at the end.

In chapter V, I recapitulate my works and reframe the content in a bigger picture. The hope is to gather more insights into how the simplest life persists and continues in its own world and within ours.

CHAPTER II
BACTERIOPHAGE P1 DOES NOT SHOW SPATIAL PREFERENCE WHEN
INFECTING *ESCHERICHIA COLI**

Introduction

Bacteriophage P1 was isolated by Giuseppe Bertani from a lysogenic strain of *Escherichia coli* named “Li” (Lisbonne and Carrère) in 1951⁴², and P1 has been well-known for its high rate of generalized transduction³. P1 is a myophage that infects *E. coli* and several other enteric bacteria. Its genome, of around 94 kb¹², is packaged in a head structure of icosahedral symmetry. The head is attached to a contractile tail that bears six kinked tail fibers^{14,200}.

The infection cycle of P1 begins with the adsorption of phage particles on the cell surface. During adsorption, Ca²⁺ ions are required⁴²⁻⁴⁴ (Fig. II.1), and the recognition receptor is identified to be a terminal glucose moiety of the lipopolysaccharide (LPS) core of the bacterial outer membrane⁴¹. The interaction of at least three tail fibers with the receptor molecules is assumed to be sufficient to stimulate viral DNA injection⁴⁵. To be more specific, the attachment of P1 tail fibers triggers the tail sheath to contract, and the tail tube is pushed through the baseplate, puncturing the cell outer membrane. It is speculated that the tail tube penetration induces the fusion between the inner and outer

* Reprinted with permission from “Bacteriophage P1 does not show spatial preference when infecting *Escherichia coli*” by Kailun Zhang, Ry Young, and Lanying Zeng, 2020. *Virology*, Volume 542, Pages 1-7, Copyright 2021 by Elsevier B.V.

membrane, which allows a direct translocation of the DNA from the phage head into the host cytoplasm⁵⁰. The injected linear DNA circularizes rapidly by the recombination between terminal redundant ends^{71,182}. Following that, the cell enters either the lytic cycle, where progeny phages are produced and the cell lyses, or the lysogenic cycle, in which the phage DNA exists as a low copy plasmid and replicates autonomously^{79,182}.

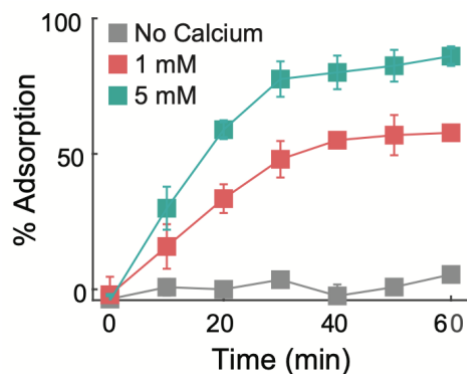


Figure II.1 The percentage of phage adsorption in bulk with different calcium concentrations in the solution.

Phages P1LZ1856 were incubated with MG1655 adding 0, 1mM or 5mM CaCl₂. The MOI is around 3. Ca²⁺ ions are required for phage P1 adsorption on *E. coli* cells. The means and standard deviations are presented (n=2).

Spatial organization is essential for all living systems. Even bacteria, the simplest forms of cellular life, can display complex internal organization^{201,202}. For example, in rod-shape bacteria, the nucleoid is located in the center of the cytoplasm, leaving the cell poles largely free of DNA. Certain functional proteins, such as protease FtsH²⁰³, and ribosomes²⁰⁴ are enriched at the cell poles. Therefore, when phage DNA is injected into the cell at different locations, the phage DNA will be exposed to different intracellular environments, which may result in altered stabilities, replication, gene expression, and DNA dynamics. In this study, we aim to investigate the localization of phage P1 on the *E. coli* cell surface, and its influence on the subsequent DNA injection and lysis-lysogeny cell fate. A previous study showed that a number of virulent and temperate phages, including P1, preferentially localized to bacterial poles²⁰³. In contrast, the P1 recognition receptor, LPS, is abundant and exhibits an even distribution around the cell periphery as observed by staining the O8 surface antigen with fluorescent lectin²⁰⁵. In order to examine the spatial distribution of P1 at the single-cell, single-virus level, we constructed fluorescent virions through capsid labeling, and found that P1 showed no preference for binding to different cellular locations. We next monitored phage DNA locations after the infection, using fluorescent *E. coli* SeqA fusion. The position of P1 DNA showed a uniform distribution along the cell. Furthermore, we constructed a cell-fate reporter system based on distinctive gene expressions in lytic and lysogenic pathways. We found the same success rate of infection against different phage adsorption locations, and there was no correlation between adsorption locations and cell fate.

Results

Fluorescent Capsid Labeling of P1 Particles

To enable the detection of individual phages, we labeled the P1 particles by fusing fluorescent proteins on the viral capsids, similar to the strategy labeling phage lambda²⁰⁶. In this case, the fluorescent phages are produced from lysogen induction. The wild type (WT) major capsid proteins (gp23)¹²⁴ are produced from the phage genome. Simultaneously, the fluorescently fused gp23-mTurquoise2 is expressed from a plasmid *in trans* (Fig. II.2A). As a result, the newly assembled phages contain a mixture of both WT and labeled capsid proteins. The specific procedures are described below.

P1 can infect a variety of Gram-negative bacteria, and an inversion system^{20,21} (C-segment) located in the P1 genome leads to the adsorption specificity to different hosts⁸⁰ by expressing alternate sets of tail fiber proteins (RSU or RS'U')²⁰⁷. Specifically, phages carrying RSU fibers (C+) are able to infect *E. coli* K12, *E. coli* B and *E. coli* C, whereas phages carrying RS'U' fibers (C-) do not normally infect these strains. In the prophage, inversions of the C-segment are accomplished by the Cin site-specific recombinase^{22,23}. Thus, the phage induced from a P1 lysogen will contain equal numbers of particles with either host specificity. The host strain we used for the infection study, MG1655, is an *E. coli* K12 derivative, meaning half of the phage virions are inert during the infection, disturbing single-cell analysis. To ensure the tail fiber type is C+, we knocked out gene *cin*, and the titer of Δcin phages (P1LZ1856) from lysogen induction doubled the titer of the WT (P1KL463) as expected.

Another feature for P1 that might misguide the single-cell observation is the variety of head sizes¹⁴. In addition to the normal infectious particles with big heads (P1B), P1 produces ~20% small (P1S) and minute (P1M) particles with similar tails. P1S and P1M can adsorb and inject their DNA normally but are not productive during infection, because they lack the capacity to hold a complete P1 genome DNA (<45% of full-length DNA)^{15,16}. In order to ensure the infectivity of phage particles, we separated the defective particles by CsCl isopycnic centrifugation based on their smaller buoyant densities⁸⁰. Images taken by transmission electron microscope showed that 95.8% (115 of 120) of the CsCl purified fluorescent phages have big heads with normal morphology (Fig. II.2B).

Next, in order to test the capsid labeling and DNA packaging efficiency, we stained the fluorescent phages with the DNA intercalating dye, 4', 6-diamidino-2-phenylindole (DAPI). As shown in Fig. II.2C, the individual phages are easily distinguishable under the fluorescence microscope, and the mTurquoise2 signal (phage head) colocalizes with the DAPI signal (phage DNA) very well. Only about 0.6% of the fluorescent phage particles examined (3 of 470) lacked the DAPI signal, and 4.3% (20 of 470) lacked the mTurquoise2 signal. After extensive purification and no apparent reduction of phage titer over three months, we conclude that the fluorescent phage is structurally stable. Furthermore, the fluorescent phage also exhibits the same lysis-lysogeny decision-making phenotype through the bulk assay (Fig. II.3).

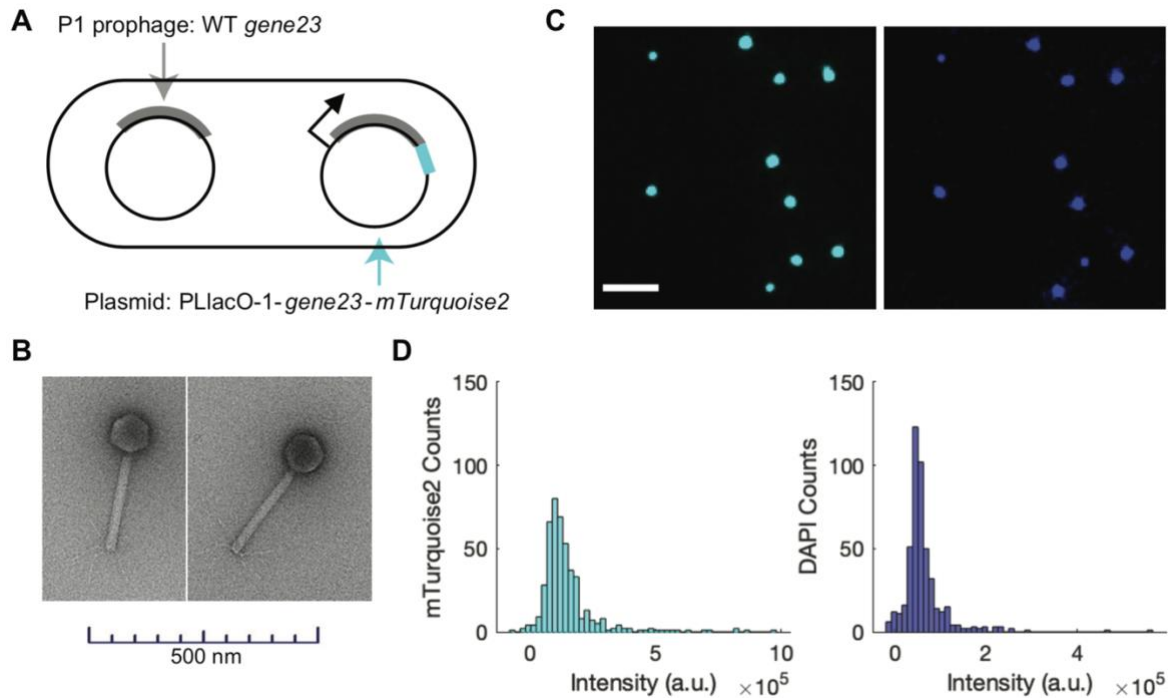


Figure II.2 Labeled phage P1 through fluorescent capsid fusion.

(A) A schematic of fluorescent phage construction. The plasmid expressing *gene23-mTurquoise2* under the control of an IPTG inducible promoter (PLlacO-1) is transformed into P1 lysogens. After lysogen induction, the fluorescent phages are produced, which assemble a mixture of both WT and labeled capsid proteins in the head. (B) Fluorescent phage morphology is examined using transmission electron microscopy. The mosaic phage exhibits normal phage morphology. Phage particles with big heads (P1B) are around 96% among all images. (C) DNA packaging efficiency of the gp23-mosaic phages. DAPI was used to label the phage genome DNA. mTurquoise2 (phage capsid; left) and DAPI (viral DNA; right) signals colocalize very well and individual phages are easily distinguishable. Only about 0.6% of the fluorescent phage particles examined (3 of 470) lacked the DAPI signal, and 4.3% (20 of 470) lacked the mTurquoise2 signal. Scale bar = 2 μ m. (D) Intensity histograms of the mTurquoise2 and DAPI signals.

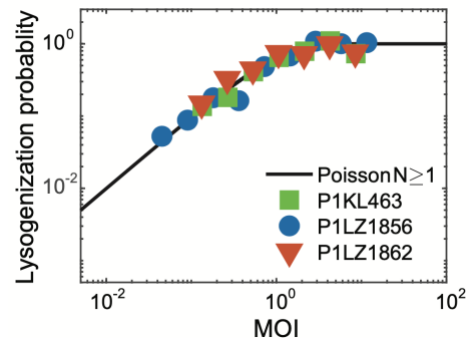


Figure II.3 Fluorescent phages lysogenize like WT phage in bulk.

Percentage of lysogenization probability is plotted against the MOI. The data of each set were normalized by the maximum value of the lysogenization probability. Both Δcin phage P1LZ1856 (blue circle), and capsid labeled phage gp23-mTurquoise2 P1LZ1862 (orange triangle) show the same lysogenic response to MOIs as the WT P1 strain, P1KL463 (green square), which follows the theoretical prediction of Poisson distribution of $N \geq 1$ (black line).

P1 Adsorption Shows No Preference on the Cell Surface

We examined phage adsorption on the cell surface using the fluorescent phages. Since the adsorption was saturated after incubating phages and cells for 30 min at 30°C from bulk measurements (Fig. II.4), we chose this time point to examine the adsorption under the microscope (Fig. II.5A). We found that P1 had a similar probability for adsorption on the cell surface, regardless if we only counted the cells with single phage attached (596 cells with MOA = 1; multiplicity of attachment) (Fig. II.5B) or total cells with MOA ≥ 1 (2613 phages in total, see Fig. II.5C). In addition, the number of phages adsorbed on the single cell follows the Poisson distribution (Fig. II.5D and Fig. II.6), indicating that the phage adsorption is an independent event, in other words, the adsorption of one phage does not affect that of the others. Since phage adsorption on the cell surface does not necessarily correspond to successful infection, we use MOA to describe the number of phages adsorbed on each cell observed in single-cell experiments, but keep using MOI as the ratio of the input phage and cell number in bulk experiments in the rest of the manuscript.

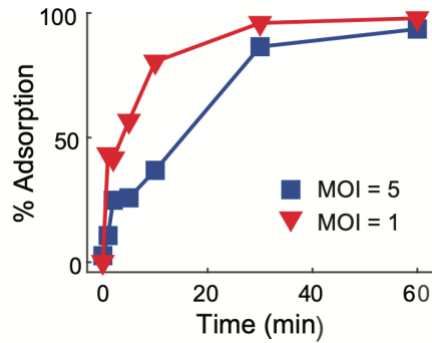


Figure II.4 The percentage of phage adsorption in bulk at different MOIs. Phages P1LZ1856 were incubated with host cells at 30°C, with MOI equals to 1 and 5. The adsorption is saturated at about 30 min.

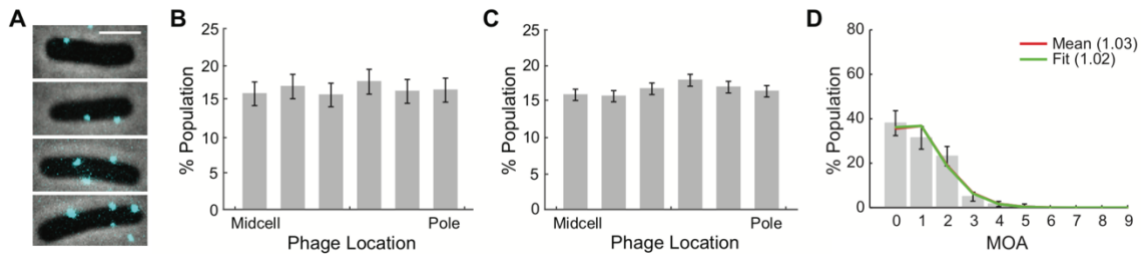


Figure II.5 Phage P1 adsorption shows no preference on the cell surface. (A) Representative images of gp23-mTurquoise2 phage P1LZ1862 adsorbed on MG1655 are shown, which allow us to collect the information of the adsorbed-phage number and location on the cell surface. Scale bar = 2 μm. (B) and (C) Distributions of infecting phages are plotted versus phage locations along the cell for MOA = 1 and MOA ≥ 1 respectively. No preferred P1 distribution was observed in the view of localization on the cell surface. (D) The percentage of phage adsorbed cells as a function of MOA. Grey bars: experimental data from a time-lapse movie. Red line: the prediction of the Poisson distribution given the mean of MOA (1.03). Green line: fit the experimental data to a Poisson probability density function and the expected number of occurrences of this function is 1.02. Experimental data are well fitted by the prediction. Therefore, the adsorption of phage P1 follows the Poisson distribution. See supplementary material for more examples (Fig. II.6). In all plots, error bars denote counting error.

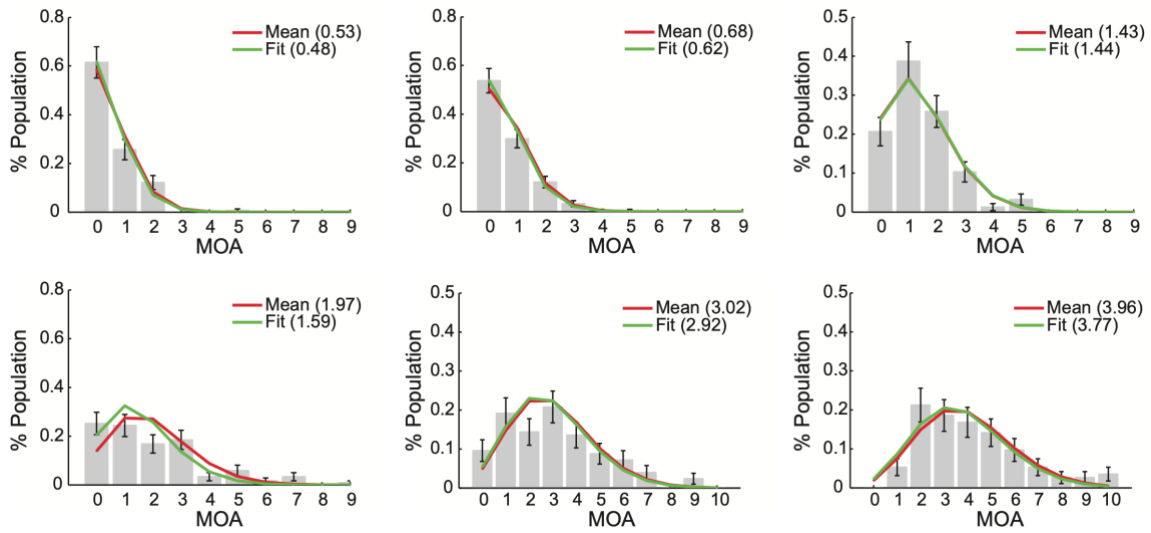


Figure II.6 The adsorption of phage P1 follows the Poisson distribution.

Shown here are data from several single-cell infection time-lapse movies with different MOIs. Also see figure II.5D. Grey bars: experimental data. Red line: the prediction of the Poisson distribution given the mean of MOA. Green line: fits the experimental data to a Poisson probability density function and calculates the expected number of occurrences of this function. Experimental data fit well with predictions. In all plots, error bars denote counting error.

Localization of Phage P1 DNA Shows No Preference in the Cytoplasm

We further tested whether there was specific spatial organization of phage DNA inside the cell. To monitor phage DNA localization upon injection, we utilized our established DNA visualization system by taking advantage of the specific binding of SeqA protein to methylated DNA GATC site^{132,206}. To do this, we prepared P1 DNA methylated and *E. coli* DNA unmethylated to allow the specific labeling of phage DNA. In particular, P1 genome DNA that contains 700 5'-GATC sites was produced from the normal lysogen induction resulting in adenine methylation of GATC sites. On the other hand, we used a host strain, LZ1387, which was defective in adenine methylation of 5'-GATC sequences (*dam*⁻) and constitutively expressed the fluorescent fusion protein SeqA-mKate2 from its chromosome¹³². Before P1 infection, the SeqA-mKate2 fusion in the *dam*⁻ host exhibits uniform cytoplasmic distribution. Upon P1 infection, SeqA-mKate2 specifically labels the initial, injected phage DNA (methylated) or the first replicated duplex (hemi-methylated) by forming foci, but not the unmethylated phage DNA or host chromosome (Fig. II.7A and B).

Next, we recorded the data of the first appearance of each SeqA-mKate2 focus in the cytoplasm with a five-minute temporal resolution. Intensities of the first fluorescent foci were fairly uniform (Fig. II.8A and B) and distributed evenly along the cell, excepting for the polar position (Fig. II.7C). The low frequency of phage DNA appeared at the cell pole might be due to: first, relatively smaller volume of the spherical pole compared to the volume of the cylinder-like nonpolar regions (see normalized data in Fig. II.8C); second, the crowded effect with many proteins and biomolecules

accumulated there²⁰⁸⁻²¹¹; third, during 5 min detection, phage DNA molecules might have moved away from the poles although they are injected in these positions. In sum, these initial phage DNA location data provide further support that P1 infection does not have spatial preference.

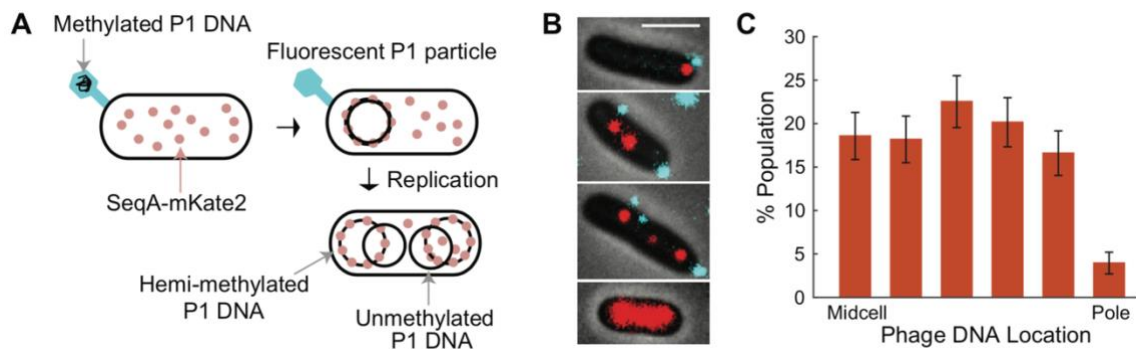


Figure II.7 Phage P1 DNA injection shows no preference for cellular positions.

(A) A schematic of phage DNA labeling through SeqA-mKate2 binding in *E. coli* strain LZ1387. The initial SeqA-mKate2 focus appearing inside the cell corresponds to the injected phage DNA. Two foci appear as the phage DNA replicates into two hemi-methylated phage DNAs. These two foci remain during the infection cycle. (B) Representative images showing phage DNAs (red spots) during the infection of gp23-mTurquoise2 phage P1LZ1862 (cyan spots). For the cell at the bottom, it has no phage infecting and thus the SeqA-mKate2 fusions distribute uniformly inside the cell. A different contrast is used for the bottom cell for better clarity. Scale bar = 2 μm. (C) The distribution of locations for the first appeared SeqA-mKate2 foci during phage infection (253 foci in total). Injected DNAs distribute evenly along the cell. Error bars denote counting error.

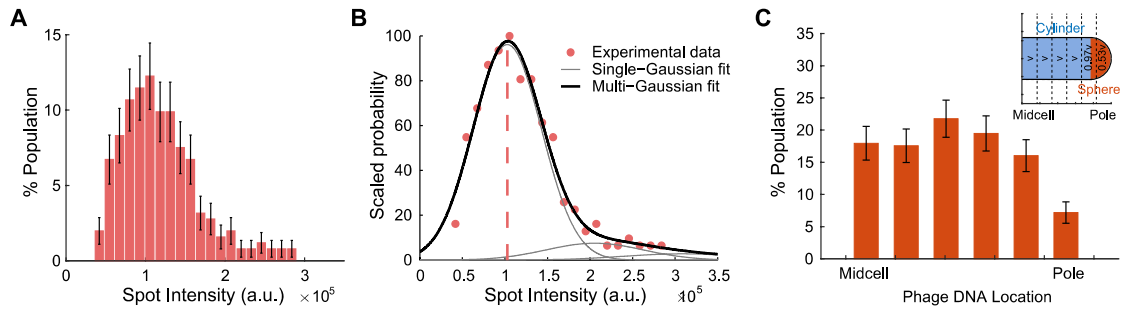


Figure II.8 Data analysis of injected viral DNA.

(A) The distribution of first SeqA-mKate2 spot intensities captured during single-cell infection movies (253 foci in total). It shows a predominant peak, corresponding to a single DNA molecule. (B) The data are well fit to a sum of Gaussians (black line) with increasing peak positions and decreasing peak heights, corresponding to one, two, three and so on DNA molecules per spot (gray lines), where each of the means and variances are constrained to being a multiple of the mean and of the variance of the first DNA peak. Salmon dots: Experimental data scaled to the maximal percentage of the distribution. The intensity of a single DNA molecule can be estimated as the mean of the first Gaussian (salmon dash line), which is 1.03×10^5 a.u. (C) The normalized distribution of locations for the first appeared SeqA-mKate2 foci based on the volume (Related to Fig. II.7C). In the insert, the vertical dish lines separate the data into six groups plotted in bar graph. The volume of the spherical polar region is about 0.53 of each cylinder-like region. In all plots, error bars denote counting error.

Assaying the Post-Infection Lysis-Lysogeny Decision with Single-Cell Resolution

In order to examine the lysis-lysogeny decision at the single-cell level, we constructed a fluorescent reporter system based on the distinct gene expression programs of the lysis and lysogeny pathways (Fig. II.9A). The infecting phage was fluorescently labeled as described in the previous section, which allows us to count the number and location of the phage (Fig. II.9B, 0 min). To report the lytic pathway, we transformed a lytic reporter plasmid (pLZ1915) into the host, carrying a fluorescently fused *gene23* (gp23-mTurquoise2) under the control of its native late promoter, LP23 (Fig. II.9B, 60 min and 100 min). In lytic cells, this fluorescent reporter forms discrete foci at the later time points during infection, which are presumably the centers of phage assembly. To report the lysogenic pathway, we constructed the phage bearing a transcriptional fusion of a fluorescent protein gene *mVenus* inserted downstream of *cI*. Protein C1, the major repressor for the lytic development, is produced once the P1 DNA is injected into the host cytoplasm. Therefore, all infected cells contain mVenus signal (Fig. II.9B, 15 min). Accordingly, the lysogenic pathway can be identified through mVenus expression followed by cell division.

The reason to choose the transcriptional fusion instead of a translational fusion to C1 is to avoid any potential interference with C1 activity since C1 binds to a multiplicity of operators (~20 sites) scattered across the P1 genome¹². In addition, we speculate that the insertion of the *mVenus* gene along with an antibiotic resistance marker (~2kb in total which is ~2% of P1 genome size) does not disturb phage morphogenesis and behavior since infectious P1 particles normally contain a DNA molecule with about 10%

terminal redundancy^{71,182,212}. To verify this, we performed bulk experiments to examine the lysogenic response of the *cI*-labeled phages, which showed a similar trend of lysogenization frequency as the unlabeled WT phages (Fig. II.10).

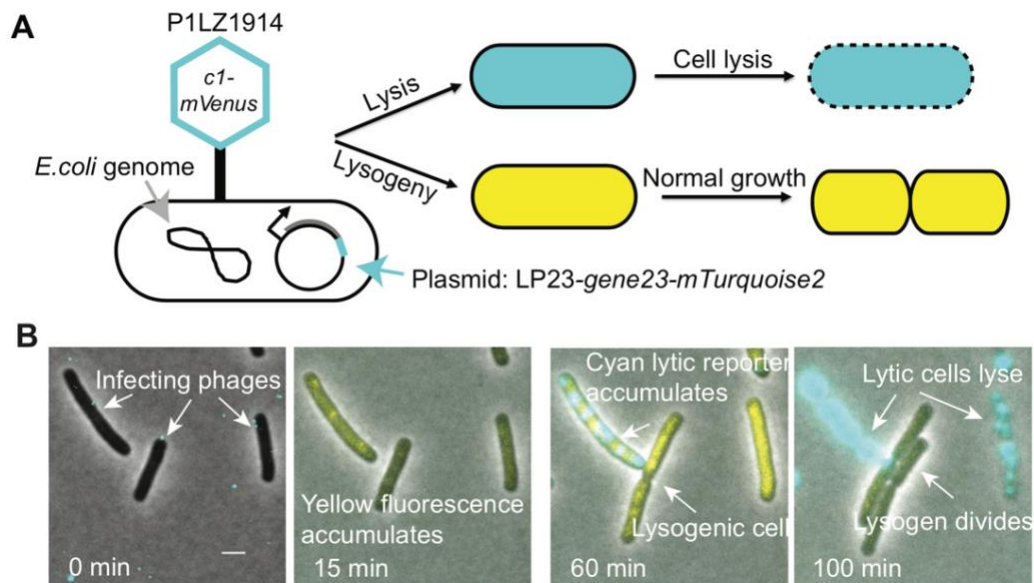


Figure II.9 Assaying the post-infection decision with single-cell resolution.

(A) A schematic description of our cell-fate assay. Multiple gp23-mTurquoise2 *c1*-labeled phages P1LZ1914 infect individual cells of *E. coli* (LZ1915). The post-infection fate can be detected in each infected cell. A successful infection can be indicated by the expression of mVenus. Choice of the lytic pathway is indicated by the intracellular production of gp23-mTurquoise2 from a plasmid with native late promoter LP23, followed by cell lysis. Choice of the lysogenic pathway is indicated by cell division after infection. (B) Frames from a time-lapse movie depict infection events. Shown is an overlay of the phase-contrast, CFP (sum of multiple z-stacks for 0 min; single z-stack at later time frames) and YFP channels. At 0 min, two cells (left two) are seen each infected by a single phage (cyan spots), and one cell on the right is adsorbed by two phages. At 15 min, all cells show mVenus signal, indicating that viral DNAs are successfully injected and phage C1 proteins are being expressed. At 60 min, the cell on the left has gone into the lytic pathway, as indicated by the production of gp23-mTurquoise2 from the LP23 on the lytic reporter plasmid. The cell in the middle has gone into the lysogenic pathway, as indicated by cell division. At 100 min, the lytic pathway has resulted in cell lysis, whereas the lysogenic cell divides and grows normally. We assume that the decreased mVenus signal inside the daughter lysogens is due to the dilution of mVenus expressed during the decision-making after lysogen division, and C1-mVenus expression is repressed in the steady lysogen cells because of autoregulation. Scale bar = 2 μ m.

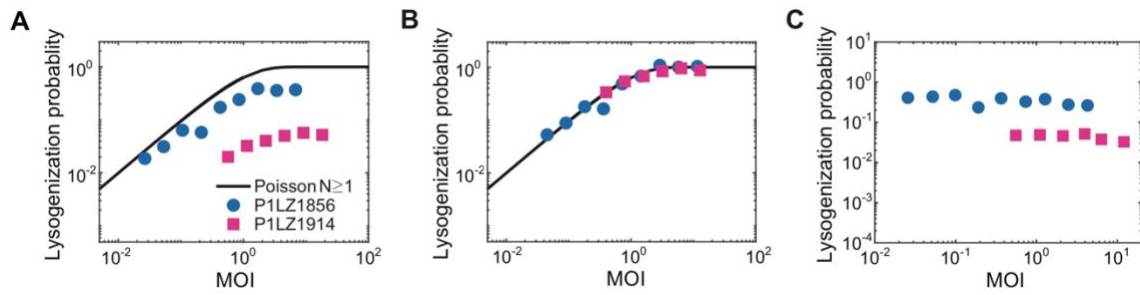


Figure II.10 *cI*-labeled phages lysogenize like unlabeled phages in bulk.

(A) The lysogenization probability is calculated based on total cell numbers. The black line shows the theoretical prediction based on the $N \geq 1$ Poisson distribution. (B) The data of each set in (A) were normalized to the Poisson curve. The gp23-mTurquoise2 *cI*-labeled phage P1LZ1914 (magenta square) shows the same lysogenic response against MOI on MG1655 as the parent P1 strain, P1LZ1856 (blue circle). (C) The lysogenization probability is calculated based on the number of infected cells. Both phage strains show a constant lysogenic response over MOI, although the lysogenization frequency of gp23-mTurquoise2 *cI*-labeled phage is lower than the parent P1 phage.

The Successful Infection and Decision-Making of P1 Are Independent of the Phage Adsorption Location

We then examined the decision-making process of P1 through time-lapse movies under the microscope. The majority of phage-attached cells (84.7%, 1083/1278 cells, 15 experiments) entered either lytic or lysogenic pathway. A small fraction of infection events (3.5%, 45/1278 cells) exhibited a halting of cell growth, and the fraction of nongrowing cells increased with MOA (Fig. II.11). The remaining fraction of the infection events (11.7%, 150/1278 cells) did not trigger mVenus or lytic mTurquoise2 signal expression, which was likely due to failed or incomplete viral DNA injection. Furthermore, at a MOA of 1, the failed infection frequency was about 16.6% (99/596 cells) regardless of where the phage was adsorbed (Fig. II.12A and B). In addition, the positions of the infecting phages did not have significant effect on the choice between lysis and lysogeny (Fig. II.12C), the lysis time (Fig. II.12D) or the gene expression (Fig. II.13). In summary, the rate of successful infection or the post-infection decisions do not depend on the site of infection.

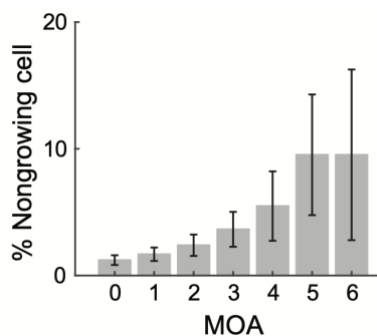


Figure II.11 The percentage of nongrowing cells increases with MOA.

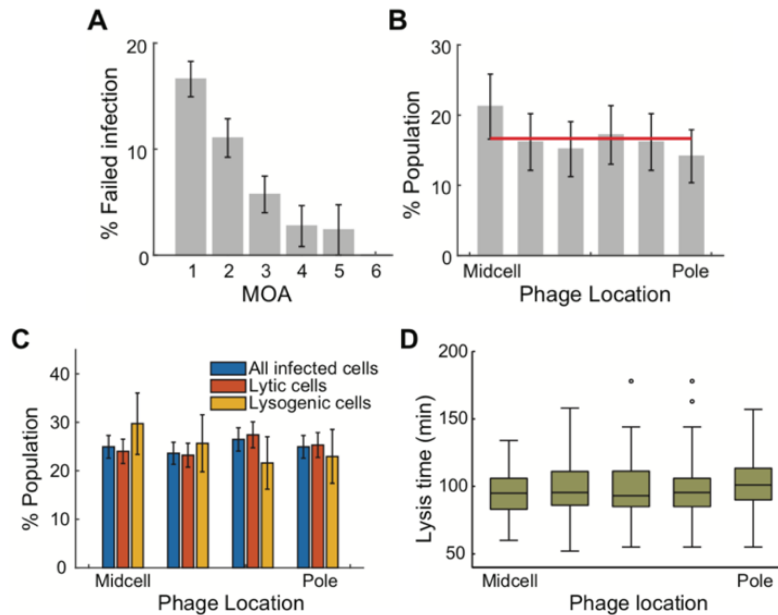


Figure II.12 The failed infection and decision-making do not depend on the initial adsorption locations on the cell surface.

(A) The percentage of failed infection as a function of MOA. The failed infection frequency is about 16.6% at MOA = 1 and decreases with increasing MOAs. (B) The percentage of failed infection against phage locations of cells at MOA = 1 shows a uniform distribution. Red line: the mean failed infection frequency of cells at MOA = 1. (C) The percentage of all infected, lytic and lysogenic cells as a function of phage locations on the cell surface. There is no significant preference for P1 lysogenization over the phage locations. (D) Box plot of the lysis time for the cells with one phage infected at different locations. We count the start of infection movies as 0 min. The average lysis time is around 98 min and there is no difference when phages adsorb at different cell locations. In A-C, error bars denote counting error.

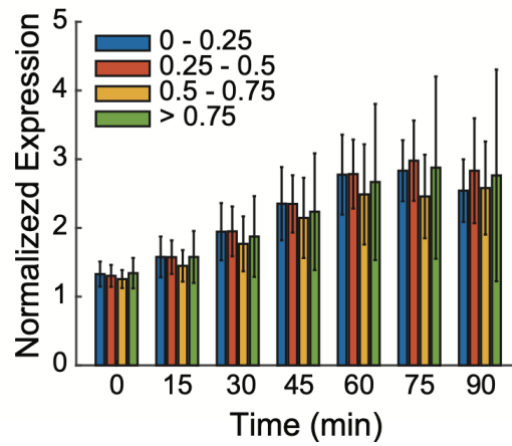


Figure II.13 Expression level of C1-mVenus of cells infected at different locations. We divided infected cells (MOA = 1) into four groups depending on infected locations and defined 0 as mid-cell and 1 as cell poles. In A-B, error bars denote counting error. In C, error bars stand for standard deviation.

Discussion

In this work, by taking advantage of single-cell and single-virus techniques, we characterized the initial steps of the bacteriophage P1 infection cycle and examined their relationship with the post-infection decisions. To visually detect the phage adsorption, we developed a plasmid-based approach to construct fluorescent P1 virions. Under our experimental conditions, although the titer of the prophage lysate (P1LZ1914) decreased about 30% compared with the unlabeled parental P1 (P1LZ1856), the fluorescent phages were structurally stable, behaved similarly to the WT phage, and bright enough to be detected under the microscope. The reduction of progeny yield might be due to the overexpression of the gp23-mTurquoise2 during lysogen growth and induction, or the trade-off of the infectious phage production for the mosaic capsid assembly.

The three principal findings of this work are: (1) P1 infection occurs uniformly along the length of the cell; (2) the likelihood of successful infection does not depend on the site of infection; (3) the outcome of the lysis-lysogeny decision is also independent of the site of infection. In all three aspects, P1 differs from the paradigmatic phage lambda.

Lambda exhibits a significant bias towards infection sites at the poles or, in predivisional or filamented cells, at mid-cell “future poles”^{127,129,203,206}. Moreover, we have previously shown that lambda infections at the poles have a lower failure rate and higher frequency of lysogenic outcome, so our findings suggest that these two well-studied temperate phages show significant diversity in important functional respects. However, in 2008 Edgar and colleagues²⁰³ reported many other phages, including P1, also exhibit a bias towards infection at the poles or future poles (mid-cell). This polar bias was suggested to

reflect important biological narratives, including optimizing successful infections. For example, together with lambda the ManYZ inner membrane protein complex was also found to show polar bias; since ManYZ has been implicated in the penetration of the lambda genome DNA into the cytoplasm, polar infections would be more likely to be successful. Moreover, the protease FstH (HflB) was also shown to exhibit polar bias, leading to the notion that polar infections would be subjected to locally enhanced degradation of the CII and CIII proteins and thus be less likely to follow the lysogenic pathway.

The polar bias of lambda infections is thus well-supported by works reported from three different research groups using a variety of methods for labeling the lambda particles^{127,129,203,206}. Moreover, a simple rationale for this bias is available in that two groups have found a significant polar bias in the localization of the LamB receptor^{127,213}. No such rationale exists for the receptors of P1 or the other phages reported to exhibit polar infection, although in each case the receptor has been determined. P1 uses LPS sugars, as does the podophage T7 and the T7-like *Yersinia* phage phiA1122, whereas the siphophage phi80, myophage T4, and T4-like *Vibrio* myophage KVP40 use the porins FhuA, OmpC and OmpK, respectively. As it seems highly unlikely that all these outer membrane proteins, much less LPS receptors, are all distributed with a polar/mid-cell bias, our own finding, that P1 attaches uniformly along the cell length, seems more consistent with expectations. Thus it is prudent to consider what differences exist between the two experimental conditions used for the conflicting P1 infection results from our work and Edgar *et al.*²⁰³. Both experiments used *E. coli* K-12 strains, MG1655

in our work, and either W3110 or C600 in theirs. Edgar *et al.* used a P1 *vir* from a laboratory collection, but no genotype was provided. We used a derivative of P1Cm *cI*-100⁵⁶, in which the *cin* gene was inactivated. The *cin* deletion keeps the P1 *cin* cassette in the (C+) orientation that generates phages that all recognize *E. coli* K12. We presume P1 *vir* as used by Edgar *et al.* was grown lytically, so that only the C+ orientation can propagate, so there should be no difference in the host range or adsorption properties. However, the labeling of the P1 virions was dramatically different. In our case, we supplied a chimeric P1 major capsid protein, gp23-mTurquoise2, *in trans* to the induced prophage, generating fluorescently labeled mosaic virions, which were unimpaired in plaque formation. For the P1 experiments, Edgar and colleagues used chemically modified phages, first derivatized with a biotin-tagged reagent that forms covalent bonds with the free amino groups of lysines and the N-termini of proteins. The biotinylated phages were then labeled with streptavidin-conjugated Quantum dots (Qdots) and used for infections. EM imaging revealed that ~50% of the Qdot labeling occurred on the tails. No quantitative data were provided for the effect of the chemical modification and labeling on the infectivity of the phage. Another difference arises in the infection conditions. We incubated phages and cells at 30°C for 30 min to allow the adsorption and viral injection. In Edgar *et al.*, no specific details are provided for the P1 infection conditions other than that they were identical to those used for the lambda experiments. This indicates that adsorptions were done with fresh logarithmically grown cells at room temperature for 5 min, after which the cells were pelleted at 2,300 ×g and resuspended in phosphate buffer. For imaging, we transferred the infected cells directly to a 1.5%

agarose slab (~1 mm thick). After 1 min, a coverslip was gently overlaid, and the sample was imaged under the fluorescence microscope at 30°C^{129,132}. Edgar *et al.* transferred the buffer-suspended cells to a coverslip coated with poly-L-lysine. None of these differences seem obviously relevant to the divergent findings. However, on balance the most striking difference is the centrifugation step featured in the protocol used by Edgar *et al.* P1 is a large myophage with multiple moving parts; as such it may be susceptible to shearing forces in its cell-adsorbed state, with its six tail fibers deployed and attached to surface receptors, especially after chemical cross-linking and Qdot decoration. In >2,000 ×g centrifugal fields, shearing forces may not be equally transmitted to virions adsorbed to the poles and lateral surfaces. In our experiments, even the gentlest treatment of infected cells, completely avoiding centrifugal pelleting and resuspension, still results in a significant percentage of “dark” infections, where the labeled virion has been lost but the infection still proceeds^{129,132}. Other factors may include the kinetics of adsorption and the absence of divalent cation supplementation in the protocols reported by Edgar *et al.* In any case, resolution of these conflicting results might be most easily achieved by real time monitoring of virion attachment using a microfluidic system that does not require specially coated surfaces for cell attachment or a washing step involving centrifugal separation.

Recognizing different outer membrane receptors for adsorption has important evolutionary meaning to bacteriophages as it defines the host range specificity and determines the infection efficiency. Utilization of LPS as the receptor acquired by phage P1 might give it the property of adsorbing at any locations along the bacterial cell

surface and guarantees a high probability of successful infection upon various host strains. In contrast, several lines of research demonstrated that phage lambda prefers to adsorb to the cell poles and the failed infection at cell poles was lower^{127,129,203}. These different spatial behaviors of P1 and lambda might reflect different infection strategies used by phages.

Methods

Media

LB broth contained per liter of distilled H₂O, 10 g Bacto tryptone, 5 g Bacto yeast extract and 5 g NaCl, and was adjusted to pH about 7.5 with NaOH. Derivative media were supplemented with the following: LBM, 10mM MgSO₄, used for generating crude lysates and in agarose slabs for single-cell microscopy; LB plate, 1.5% agar; LBCM plates, 1.5% Bacto agar and 12.5 µg mL⁻¹ chloramphenicol. SM buffer (50 mM Tris-HCl pH 7.5, 100 mM NaCl, 8 mM MgSO₄) was used as a phage storage buffer. NZYM was used for phage titration, supplemented with 1.5% or 0.7% Bacto agar for plates and top agar, respectively.

Bacterial Strains, Phages, Plasmids and Primers

Bacterial strains, phages, plasmids and primers used are described in Table 2.1 and Table 2.2.

In-frame deletion of *cin* in P1Cm *cI-100*

P1Cm was derived from P1*kc* that obtained chloramphenicol resistance from the R-factor R₁₄. Hereafter, P1Cm *cI-100* is a thermoinducible mutant of P1Cm⁵⁶. We used the lambda red recombination method²¹⁴ to recombine the *Frt-Kan^R-Frt* sequence at *cin*

locus in the P1 genomic DNA. The *Frt-Kan^R-Frt* resistance cassette (consisting of the kanamycin resistance gene and its promoter flanked by the two flippase recognition target (FRT) sequences) was amplified from pKD4 (primer 1 and 2) with ~50 nt appended homolog regions beside gene *cin*, and transformed into KL463 lysogen with pKD46 via electroporation. Each electroporation reaction contained 100 ng purified DNA and 100 μ l competent cells in a 0.2 cm cuvette and was transferred in a Bio-Rad MicroPulserTM electroporator. Cells were recovered in 1 ml SOC solution for 1-2 hours at 30°C and plated on LB CM (12.5 μ g/ml) Kan (30 μ g/ml) plates at 30°C overnight. Then CM^R and Kan^R colonies were selected and verified by PCR.

Construction of gp23-mTurquoise2 expression plasmid

We constructed the plasmid containing the P1 gene23 without a stop codon, a 45bp linker sequence and mTurquoise2 under the control of an IPTG inducible promoter PLlacO-1. We inserted the gene23-linker (primer 3 and 4) and mTurquoise2 (primer 5 and 6) into pZE12luc with NcoI, SphI and AvrII, and then transferred the whole fragment from PLlacO-1 to mTurquoise2 (primer 7 and 8) into pACYC177 at the sites of HindIII and XhoI to maintain the ampicillin resistance. In order to achieve a uniform IPTG induction, pLZ1903 was transformed into the MG1655 lacIq lacY- strain for gp23-mTurquoise2 expression.

Construction of lytic reporter plasmid

The late promoter LP23 can only be activated by the phage late gene activator Lpa when entering the lytic pathway during P1 infection¹². The lytic reporter plasmid contains *gene23-linker-mTurquosie2* downstream of LP23 between AatII and PstI

(primer 4, 5, 9, and 10) in pBR322, which can indicate both the cell fate and the localization of newly produced phages. We transformed pLZ1915 into MG1655 or other strains acting as the host cell during single-cell infection assays.

Transcriptional labeling of *cI* on the P1 genome

Gene *cI* and RBS-*mVenus* (gBlock) was ligated into pZE12luc at NcoI, SphI and AvrII. A *Kan^R* cassette (primer 11 and 12) was inserted at AvrII (pLZ1883). DNA sequence *cI*-RBS-*mVenus*-*Kan^R* was amplified from pLZ1883 (primer 13 and 14) with ~50 nt appended homolog regions beside gene *cI*, and transformed into LZ1856 lysogen with pKD46 under electroporation. We performed the electroporation reaction as described above. Cells were recovered in 1 ml SOC solution for 1-2 hours at 30°C and plated on LB CM (12.5 µg/ml) Kan (30 µg/ml) at 30°C overnight. Then CM^R and Kan^R colonies were selected and verified by PCR. These lysogens were then induced as described later and *cI*-labeled phages were lysogenized into MG1655 for maintenance.

Table II.1 Bacterial Strains, Phages and Plasmids used in this work.

| Strain # | Genotype | Comments | Source |
|----------------|---|---|----------------------|
| MG1655 | F-, <i>lambda</i> , <i>rph-1</i> | Wild type <i>E. coli</i> ; indicator strain of phage titration and lysogenization in bulk | Lab stock |
| KL463 | F-, <i>lacZ105</i> (Am), <i>relA1</i> , <i>rpsL221</i> (strR), <i>thiE1</i> , P1Cm, <i>cI-100</i> (ts) | Original phage stock | Gift from Jason Gill |
| LZ1387 | MG1655 <i>seqA-mKate2</i> , <i>Cm^R-Frt</i> , Δ <i>dam::Kan^R</i> | Strain with SeqA reporter, <i>dam</i> deletion | ref. ¹³² |
| LZ1914 | MG1655 <i>lacIq</i> , <i>lacY</i> , P1Cm, <i>cI-100</i> Δ <i>cin</i> , <i>cI-RBS-mVenus-Kan^R</i> [pACYC177 P _L lacO-1- <i>gene23-mTurquoise2</i>] | Strain to produce gp23- <i>mTurquoise2</i> <i>cI</i> -labeled phages | This work |
| LZ1915 | MG1655 [pBR322 LP23- <i>gene23-mTurquoise2</i>] | Host strain with lytic reporter plasmid for single-cell infection movies | This work |
| Phage | | | |
| P1KL463 | P1Cm, <i>cI-100</i> | Wild type phage | This work |
| P1LZ185 6 | P1Cm, <i>cI-100</i> , Δ <i>cin</i> | Phage with fixed tail fibers | This work |
| P1LZ186 2 | P1Cm, <i>cI-100</i> , Δ <i>cin</i> | gp23- <i>mTurquoise2</i> mosaic phage | This work |
| P1LZ191 4 | P1Cm, <i>cI-100</i> , Δ <i>cin</i> , <i>cI-RBS-mVenus-Kan^R</i> | gp23- <i>mTurquoise2</i> <i>cI</i> -labeled phage | This work |
| Plasmid | | | |
| pLZ1903 | pACYC177 P _L lacO-1- <i>gene23-mTurquoise2</i> | Provides fluorescently labeled gp23 during lysogen induction to form fluorescent phages | This work |
| pCP20 | | Temperature sensitive plasmid which recombines flanking FRT sites to remove DNA inserts | Gift from Jason Gill |
| pKD4 | | PCR template of <i>Frt-Kan^R-Frt</i> fragment | Gift from Jason Gill |
| pKD46 | | Temperature sensitive plasmid which inserts DNA using homologous recombination | Gift from Jason Gill |
| pLZ1883 | pZE12luc <i>cI-RBS-mVenus-Kan^R</i> | For <i>cI</i> labeling | This work |
| pLZ1915 | pBR322 LP23- <i>gene23-Turquoise2</i> | Lytic reporter plasmid | This work |

Table II.2 Primers (5' – 3') used in this work.

| Primer | Sequence |
|---------------|---|
| 1 | GTGATTTCCACACATACTGGTTTTTGTTAATTA AAAATCCGCAGCT TGCTAGTGTAGGCTGGAGCTGCTTC |
| 2 | GGGATCTTTTCACCGCTGGTACCGAGTTCTCTTAAACCAAGGTTT AGGATACATGGGAATTAGCCATGGTCC |
| 3 | ACTGCCATGGAGTTGAGTAACTTACGCGAATACCAGAATCGTAT TGC |
| 4 | CATGGCATGCAGTGCCACCAGAACCTCCACC ACTTCCTCCGCCA GAACCGAGACCCTCAGAGTCACCGGCATCAATCGTG |
| 5 | ACTGGCATGCATGGTGAGCAAGGGCGAGGAG |
| 6 | TAGCCCTAGGTTACTTGTACAGCTCGTCCATGCCG |
| 7 | CCTGAAGCTTAATTGTGAGCGGATAACAATTGACATTGTG |
| 8 | TCGTCTCGAGTTACTTGTACAGCTCGTCCATGCC |
| 9 | AGTCGACGTCTGCGCTTGATAACAAAGGAAGCC |
| 10 | AGTCCTGCAGTTACTTGTACAGCTCGTCCATGCC |
| 11 | AGTCCCTAGGGTGTAGGCTGGAGCTGCTTC |
| 12 | AGTCCCTAGGACATGGGAATTAGCCATGGTCC |
| 13 | AGCCGCAAACTAAGAAGGGG |
| 14 | AAGCTCTGGCATGGCTTAATGAATAACTCATTAACCATGCCGGA TGGA AACATGGGAATTAGCCATGGTCC |

Bacteriophage Assays

Production of phage lysates

Phage lysates were produced by thermal induction of phage lysogens. Briefly, a single colony of desired lysogen was grown in 1 ml LB with appropriate antibiotics overnight at 30°C. The overnight culture was diluted for 100-fold in LBM and grown at 30°C until OD₆₀₀ ~0.5. P1 or a P1 mutant was thermally induced by shifting the culture to 42°C in the shaking water bath (180 rpm) for 30 min. Then, the culture was shaken at 37°C, 180 rpm, for 1 hour till OD₆₀₀ ~0.1. We collected the lysate in a centrifuge tube and mixed with chloroform (2%) for about 15 min at room temperature (RT) for thorough lysis. The lysate was centrifuged at 10,000 ×g for 10 min at 4°C and sterilized by the passage of the supernatant through a 0.2 µm filter (VWR International Cat. No. 28145-477). The gp23-mTurquoise2 phages were obtained by inducing the lysogen (LZ1914). During the lysogen growth, add IPTG with the final concentration of 0.075 mM when OD₆₀₀ approaching 0.1, to provide a proper amount of gp23-mTurquoise2 for mosaic phage assembly.

Phage titration assay

Our protocol was based on previous assays^{17,49,215} with some modifications. An overnight culture of indicator strain MG1655 was diluted 100-fold in LBM and grown at 37°C to OD₆₀₀ ~0.4. Next, we kept the cell culture on ice and added CaCl₂ of 5 mM. The phage stock was diluted in SM buffer to an estimated 10³-10⁴ pfu/ml (plaque forming units per milliliter). We incubated 100 µl of the diluted phages with 300 µl of host solution for 20 min at RT. The phage-cell mixture was then added into 4 ml of 50°C

molten NZYM top agar and plated on pre-dried NZYM agar plates. The plates were allowed to set for 10 min at RT and incubated overnight at 42°C. The titer was determined as the ratio of plaques appearing and the dilution factor.

Phage purification by ultracentrifugation

The crude lysate, obtained from the thermal induction in 500 ml LBM as described above, was centrifuged in a Sorvall GSA rotor at 10,000 rpm for 20 min, 4°C. The supernatant was transferred into a new bottle. After incubating with 1 µg/ml DNase and 1 µg/ml RNase for 1-2 hours at RT, the lysate was concentrated by overnight centrifuge (~16 hours) in the Sorvall GSA rotor at 10,000 rpm, 4°C. We soaked the resulting phage pellet in 2 ml cold SM buffer and extracted the phage solution after a 48-hour incubation. Phages were then purified by equilibrium centrifugation in 1.40-1.45 g/ml cesium chloride using the Beckman 70.1Ti rotor at 45,000 rpm for 24-26 hours, 4°C. The phage band (Fig. II.14) was extracted with 18-gauge needles and dialyzed against SM buffer in Slide-A-Lyzer 3500 MWCO dialysis cassettes (Thermo Scientific).

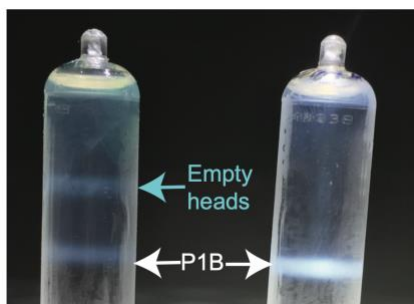


Figure II.14 Phage bands after ultracentrifugation through CsCl equilibrium gradients.

White arrows point to the P1 phage bands of normal size particles for both gp23-mTurquoise2 phages (P1LZ1914, left) and WT phages (P1KL643, right). The gp23-mTurquoise2 phage tube (left) shows another band (cyan arrow) above is presumably the empty capsids.

Bulk lysogenization-probability assay

We measured the lysogenization probability as a function of the MOI. An overnight culture of MG1655 was grown in LB at 37°C. Cells were diluted 1000-fold into LBM and grown at 37°C to OD₆₀₀ ~0.4, chilled, and CaCl₂ was added to a final concentration of 5 mM. Then 100 µl of the cell was added to 100 µl of phage solutions with different concentrations. After a 30 min-incubation at 30°C, we transferred 20 µl of the mixture into 980 µl ice-cold LB or SM buffer to stop the adsorption process. Aliquots in LB media were plated on LBCM plates and incubated overnight at 30°C. Lysogen concentrations were determined by counting the number of CM^R colonies. To examine the concentration of non-adsorbed phages, we centrifuged down the aliquots in SM buffer and titrated the supernatant on MG1655. Pre-infection phage and bacteria concentrations were measured using plate assays as well. The lysogenization probability of all cells or of the infected cells (determined from the MOI using the Poisson distribution with cumulative probability ≥ 1) was plotted as a function of the MOI on a log-log scale.

Bulk phage adsorption assay

The adsorption of P1 was determined by measuring the non-adsorbed phages during phage-cell incubation. An overnight culture of MG1655 was grown in LB at 37°C. Cells were diluted for 100-fold into LBM and grown at 37°C to OD₆₀₀ ~0.4, chilled, and CaCl₂ was added to certain final concentration. 100 µl cells were mixed with 100 µl phages. We transferred 20 µl mixture into seven 1.5 ml centrifuge tubes for different time-point observations. At certain time points of the 30°C incubation, we

added 980 μ l ice-cold SM buffer into one of the tubes, to stop the adsorption. All tubes were centrifuged for 2 min at maximal speed and 200 μ l of the supernatant were taken to test the concentration of the non-adsorbed P1. The adsorption rate was calculated by one minus the ratio between non-adsorbed phages and pre-infected phages.

Single-cell Infection Assay

DNA injection on SeqA-mKate2 strain

An overnight of LZ1387 was diluted for 100-fold in LBM and grown to OD_{600} ~0.4, then $CaCl_2$ was added to 5 mM. Purified P1LZ1856 phages were mixed with the cell to reach an MOI around 1, followed by incubation for 5 min at RT to allow some adsorption. 1 μ l of the sample was placed on 1 mm 0.15% LB agarose pad resting on a small coverslip (18 x 18 mm, Fisher Scientific). After 1 min, a large coverslip (24 x 50 mm, Fisher Scientific) was gently overlaid and the sample was imaged under the microscope at 30°C.

For the DNA injection movies, 3 z-stacks at spacing of 300 nm were taken in the DNA reporter channel throughout the whole movie to track the DNA focus. Cells were imaged at multiple stage positions (typically 12) in phase contrast (100 ms exposure for cell recognition) and Far Red (100 ms exposure for SeqA-mKate2 foci) channels at time intervals of 5 min for 3 hours in total. The movies recorded the processes for the DNA injection as foci appeared in the infected cells. Some of the infection events happened before imaging, as we could observe that some cells formed a fluorescent focus at 0 min (42 out of 253 DNA foci).

Decision-making examination

An overnight of LZ1915 was diluted for 100-fold in LBM and grown to $OD_{600} \sim 0.4$, then $CaCl_2$ was added to 5 mM. Purified P1LZ1914 phages were mixed with the cell to reach an MOI of 0.1-7, followed by incubation for 30 min at 30°C to trigger both phage adsorption and viral DNA injection. 1 μ l of the sample was placed on 1 mm 1.5% LB agarose pad resting on a small coverslip (18 x 18 mm, Fisher Scientific). After 1-2 min, a large coverslip (24 x 50 mm, Fisher Scientific) was gently overlaid and the sample was imaged under the microscope at 30°C.

To localize all phages surrounding the cells, a series of 7 z-axis images at spacing of 300 nm were taken through the CFP channel using a 500 ms exposure for each. Cells were imaged at multiple stage positions (typically 16) in each experiment. During the time-lapse movie, the sample was imaged in phase contrast (100 ms exposure for cell recognition), YFP (300 ms exposure for phage C1-mVenus expression), and CFP (100 ms exposure for lytic reporter signal) channels at time intervals of 5 min until cell fate was visible (3 hours in total).

Microscopy Imaging

Imaging was performed on a Nikon Eclipse Ti inverted epifluorescence microscope using a 100x objective (Plan Fluo, NA 1.40, oil immersion) with a 2.5x TV relay lens, within a cage of incubator (InVivo Scientific) at 30°C, and acquired using a cooled EMCCD (electron multiplying charge-couple device) camera (IXON 897, Andor, Belfast, UK). Cells were imaged under the phase-contrast and other fluorescent filter cubes, which were introduced as follows (Xnm, Yex [bandwidth] excitation

filter/dichroic beamsplitter wavelength/Xnm, Yem [bandwidth] emission filter/company, product #): CFP (436nm 20ex/455nm/480nm, 40em/Nikon, 96361), YFP (539nm, 21ex/556nm/576nm, 31em/Chroma, 49309), Far red (592nm, 21ex/610nm/630nm, 30em/Chroma, 49310).

When presenting microscopy images in our figures and movies, uniform contrast settings are applied for each separate channel throughout the entire figure subpanels or movie, unless otherwise stated.

Data Analysis

DNA packaging efficiency

We stained the phage with DAPI to examine the labeling efficiency of fluorescent phages. 10 μ l of purified phage solution (10^9 - 10^{10} pfu/ml) was incubated with 10 μ l of DAPI (10 μ g/ml) at RT for 10 min. We applied 1 μ l of the mixture for imaging under the fluorescence microscope with 5 z-axis slices taken at intervals, using 300 ms exposure in the CFP and DAPI channels. Typical images were seen in Figure II.2C. The images were analyzed using MATLAB scripts for fluorescent foci counts and intensity plot.

Phage localization on cell surface

To determine if there is a localization preference of phage P1 adsorption on *E. coli* cell surface, we measured the cell length (l) and the distance of the adsorbed phage towards one of cell poles (d). We calculated relative positions as the absolute number of $1-2d/l$, as a consequence that the mid-cell was 0 and cell poles were 1. The data were

sorted into 6 groups depending on different phage positions and plotted in bar graphs showing the percentage of each group (Fig. II.3B and C).

Analysis of injected DNA

Microscope images of the DNA injection were analyzed via a MATLAB-based software package called MicrobeTracker Suite²¹⁶. We first used MicrobeTracker program to outline the cells that had the fluorescent SeqA-mKate2 focus just appeared. Next, we utilized other tools or supporting functions in the suite to determine the profile of the signal along the cell, i.e., used the SpotFinder to detect the fluorescent foci inside cells and displayed the data as the cell length, the time of appearance for the fluorescent foci, the intensity of individual foci and their polarity of localization. All data were saved in comprehensive MATLAB format and processed by homemade MATLAB scripts. We plot the distribution of relative localization of the fluorescent foci along the cell.

Analysis of time-lapse movies

Movie images were analyzed firstly using the cell recognition program Schnitzcell (gift of Michael Elowitz, California Institute of Technology), in order to generate cellular index. The numbers and positions of phages attached on the cell surface, as well as cell lengths were measured manually using the supporting tools of NIS element program. Cell fates and lysis times for each cell was recorded as well. All subsequent data analysis was performed in MATLAB.

Estimating the infection efficiency

We observed that, in some cases, adsorbed phages were seen on the cell surface, but the cell grew normally with neither lysis nor lysogeny detected, similar to phage lambda infection¹²⁹. We define those events as “failed infections.” In our experiments, the rate of failed infection at a given MOA was defined as the number of failed infections divided by total number of infected cells with that MOA. At MOA = 1, the failed infection rate was 16.6% (99 of 596). The rate of failed infection at different phage-attached locations on the cell surface was defined as the number of failed infections at certain cell position divided by total number of infected cells with MOA = 1.

“Dark” infections

Similar to phage lambda infection¹²⁹, a fraction of the cells exhibited dark infections: cells without any observed infecting phages on the cell surface, exhibiting lysis or lysogeny. With careful treatment of the sample, the dark infection rate was ~20% (120 cells at MOA = 0 showing mVenus signal, compared to 596 cells with MOA = 1), which is higher than the unlabeled phage fraction (~5%). The calculation is based on the assumption that dark infections were mainly MOA = 1 events. We hypothesize that these dark infections are mainly due to the phages failing off after injecting their DNA into the host cell. Another possibility is that some cells may divide into two daughter cells during the 30 min incubation, resulting in an infected daughter cell without an observed infecting phage.

Cells exhibiting halted growth

We observed that some cells did not grow during the course of the time-lapse microscopy. The percentage of cells exhibiting halted growth, as a function of the MOA, is plotted in Fig. II.11. For MOA = 0 (i.e., uninfected cells), ~2% of the cells did not grow. At higher MOAs, the percentage of nongrowing cells increased drastically. This is consistent with the observations in the bulk lysogenization experiments that the lysogeny possibility decreases when the MOI is getting higher.

CHAPTER III

INTERACTIONS BETWEEN VIRAL REGULATORY PROTEINS ENSURE A CONSTANT PROBABILITY OF HOST OUTCOME DURING INFECTION

Introduction

Bacteriophages (phages) and phage-like plasmids play a prominent role in the dissemination of adaptive traits that allow for stable colonization and persistence of multidrug resistance in pathogenic bacteria^{1,11,153,168-172,217-220}. A better understanding of their contribution to pathotype spread and adaptation is important. Phage P1 was discovered from a lysogenic strain of *E. coli* about 70 years ago⁴². In terms of the ability to inject its DNA, P1 has the broadest known host range, spanning from a variety of Gram-negative enteric bacteria, e.g., *E. coli*, *Shigella dysenteriae*⁴² and *Salmonella typhimurium*¹⁷³⁻¹⁷⁶, to soil bacteria, including *Pseudomonas aeruginosa*^{176,177}, *Acetobacter suboxydans*¹⁷⁶ and *Myxococcus xanthus*^{80,125}. For *E. coli* as a host, the infection cycle of P1 begins with the adsorption to the cell surface by recognizing the terminal glucose moiety of the lipopolysaccharide (LPS) core region⁴¹. The interaction of at least three of the six tail fibers with receptor molecules is assumed to be sufficient to stimulate the injection process¹⁹. Injected viral DNAs can be protected from host Type I Restriction-Modification (RM) system by phage anti-restriction proteins^{18,49,178}. Following DNA injection, the infected cell enters either the lytic cycle, where progeny phages are produced and the cell lyses, or the lysogenic cycle, in which the phage DNA exists as a low-copy plasmid and replicates autonomously. At the molecular level, the

lysis-lysogeny decision is controlled by the interactions between the components of the regulatory network (Fig. III.1). Briefly, the major repressor of P1, C1, is expressed immediately after phage infection, and binds to 22 operator sequences widely dispersed over the P1 DNA to repress lytic gene expression. For example, C1 controls the expression of RepL that is responsible for vegetative DNA replication and Lpa that activates the late promoter serving viral morphogenesis and lysis genes^{12,221,222}. Coi (*c_one* inactivation) is an anti-repressor binding to C1 to inactivate its function<sup>223-
225</sup>, whereas the corepressor Lxc (*l*owers *e*xpression of *c_l*) increases C1 binding affinity through forming a ternary complex with C1 and operator DNA and inhibits the ability of Coi to dissociate the operator-C1 complex^{74,75,78}. Moreover, the heterodimeric complex of Ant1 and Ant2 proteins also functions as an anti-repressor while the *trans*-acting *c4* RNA represses the synthesis of Ant proteins (Fig. III.1; see more detailed review⁶⁷).

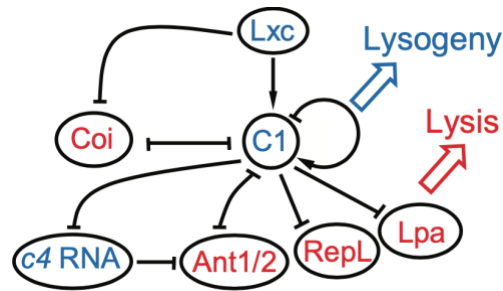


Figure III.1 A schematic of P1 lysis-lysogeny regulatory network.

Blue players contribute to lysogeny development and red players lead to lytic growth. Briefly, the major repressor C1 is expressed immediately after infection and binds to 22 operator sequences across the P1 genome to repress the lytic functions. One of these operators overlaps the promoter expressing *coi*. *Coi* is the major anti-repressor binding to C1 to inactivate its function. *Lxc* serves as a co-repressor that enhances the affinity of C1 to the bound operators and inhibits the ability of *Coi* to dissociate C1-operator complexes. *Ant 1* and *Ant 2* are anti-repressors, and *c4 RNA* represses the synthesis of *Ant* proteins. *RepL* is responsible for vegetative DNA replication and *Lpa* activates the late promoter in the lytic development.

Some studies suggest that the initial choice between lysis and lysogeny relies on the relative synthesis rate of the main competing pair, C1 and Coi^{12} , but no quantitative evidence has been available to determine the relationship between this competition and the final lysis-lysogeny decision. In addition, the benefits for P1 acquiring different regulatory components besides the major competing pair are not clear. Regrettably, the studies of P1 regulatory circuitry halted prematurely with the death of its prime mover, Heinz Schuster^{67,74,78,224-228}. Further, the interest in P1 was reduced since it does not contain cargo genes of clinical interest (e.g., stress resistance and nutrient acquisition) and, being a temperate phage, P1 has been not considered for antibacterial therapeutic applications (phage therapy). However, recent advances in sequencing technologies have allowed the identification of numerous P1 phage-like plasmids in bacteria and human pathogens^{168-172,217,220}, suggesting their capabilities to serve as specific vehicles for the spread and the maintenance of virulence and antimicrobial resistance in both clinical and livestock production settings^{11,171}. For example, pTZ20_1P, isolated from a porcine commensal *E. coli* and carrying multiple antibiotic resistance markers, was able to lysogenize a commensal *E. coli* strain with consequent transfer of resistance¹⁷¹. Moreover, the sequencing data showed that genes contributing to the lysogeny establishment were greatly similar to the genes of the regulatory network of P1¹⁷¹. Therefore, a thorough study of P1 life cycle and mechanism of its lysogeny establishment is important to understand the phage-driven antimicrobial resistance emergence and pathogen adaptation, which will benefit the development of novel therapeutic methods.

Studies of other temperate phages revealed that the lysis-lysogeny decision is highly dependent on the environmental conditions by detecting the host availability, or the virus-cell ratio. For phage λ , one of the simplest paradigms for cell-fate decision-making, the probability of lysogeny increases with multiplicity of infection (MOI, the number of phages infecting a cell) and approaches 100% when MOI is sufficiently large^{129,229,230}. Upon infection of the *Vibrio* phage 882, a quorum sensing factor expressed from the host cell is utilized to make the lysis-lysogeny decision^{231,232}. Moreover, during infection, some *Bacillus* phages produce a 6 amino acid peptide, designated as arbitrium that accumulates in the medium. In turn, high levels of arbitrium cause subsequent phage infections to bias towards lysogeny^{233,234}. These and other strategies are used by the phages to determine whether there are enough host cells for the infection by progeny phages, ensuring a high efficiency of genome propagation. By contrast, phage P1 has been reported lacking the sensitivity to the virus-cell ratio. Previous studies by G. Bertani¹³⁰ and J. Rosner⁵⁶ at the bulk level showed constant probabilities of lysogeny regardless of MOI: 80-90% of *S. dysenteriae* cells were lysogenized at 20°C when infected by the P1 strain isolated originally from the lysogenic *E. coli* Li⁴²; ~30% of the *E. coli* cells were lysogenized at 30°C by the thermoinducible P1 strain (P1CMcI-100)⁵⁶. The constant probability of lysogeny irrespective of host availability, together with P1's ability for prophage maintenance, such as Type III RM¹⁷⁹⁻¹⁸¹, autonomous replication^{79,182} and toxin-antitoxin systems^{183,184}, may suggest that for P1 there is a fitness advantage to propagate its genomic information as a

plasmid. The ability to establishment and maintenance as plasmid can be beneficial to the dissemination of the cargo genes carried by P1 or P1 phage-like elements.

In this work, we set out to examine the infection process of phage P1 at the level of individual phage and cell with a spatiotemporal resolution, sufficient to quantify the relevant subcellular parameters and to evaluate the contribution of each parameter to the observed cell-fate decisions. Using our system, we first investigate the mechanism of P1 MOI-independent lysogenization through linking the regulatory gene expression with cell fate by a simple genetic model. We also find that MOI-dependency can be imposed by increasing the distances between the co-infecting phages. Taken together, our study provides a new decision-making model that expands our understanding of temperate phages. These, in turn, give us insight in how the fitness of different phages end up in distinctive decision-making behaviors and also allow us to evaluate their contributions to pathogenicity development.

Results

The Probability of Lysogeny Is Independent of the Number of Infecting Phages at the Single-Cell Level

In order to study P1 lysogenization at the single-cell level, we constructed a fluorescent reporter system to monitor individual decision-making events under the microscope, as described previously¹²⁸. Briefly, to record the number of phages infecting each *E. coli* cell, P1 virions were labeled by fusing fluorescent proteins to phage capsids. During the time-lapse movies, the lytic pathway was followed through a reporter plasmid expressing mTurquoise2 from the PL23 promoter, which is dependent on the

late gene activator, Lpa; the indicator for the lysogenic pathway was a C1-mVenus fusion protein followed by cell division (Fig. II.9). Using this reporter system, we examined the effect of MOI on the cell fate. In agreement with previous bulk experiments using phage carried chloramphenicol resistance as a readout⁵⁶, our single-cell measurements demonstrated that the probability of lysogeny is constant over different MOIs (Fig. III.2).

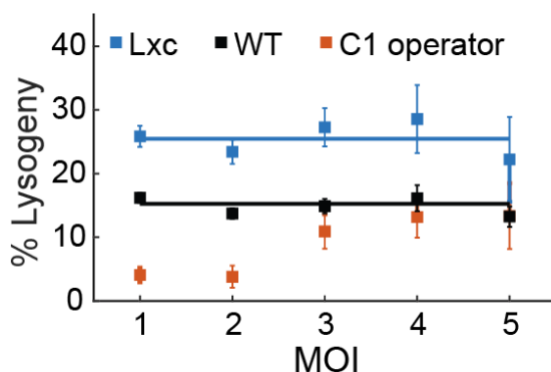


Figure III.2 The probability of lysogeny is independent of the number of infecting phages at the single-cell level.

The probability of lysogeny remains constant over MOI for WT cells at ~14.53% (black, cell sample sizes for MOI 1 to 5 are 457, 277, 168, 62 and 68 respectively) and for Lxc overexpressed cells at ~26.58% (blue, cell sample sizes for MOI 1 to 5 are 295, 132, 55, 38 and 15 respectively). For cells with more C1 operator sequences (red, cell sample sizes for MOI 1 to 5 are 147, 111, 44, 14 and 9 respectively), the probability of lysogeny increases with MOI at lower MOIs and returns to the normal level at MOI > 3. Error bars denote counting errors.

Considering that some proteins encoded by P1, e.g., the superimmunity protein Sim, may act to prevent superinfecting phages injecting their DNAs into the cytoplasm of infected cells^{53,54}, we first tested if all the phages attached on the cell surface were able to inject their DNA. To examine the number of injected DNAs, we utilized our established DNA visualization system by taking advantage of the specific binding of SeqA proteins to the methylated GATC sites^{128,132,206}. In particular, during phage infection, the SeqA-mKate2 fusion proteins constitutively expressed in the methylation deficient host cells (LZ1387, a Δdam variant) bind to the methylated P1 DNA but not the host DNA, allowing us to track the viral DNAs as fluorescent spots. The intensity of SeqA-mKate2 protein (i.e. viral DNA) at the beginning of the phage infection was measured and the injected DNA copy number was calculated based on the single DNA intensity. Meanwhile, as each phage particle was fluorescently labeled by mTurquoise2, we can count the number of phages that attached on the cell surface and predict the injected DNA number based on failed and dark infection frequencies (see details in Methods). We observed a nearly perfect positive correlation between the actual injected DNA number and predicted DNA copy number (Fig. III.3). This indicated the success of multiple infection and the independence of DNA injection process from different phages adsorbing on the same cell.

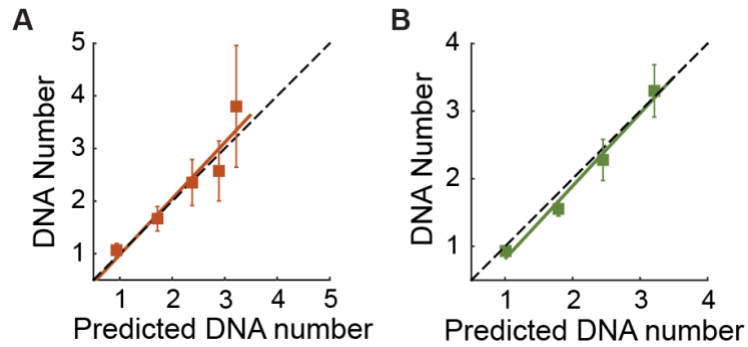


Figure III.3 The injected DNA copy number correlates with prediction very well.

(A) The injected DNA copy number was tested in SeqA-mKate2 DNA virtualization system. Cell sample sizes for MOI 1 to 5 are 83, 33, 17, 14 and 5 respectively. Filled squares: experimental data. Red line: linear fit. Black dashed line: diagonal indicating the ideal positive correlation. Error bars denote standard error of the mean. (B) The injected DNA copy number was tested in *tetO*/TetR-FP DNA virtualization system. Cell sample sizes for MOI 1 to 4 are 144, 65, 16 and 12 respectively. Filled squares: experimental data. Green line: linear fit. Black dashed line: diagonal indicating the ideal positive correlation. Error bars denote standard error of the mean.

Build A Simple Genetic Model to Elucidate MOI-Independent Decision-Making

To understand the underlying mechanism of this MOI-independent cell lysogeny, we sought a minimal genetic model based upon the regulatory network of P1 (Fig. III.1). Given the central role of the major repressor, we hypothesized that C1 activity is a cell-fate deterministic factor. Based on the P1 regulatory circuitry, C1 activity can be affected by different parameters, e.g., the expression level of C1 compared with its inhibitor Coi, the level of the corepressor Lxc and the number of intracellular C1 binding sites (22 sites per P1 DNA). We first compared C1 expression level in lytic and lysogenic cells by tracking C1-mVenus intensity using the decision-making reporter system¹²⁸. As expected, cells entering the lysogenic pathway showed higher C1 signal on average than those entering the lytic pathway, though it was not always true for every single cell trajectory (Fig. III.4A). Next, we tested whether the decision-making outcome could be manipulated by varying the intracellular C1 activity. To enhance C1 activity, we overexpressed corepressor Lxc from plasmids in host cells. Indeed, host cells with higher Lxc expression levels exhibit higher probabilities of lysogeny at both the bulk level (Fig. III.4B) and the single-cell level (Fig. III.2). Interestingly, the probability of lysogeny was still independent of MOI (Fig. III.2). On the other hand, to reduce the C1 activity, we introduced more C1 operator DNA sequences from a plasmid (~15 sites per cell) and found a reduction of the lysogeny probability at low MOIs (1 and 2) (Fig. III.2), although not at higher MOIs, where changes of the number of C1 binding sites were relatively low hence showed less effect on C1 function. In summary, these data suggest that C1 activity is a deterministic factor of P1 decision-making.

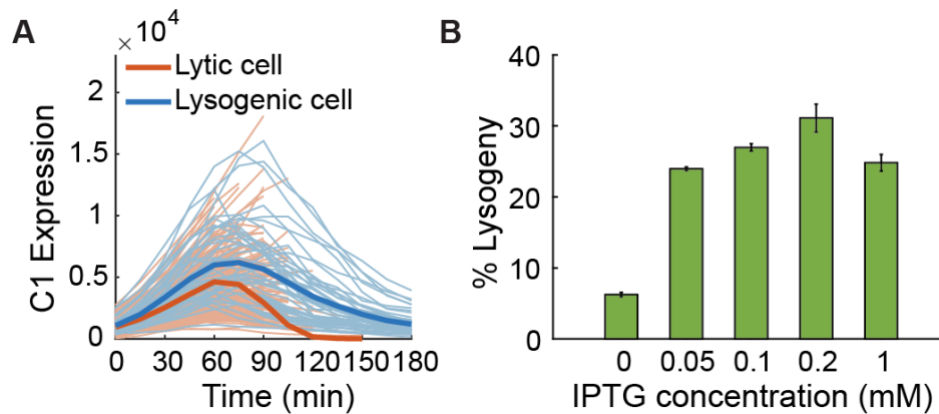


Figure III.4 Influence of C1 activity on P1 lysogenization.

(A) C1-mVenus intensities in lysogenic cells are higher on average than those in lytic cells overtime. Bold line: mean intensities. Light line: C1 expression trajectories of each individual cell. Blue: Lysogenic cells, n = 47. Red: Lytic cells, n = 165. (B) The probability of lysogeny upon the infection of *E. coli* cells with different expression levels of Lxc at the bulk level (MOI = 1), by fluorescent phage P1LZ1914. Lxc is induced with certain concentrations of IPTG from PLacO promoter. The error bars denote counting errors.

We then hypothesized that C1 activity of each infecting phage was constant in cells with different MOIs, which led to the MOI-independent lysogenization. Initially, we defined the total C1 activity in an infected cell as the amount of free C1, i.e., (C1-Coi), based on their antagonized functions, and assumed that the free C1 of each infecting phage, i.e., (C1-Coi)/MOI was a constant. To test this, we compared the gene expression of *c1* and *coi* simultaneously at different bulk MOIs (0.2, 1 and 5), measured by single molecule fluorescence in situ hybridization (smFISH)²³⁵. DNA FISH and qPCR data (Fig. III.5) suggested that viral DNA replication began around 30 min after infection, so we focused on mRNA levels at 20 min and 30 min.

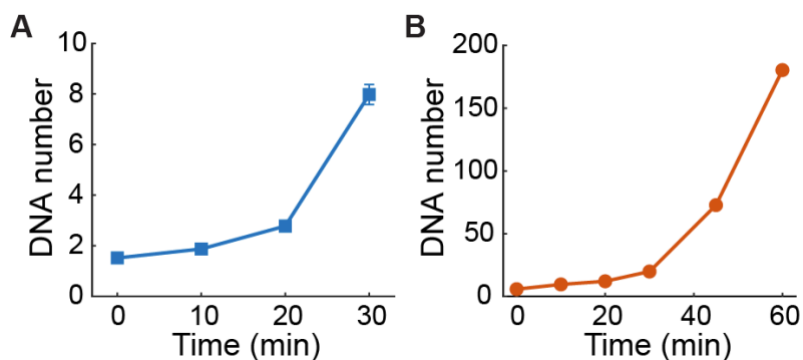


Figure III.5 P1 DNA replication during infection.

(A) Plot of DNA copy number overtime tested using DNA FISH at bulk MOI = 0.2. Error bars denote standard error of the mean. (B) Plot of DNA copy number overtime tested using qPCR at bulk MOI = 1.

Fluorescent probes were designed to target *cI* or *coi* mRNA so that we could quantify them separately (Fig. III.6A and B). According to the Poisson distribution¹²⁸, at bulk MOI of 0.2, 1, and 5, the estimated proportions of infected cells were about 18%, 63% and 99% out of total cells, respectively. From the smFISH experiments, the percentage of infected cells (cells showed *cI* or *coi* signal) were consistent with our predictions (Fig. III.7). However, the level of (*cI-coi*)/MOI decreases against MOIs instead of remaining constant (Fig. III.6C). This suggested that, in order to achieve MOI-independent lysogenization, there would be other components that work together to diminish the effect of MOI. Based on the aforementioned regulated function of Lxc, we decided to define C1 activity considering both (C1-Coi) and Lxc. Since none of the promoters that drive the transcription of *lxc* is under the control of C1 or other factors, we suppose that Lxc is constitutively expressed upon infection and Lxc level is positively correlated with MOI, i.e. $Lxc \propto MOI$. As shown in Fig. III.6D, *lxc* RNA number increased with MOI from smFISH experiments. Together with the observation that (*cI-coi*)/MOI decreased with MOI (Fig. III.6C), our simple model became [(C1-Coi)×Lxc]/MOI which remained constant. To test this, we quantified the mRNA expression of *cI*, *coi* and *lxc* in the same cell during phage infection using smFISH. Indeed, the results showed that [(*cI-coi*)×*lxc*]/MOI was similar at different bulk MOIs (Fig. III.6E). These data support our model for MOI-independent lysogeny and indicated the importance of Lxc for maintaining a set frequency of lysogeny during P1 infection.

To abolish Lxc function in maintaining the probability of cell lysogeny, we overexpressed Lxc, thus Lxc level becomes a constant in all infection events and Coi

activity can be ignored. In this scenario, cell fate should be simply determined by $C1/MOI$. As we expected, cI/MOI remains similar for different MOIs (Fig. III.F) during the infection of the *Lxc*-overexpressed hosts, corresponding to the unchanged probabilities of lysogeny over different MOIs in single-cell tests (Fig. III.2). In summary, $C1$ activity regulating each phage, dependent on the expression level and the interaction between the gene products of *cI*, *coi* and *lxc*, is a constant during infection with different numbers of P1 virions, which results in an MOI-independent lysogenic response.

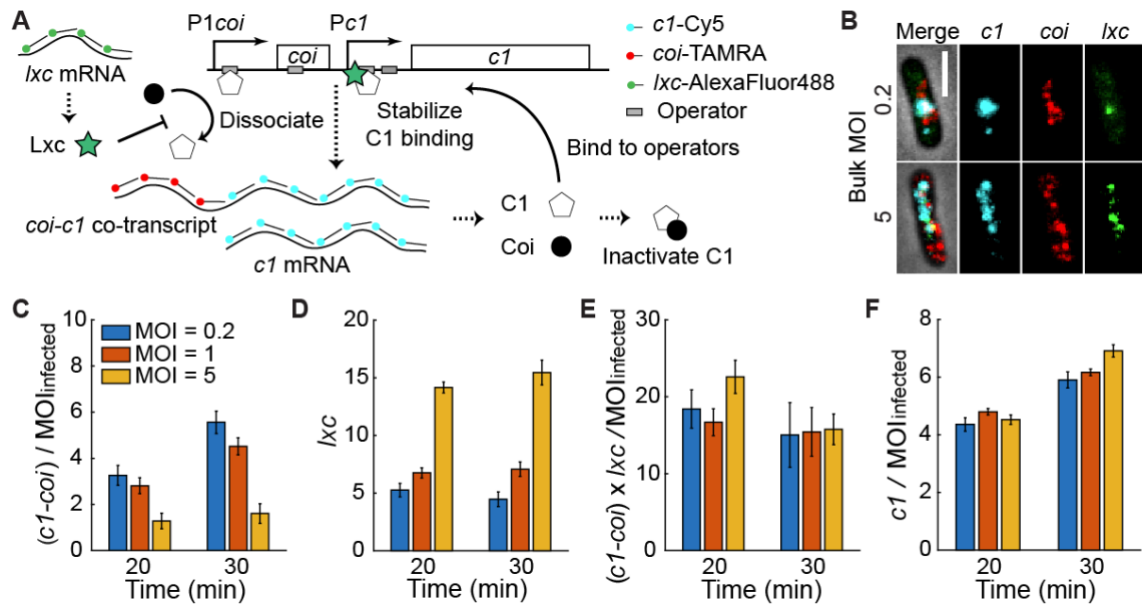


Figure III.6 The interaction of C1, Coi and Lxc leads to MOI-independence of P1 lysogenization.

(A) A schematic of *coi-cl* operon and smFISH method. C1 is expressed from two promoters ($P1_{coi}$ and $P1_{c1}$) while Coi is only expressed from $P1_{coi}$. C1 is able to inhibit both $P1_{coi}$ and $P1_{c1}$ through binding to the adjacent operators. Coi forms a 1:1 complex with C1 to inactivate C1 function. Lxc promotes C1's binding affinity to its operators. (B) Representative images showing mRNA expression at 30 min after infection at bulk MOI = 0.2 (top) and 5 (bottom). Cyan: *c1*; Red: *coi*; Green: *lxc*. Scale bar = 2 μ m. (C) $(c1-coi) / MOI_{infected}$ per cell decreases with MOI. (D) *lxc* level per cell increases with MOI. (E) C1 activity depends on $[(C1-Coi) \times Lxc] / MOI$. $[(c1-coi) \times lxc] / MOI_{infected}$ is similar at different MOIs. (F) In Lxc overexpressed host cells, C1 activity depends on $C1 / MOI$. $c1 / MOI_{infected}$ is similar at different MOIs. In all plots, error bars denote standard error of the mean.

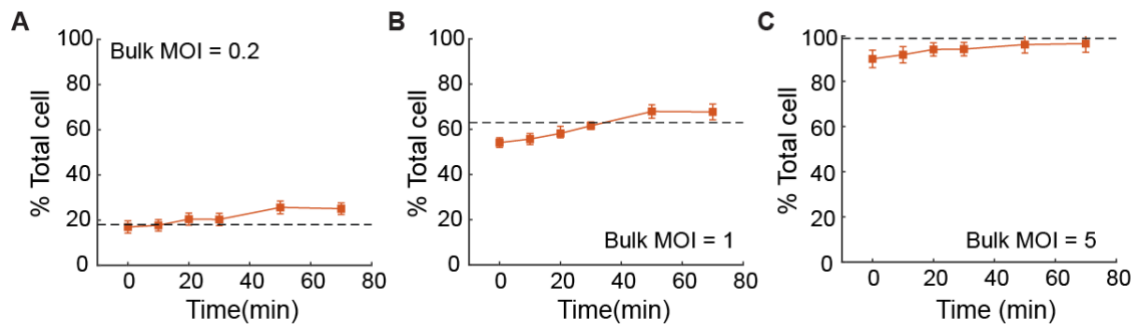


Figure III.7 Percentage of infected cells over total cells using smFISH assay. Black dashed lines are the predicted infection rate 18%, 63% and 99% at bulk MOI of 0.2, 1 and 5 respectively, calculated based on Poisson distribution formula. The error bars denote counting errors.

Imposition of the MOI-Dependency

Recent studies of phage λ showed that the MOI dependence in cell fate was due to the individual lysis-lysogeny decision of each infecting phage, and only unanimous lysogenic decisions by all phages led to cell lysogeny^{129,131,132,134}. In contrast, the MOI independence of P1 lysogenization may imply that the infecting phages make an ensemble decision. To explore this, we examined phage DNA interactions inside the cell using a *tetO*/TetR-FP DNA visualization system^{131,236}. Basically, we replaced *darB*^{17,49}, a gene nonessential for P1 decision-making, with 120 \times *tetO* sequences in the phage DNA. Upon infecting the host cell harboring a plasmid constitutively expressing TetR-mNeonGreen, all injected and replicated phage DNAs are bound and labeled at *tetO* sites by fluorescent TetR-mNeonGreen proteins, forming foci or clusters (Fig. III.8A and B). During the infection process, some interesting DNA behaviors were detected (Fig. III.8A): (1) one of phage DNAs replicates faster than the other resulting in an unsynchronized pattern; (2) phage DNAs physically moved together; and (3) viral DNAs located at different cell areas showed synchronized replication patterns. Asymmetric levels of DNA replication might be due to the uneven distribution of intracellular machineries, suggesting that phages making decisions individually, defined as individual DNA behavior. In contrast, DNAs that move together and show synchronized replication pattern would indicate that the infecting phages shared regulatory products to regulate each other and made decisions as one, i.e., non-individual behaviors (Fig. III.8C and Fig. III.9A).

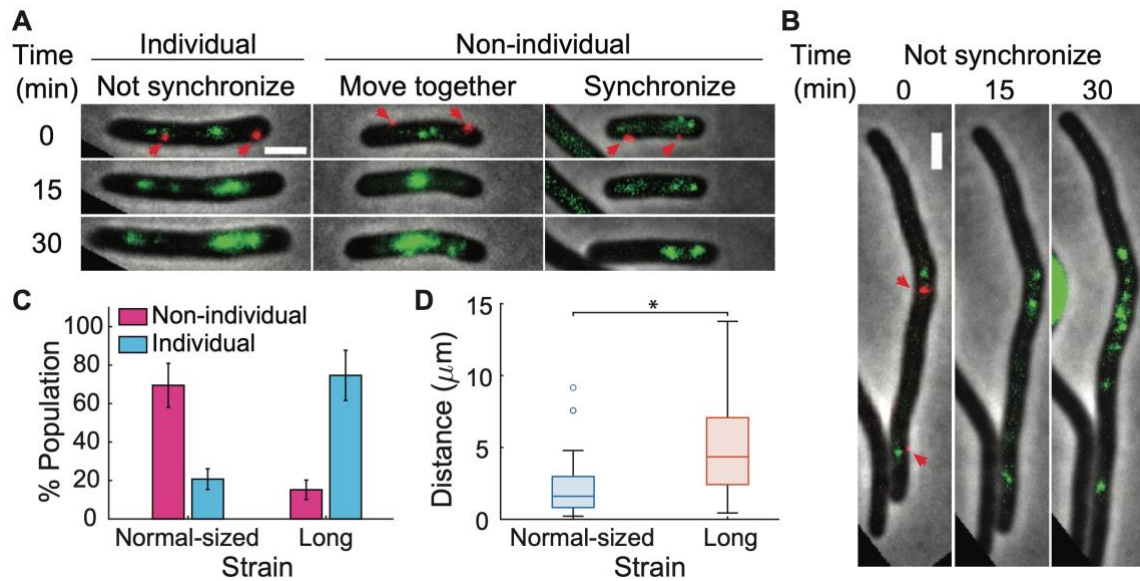


Figure III.8 P1 virions infecting the same host cell make an ensemble lysis-lysogeny decision.

(A) Representative images showing phage DNA behaviors in normal-sized *E. coli* cells with MOI = 2 (Green signals represent TetR-mNeonGreen bound phage DNAs): (1) One of phage DNAs replicates faster than the other resulting in an unsynchronized pattern; (2) Phage DNAs physically moved together; and (3) Viral DNAs located at different cell areas showed synchronized replication patterns. Red arrows point out infecting phages located on the cell surface at 0 min. (B) Representative images showing unsynchronized phage DNA behaviors in long cells with λ Kil expression (MOI = 2). Scale bar = 2 μ m. (C) Bar plot shows that more non-individual DNA behaviors in normal-sized cells (n = 82) versus more individual phage DNA behaviors in long cells (n = 79). The error bars denote counting errors. (D) Box plot of the distance between co-infecting phages on the surface of long cells (red, n = 121) is much larger than that in normal-sized cells (blue, n = 113) at MOI = 2. *p < 0.001 as determined by Student's t test.

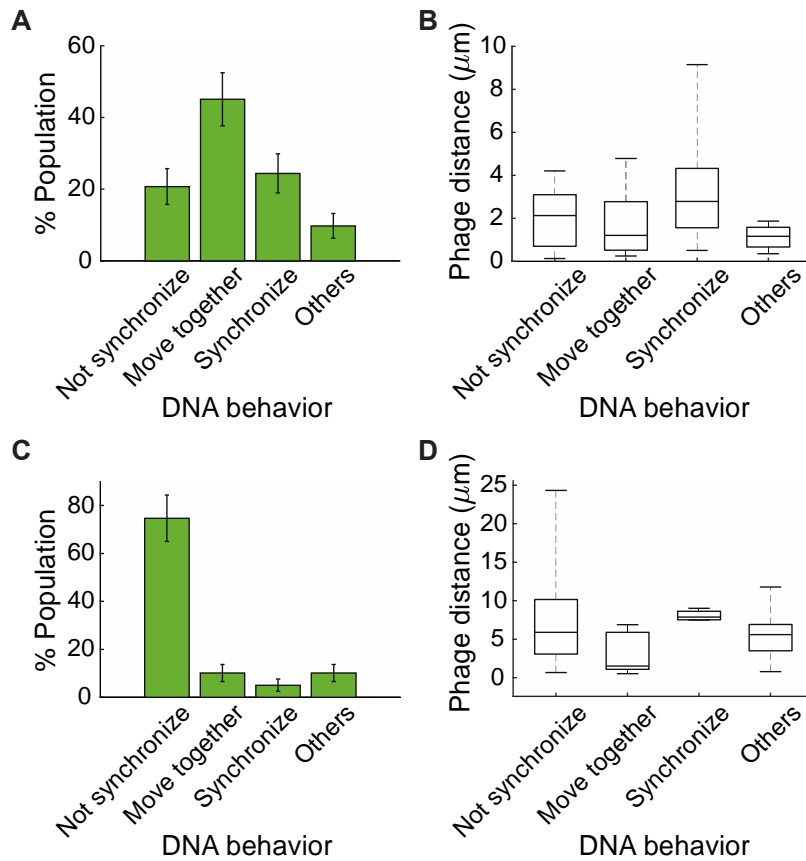


Figure III.9 P1 DNA behaviors during infection on different host strains.

(A and C) Probability of cells with different DNA behaviors tested in normal-sized and long cells (See also Fig. III.8). Error bars denote counting error. (B and D) Distance between phages on normal-sized and long cells at MOI = 2. Others indicate the cell with only one phage DNA spot at 0 min probably due to failed infection.

To test whether we could suppress this ensemble behavior, we increased the distances of phages by infecting a much longer cell (Fig. III.10A and B). Increased cell length was achieved by expressing the Kil protein of phage λ from a plasmid; Kil inhibits *E. coli* cell division, causing cells to grow into long filaments^{237,238}. For simplicity, we only analyzed the infected cells at an MOI of 2. We supposed that the larger distance between infecting phages (Fig. III.8D) would inhibit the efficient *trans* regulation and thereby lead to individual decision-making. Using this *tetO*/TetR-mNeonGreen DNA visualization system, we observed more unsynchronized DNA replications during the infection of long filamentous cells, suggesting a higher level of the individuality of co-infecting phages (Fig. III.8C and III.9C). Next, we tested P1 lysogenic response in long cells. In both bulk and single-cell experiments, the probability of cells undergoing lysogeny increased with MOI instead of being a constant value (Fig. III.10C and D, Fig. III.11). In summary, these data indicate that infecting P1 phages are more likely to make the ensemble decision and lead to MOI-independent lysogenization when they can efficiently regulate each other in the scenario of normalized cells; on the other hand, phages can make individual decisions and lead to MOI-dependent lysogenic response when the distance between them is large enough to diminish the *trans* regulation.

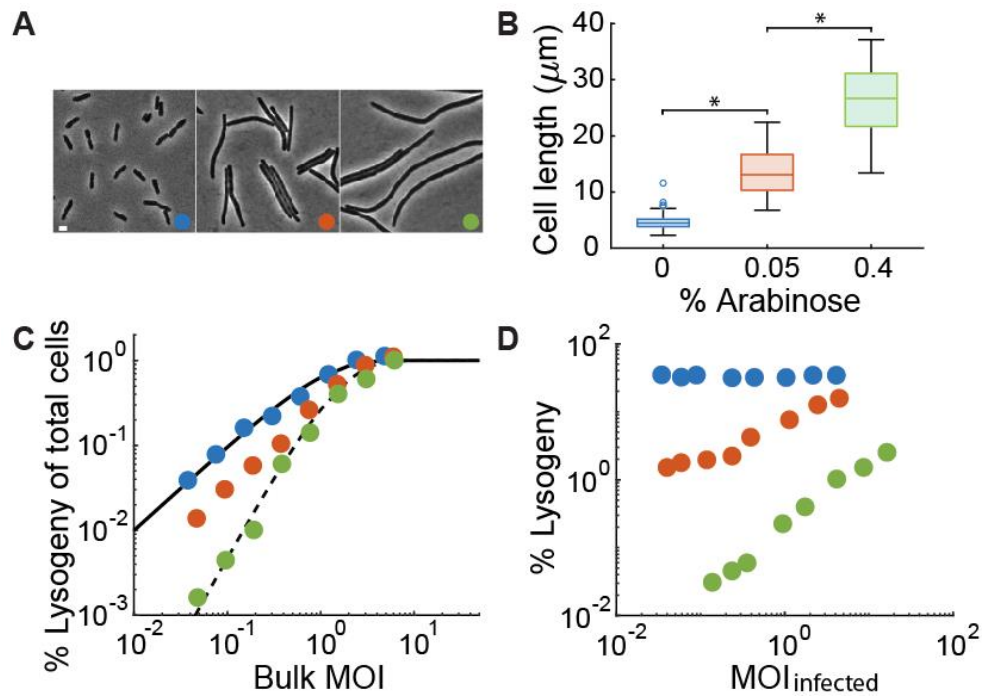


Figure III.10 P1 shows MOI-dependent lysogenization tested at the bulk level.

(A) Representative images for comparison of the cell length between normal-sized and long cells using different concentrations of L-Arabinose for λKil induction. Scale bar = 2 μm . (B) Quantification of cell length from (A). The mean lengths are 4.63 μm ($n = 231$), 13.69 μm ($n = 110$) and $\geq 26.36 \mu\text{m}$ ($n = 37$, some long cells could not be measured since they were larger than the imaging field of frame) for normal-sized and long cells induced with 0.05% and 0.4% L-Arabinose, respectively. * $p < 0.001$ as determined by Student's t test. (C) P1 shows different lysogenic responses in cells with different lengths as function of bulk MOI, which is equal to (total phage/total cell). Data are shifted with the maximum % lysogeny of 100%. In normal-sized host (blue), the probability of P1 lysogeny follows the theoretical prediction of Poisson distribution of $N \geq 1$ (solid black line). In long cells induced cells with 0.4% L-Arabinose (green), the probability of P1 lysogeny follows the theoretical prediction of Poisson distribution of $N \geq 2$ (dashed black line). Probability of P1 lysogeny in long cells induced cells with 0.05% L-Arabinose (red) locates between Poisson distribution of $N \geq 1$ and $N \geq 2$. (D) The probability of lysogeny is calculated based on the number of infected cells. In normal-sized host it shows a constant lysogenic response over $\text{MOI}_{\text{infected}}$, which is (total phages – nonadsorbed phage)/total cell. However, the probability of lysogenization in long cells are relatively lower than in normal-sized cells and increases against $\text{MOI}_{\text{infected}}$, tested at the bulk level.

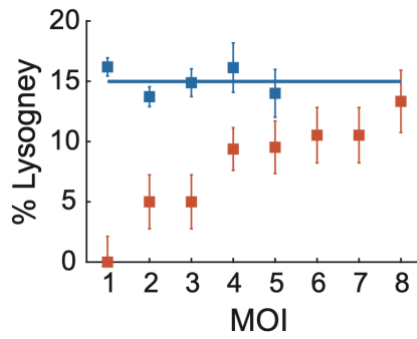


Figure III.11 The MOI-dependent lysogenization is gained by enhancing the distance between infecting phages.

The probability of lysogeny increases with MOI at the single-cell level (orange; cell sample sizes for MOI of 1 to 8 are 22, 20, 20, 32, 21, 19, 19 and 15 respectively). Blue: the probability of lysogeny upon the infection of normal-sized *E. coli* cells (see also in Fig. III.2). Error bars denote counting error.

Discussion

In this work, we investigated the underlying mechanism of how P1 enters its lysogenic state, in terms of its gene regulatory circuitry which is conserved in P1 phage-like plasmids¹⁷¹. By taking advantage of single-cell techniques, we first demonstrated the MOI-independent lysogenic response at the single-cell level (Fig. III.2) and then proposed its mechanism with a simple model: C1 activity of each infecting phage, defined as $[(C1-Coi) \times Lxc] / MOI$, was regulated to be a constant value over different MOIs, resulting in the similar probabilities of lysogeny (Fig. III.12A). Given that *Lxc* has no homologs in phage λ , the function of *Lxc* in maintaining the probability of lysogeny suggests that phage P1 uses a totally different gene regulation at the molecular level to guide its lysis-lysogeny decision. Furthermore, compared with the individuality of phage λ for decision-making^{129,131,132,134}, the independence of MOI for the phage P1 lysogenic response strongly signals that the infecting phages make a group decision. To test this hypothesis, we examined the interaction of injected viral DNAs in normal-sized *E. coli* cells with an MOI of 2 and observed more non-individual DNA behaviors (>80%) than the individual ones. Among these, the cases where the unsynchronized replication of P1 DNAs can be seen as phage individuality, i.e., co-infecting phages make different decisions due to the uneven intracellular environment, e.g., bacterial nucleoid is located in the center of the cytoplasm, leaving the polar regions largely free of DNA, while certain functional proteins, such as osmosensory transporter ProP^{204,239}, and ribosomes²⁰⁴ are enriched at the cell poles. After the individual decision-making of each P1, the decisions by all phages probably integrate into the final cell outcome as

lysis or lysogeny, similar with phage λ . On the other hand, the majority of P1 DNAs exhibited non-individual behaviors as they moved together or showed synchronized replication patterns. In addition, the proportion of non-individuality was supposed to be even higher in the cells with higher MOIs given the increased viral concentration, which results in an overall MOI-independent cell outcome. Furthermore, we found that a large separation among P1 virions infecting the same cell prompted the individual decision-making and in long cells the lysogenic response was changed to be dependent of MOI (Fig. III.12B). The imposed MOI-dependency of P1 lysogeny could be a consequence of the individual decision made by each infecting phage followed by phage voting, similar with the decision-making process of phage λ . However, the association between the levels of phage individuality and different lysogenic responses upon P1 infection is remained to be examined. An alternative assumption is that P1 lysogenization is dependent on the viral protein dosage. As shown in Fig. III.2, at low MOIs (1 and 2), the probability of lysogeny is lower in cells with more C1 binding sites than in WT cells; while at higher MOIs, it returns back to the WT level. This suggests that there is a threshold of operator numbers, compared to C1 concentration, that alters the cell-fate choices. Similarly, the changes of lysogenic response in long cells might be related with the varied gene dosages at different MOIs.

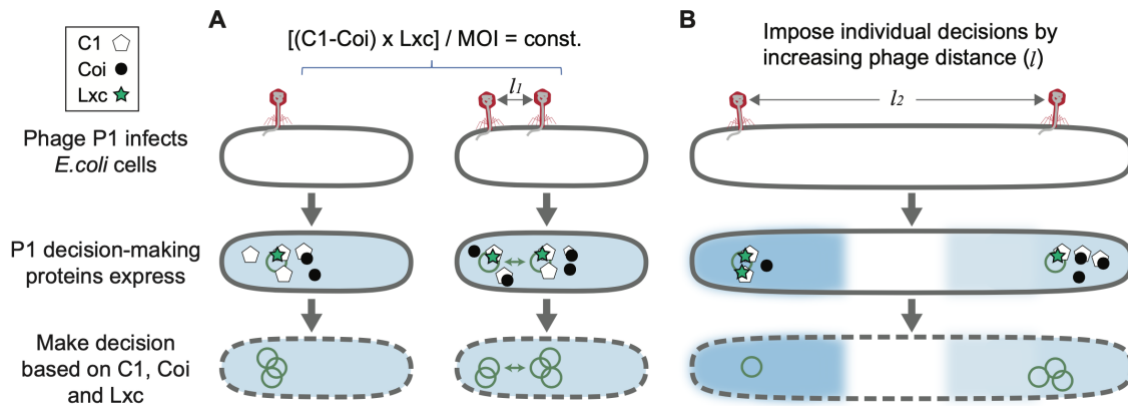


Figure III.12 The model of P1 lysis-lysogeny decision-making mechanism.

(A) The lysis-lysogeny decision-making of P1 is independent of MOI. All infecting phages make a group decision inside the host cell due to the *trans* regulation (green double-sided arrow). The constancy of C1 activity of each phage, $[(C1-Coi) \times Lxc] / MOI$, results in a robust lysogenic response against the number of phages infecting an individual cell. (B) A different lysogenic pattern is imposed by increasing phage distances infecting the same host cell. It suggests individuality of choices between lysis and lysogeny of individual phages that are not able to share regulatory components effectively. Blue intensities indicate C1 activities and darker color evinces higher activity, which is regulated by the expression levels and interactions between C1 (white pentagon), Coi (black circle) and Lxc (green asterisk).

The striking differences between phage P1 and phage λ may suggest distinctive strategies developed by these two phages for efficient genome propagation, which is essential for all organisms to survive in the fluctuating environment. Phage λ can only infect a subclass of *E. coli* strains, perhaps the ultimate ‘specialist’, implying the limited availability of host cells in natural conditions. Additionally, phage λ uses an outer membrane protein LamB as its receptor, which shows helical or ring-like patterns on cell surface¹²⁷, contributing to the preferential adsorption to cellular poles^{129,203}. The use of polar adsorption augments the infection specificity at the cost of a higher rate of failed infection^{128,129}. Thus, the ability to sense the amount of host cells for the infection of progeny phages is important: the injected phage DNA will be replicated and packaged into new progeny viral particles under conditions where host cells are not limiting; whereas viral DNA will stay dormant in the host when not enough host was available. Moreover, the MOI dependency of λ has been found relying on the individuality of each infecting phage, in which co-infecting phages make individual lysis-lysogeny decisions and the host cell integrates these decisions to result in lysis, lysogeny or lyso-lysis²⁴⁰. In contrast, phage P1 can be regarded as a ‘generalist’ with the ability to inject its DNA into a very broad spectrum of Gram-negative hosts. It recognizes evenly distributed LPS molecule as its receptor, leading to the non-specific adsorption to the cell surface¹²⁸. The broad host range and the high probability of successful DNA injection¹²⁸ reduce the need to sense the availability of host bacteria. It may also reflect phage’s real-world experience, in having to deal with diverse cytoplasmic environments where the lytic pathway may be problematical and less attractive in terms of fitness, as for the needs of

different strategies to replicate a large number of viral DNAs; while the establishment of a stable lysogen becomes preferred. Thus, P1 makes the lysis-lysogeny decision regardless of MOI and in general more biased towards lysogeny. Furthermore, during lysogenization, P1 was maintained as a self-replicating plasmid^{79,182}. First, the plasmid format gives P1 prophage more freedom from host cell's control, such as on DNA replication where P1 uses its own origin and replication system¹², and on protein synthesis, considering the effects of the chromosome position on the gene expression profile in bacteria²⁴¹. Second, together with the aforementioned capabilities of plasmid maintenance^{79,179-184} and the separated distribution of genes with related function on the viral genome¹², P1 perhaps evolves directly from an intracellular plasmid through acquiring phage related elements. These suggest a distinct evolutionary lineage of P1 with other temperate phages. In sum, the formation of stable plasmids is probably the priority for phage P1 during infection, and a robust lysogenic response over host availability will help ensure this process. Essentially, the autonomy and constant lysogenization makes P1 an ideal backbone to carry and spread cargo genes during virulence dissemination. On the other hand, the P1 phage particle is more likely to serve for lateral gene transfer between various bacteria strain, which is less essential for P1 propagation.

Methods

Rich Defined Media

Neidhardt EZ Rich Defined medium²⁴² was used for DNA visualization experiments due to its low background and fluorescence. It contained per liter of distilled H₂O, 1× MOPS Mixture (Teknova #M2101), 1.32 mM K₂HPO₄ (Teknova #M2102), 1× ACGU solution (Teknova #M2103) and 1× Supplement EZ (Teknova #M2104). Carbon source was added when starting cell culture.

Bacterial Strains, Phages, Plasmids and Primers

Bacterial strains, phages, plasmids and primers used are described in Table III.2 and Table III.3.

Construction of Lxc expression plasmid

We constructed the plasmids containing the P1 *lxc* gene under the control of an IPTG inducible promoter PLlacO-1. We inserted the *lxc* (primer 1 and 2) into pZE12luc with NcoI and SphI (pLZ1931), and then transferred the whole fragment from PLlacO-1 to *mTurquoise2* (primer 3 and 4) into pACYC177 at the sites of BamHI and PstI to maintain the kanamycin resistance (pLZ1933). In order to achieve a uniform IPTG induction, constructed plasmids were transformed into the MG1655 *lacIq lacY⁻* strain for Lxc expression.

Construction of Lxc expression plasmid

There are 22 C1 binding operators dispersed on the P1 genome. The 17 bp operator consensus sequence is asymmetric and reported in a previous work¹² as ATTGCTCTAATAAATTT. One copy of the consensus operator sequence was designed

in primer 5 and amplified with primer 6 from pACYC177. PCR fragments were ligated into pACYC177 between BamHI and PstI. We transformed the plasmid into MG1655 or other strains acting as the host cell during single-cell infection assays.

Construction of *tetO* phage

The *tetO*-recombination plasmid (pLZ1981) was constructed to replace part of the *darB* region of P1KL1856. Specifically, a 120×*tetO*-KanR array digested from pLAU39²³⁶ (EcoRI and Sall), a homology region (H1) inside *darB* (primer 7 and 8) and a Kanamycin resistance gene (primer 9 and 10) with its promoter were ligated into a pUC19 backbone using Gibson Assembly. Another homologous region (H2) inside *darB* (primer 11 and 12) was then ligated into the assembled plasmid with Sall and HindIII. Next, we used the lambda red recombination method²¹⁴ to recombine the *H1-Kan^R*-120×*tetO-H2* sequence in the P1 genomic DNA. This DNA sequence was digested from pLZ1981 with NdeI and HindIII and transformed into LZ1856 lysogen with pKD46 under electroporation. Each electroporation reaction contained 100 ng purified DNA and 100 μl competent cells in a 0.2 cm cuvette and was transferred in a Bio-Rad MicroPlulserTM electroporator. Cells were recovered in 1 mL SOC solution for 1-2 hours at 30°C and plated on LB CM (12.5 μg mL⁻¹) Kan (30 μg mL⁻¹) plates at 30°C overnight. The genomic construct was then verified by sequencing. P1 240×*tetO* phage was also constructed but had low titer from lysogen induction, probability due to inefficient DNA replication during single infection (Fig. III.13 and Table III.1).

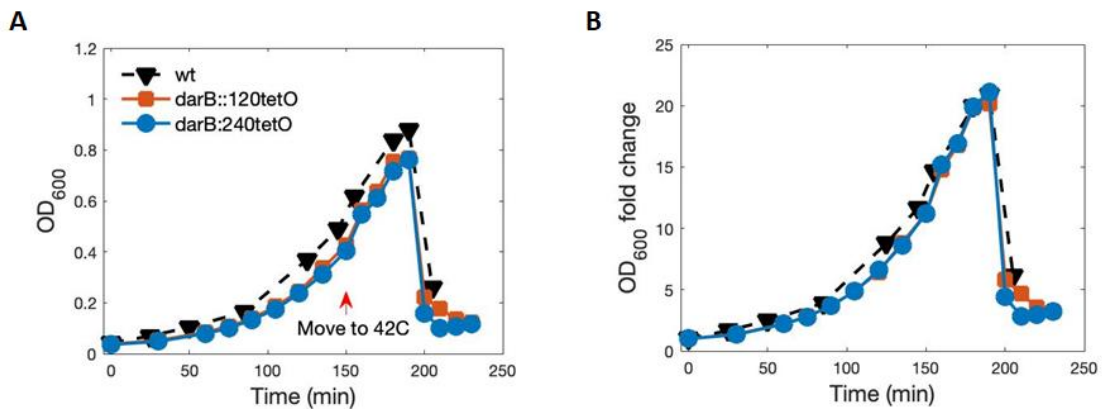


Figure III.13 Test the effect of *tetO* insertions in viral DNA on P1 lysogen growth and induction.

Lysogen cells are grown in 30°C and transfer to 42°C for thermal induction (red error). OD₆₀₀ is tested overtime (A) and is normalized to the initial time point for a more intuitive comparison (B). P1 strains with 120 (red square) or 240 (blue circle) *tetO* repeats replacing *darB* sequence shows a similar growth rate and lysis time with WT stain (black triangular). Together with the normal phage production from lysogen induction (Table 3.1), we conclude that the *tetO* insertions have no influence on P1 lysogen and phage behaviors.

Table III.1 Titer of P1*tetO* phages.

| Phage Strain | Capsid Labeling | Titer (pfu/mL) |
|--|-----------------|----------------------|
| P1 <i>darB</i> ::120 <i>tetO</i> - <i>Kan</i> ^R | None | 2.4×10 ¹⁰ |
| P1 <i>darB</i> ::240 <i>tetO</i> - <i>Kan</i> ^R | None | 7.8×10 ⁹ |
| P1 <i>darB</i> ::120 <i>tetO</i> - <i>Kan</i> ^R | mTurquoise2 | 1.4×10 ¹⁰ |
| P1 <i>darB</i> ::240 <i>tetO</i> - <i>Kan</i> ^R | mTurquoise2 | 2.1×10 ⁹ |

Table III.2 Bacterial Strains, Phages and Plasmids used in this work.

| Strain # | Genotype | Comments | Source |
|--------------|--|--|---------------------|
| MG1655 | F-, <i>lambda</i> , <i>rph-1</i> | Wild type <i>E. coli</i> ; indicator strain of phage titration and lysogenization in bulk; host stain in smFISH assays | Lab stock |
| LZ1387 | MG1655 <i>seqA-mKate2</i> , <i>Cm^R-Frt</i> , <i>Δdam::Kan^R</i> | Strain with SeqA reporter, <i>dam</i> deletion | ref. ¹³² |
| LZ1914 | MG1655 <i>lacIq</i> , <i>lacY</i> , P1 <i>Cm</i> , <i>cI-100 Δcin</i> , <i>cI-RBS-mVenus-Kan^R</i> [pACYC177 P <i>lacO-1-gene23-mTurquoise2</i>] | Strain to produce gp23- <i>mTurquoise2 cI</i> -labeled phages | ref. ¹²⁸ |
| LZ1915 | MG1655 [pBR322 LP23- <i>gene23-mTurquoise2</i>] | Host strain with lytic reporter plasmid for single-cell infection movies | ref. ¹²⁸ |
| LZ1931 | MG1655 <i>lacIq</i> , <i>lacY</i> , [pZE12 <i>luc</i> P <i>lacO-1-lxc</i>] | Lxc overexpression strain used in bulk lysogenization assay | This work |
| LZ1937 | MG1655 <i>lacIq</i> , <i>lacY</i> , [pACYC177 P <i>lacO-1-lxc</i>] [pBR322 LP23- <i>gene23-mTurquoise2</i>] | Lxc overexpression strain used in single-cell infection movies | This work |
| LZ1938 | MG1655 <i>lacIq</i> , <i>lacY</i> , [pACYC177 P <i>lacO-1-lxc</i>] | Lxc overexpression strain used in smFISH assay | This work |
| LZ1952 | MG1655 [pBR322 LP23- <i>gene23-mTurquoise2</i>] [pACYC177 C1operator] | Host cells with extra C1 operators for single-cell infection movies | This work |
| LZ2001 | MG1655 [pZS24 P <i>ftsK</i> - <i>tetR-mNeonGreen</i>] | Host strain of <i>tetO</i> /TetR-FP DNA visualization system | Lab stock |
| LZ2504 | MG1655 <i>lacIq</i> , <i>lacY</i> , P1 <i>Cm</i> , <i>cI-100 Δcin</i> , <i>darB::120tetO-Kan^R</i> [pACYC177 P <i>lacO-1-gene23-mTurquoise2</i>] | Strain to produce gp23- <i>mTurquoise2 120×tetO</i> phages | This work |
| Phage | | | |
| P1LZ1856 | P1 <i>Cm</i> , <i>cI-100</i> , <i>Δcin</i> | Phage with fixed tail fibers | This work |
| P1LZ1914 | P1 <i>Cm</i> , <i>cI-100</i> , <i>Δcin</i> , <i>cI-RBS-mVenus-Kan^R</i> | gp23- <i>mTurquoise2 cI</i> -labeled phage | This work |
| P1LZ2504 | P1 <i>Cm</i> , <i>cI-100 Δcin</i> , <i>darB::120tetO-Kan^R</i> | gp23- <i>mTurquoise2 tetO</i> phage | This work |

Table III.2 Continued.

| Plasmid | | | |
|----------------|--|---|-------------------------|
| pLZ1903 | pACYC177 PLlacO-1- <i>gene23-mTurquoise2</i> | Provides fluorescently labeled gp23 during lysogen induction to form fluorescent phages | This work |
| pKD46 | | Temperature sensitive plasmid which inserts DNA using homologous recombination | Gift from Jason Gill |
| pLZ1915 | pBR322 LP23- <i>gene23-</i> <i>Turquoise2</i> | Lytic reporter plasmid | This work |
| pLZ1931 | pZE12luc PLlacO-1- <i>lxc</i> | Lxc expression under the control of IPTG | This work |
| pLZ1933 | pACYC177 PLlacO-1- <i>lxc</i> | Lxc expression under the control of IPTG | This work |
| pLZ1950 | pACYC177 C1operator | Plasmid with one copy of the consensus C1 operator sequence | This work |
| pLZ1981 | pUC19 <i>H1-proKan^R-</i> <i>120tetO-H2</i> | The recombination plasmid to replace part of the <i>darB</i> region of P1KL1856 with <i>tetO</i> arrays. | This work |

Table III.3 Primers (5' – 3') used in this work.

| Primer | Sequence |
|--------------------|--|
| 1 | GCGACCATGGGATTGAAAAAGCGATACTACACAGTAAAG C |
| 2 | TGCAGCATGCGGTGAGCAAACAGCCATAATTG |
| 3 | CATGGGATCCCTCGAGAATTGTGAGCGGATAAC |
| 4 | CATGCTGCAGGTATTACCGCCTTTGAGTGAGC |
| 5 | GCGAGGATCCATTGCTCTAATAAATTTAGAGCGCACGAA TGAGGGC |
| 6 | ATTACTGCAGGTATCACGAGGCCCTTTCGTCTTC |
| 7 | ATTGTA CTGAGAGTGCACCATATGGATGTTGCCAGTTATG GC |
| 8 | CAAGGGTACCGATCGCGAGTGAGATCAC |
| 9 | ACTCGCGATCGGTACCCTTGCAGTGGGCTTACATG |
| 10 | ATAGAGACTCGAGGGATCCGAATTCTCAGAAGA ACTCGTC AAGAAGG |
| 11 | ACGTGTCGACCACCAATGCCATTTTCGGTACCC |
| 12 | TGTCAAGCTTAAGGGCCAGGTTTATCCGATCAG |
| dnafish-P1-for | CAACGAACCAGGTAGCCGGAATGTG |
| dnafish-P1-rev | AGCACAACCATCAACCAGCGCCAAA |
| qPCR- P1DNA-for | CTCTGCCC GTTATTTGTGGTGT |
| qPCR- P1DNA-rev | AGTCCGCTCGCTCTGTGTAG |
| dxs-for | CGAGAAACTGGCGATCCTTA |
| dxs-rev | CTTCATCAAGCGGTTTCACA |

Bulk Lysogenization Assay

We measured the probability of lysogeny as a function of the MOI. An overnight culture of host strain was grown in LB at 37°C. Cells were diluted 1000-fold into LBM and grown at 37°C to OD₆₀₀ ~0.4, chilled, and CaCl₂ was added to a final concentration of 5 mM. Then 100 µL of cells were added to 100 µL of phage solutions with different concentrations. After a 30 min-incubation at 30°C, we transferred 20 µL of the mixture into 980 µL ice-cold LB or SM buffer to stop the adsorption process. Aliquots in LB media were plated on LBCM plates and incubated overnight at 30°C. Lysogen concentrations were determined by counting the number of CM^R colonies. To examine the concentration of nonadsorbed phages, we centrifuged down the aliquots in SM buffer and titrated the supernatant on MG1655. Total phage and bacteria concentrations were measured using plate assays as well. Bulk MOI = total phage/total cell. The probability of lysogeny of all cells or of the infected cells (determined from the bulk MOI using the Poisson distribution with cumulative probability ≥ 1) was plotted as a function of the MOI on a log-log scale. MOI_{infected} is calculated by (total phages – nonadsorbed phage)/total cell. λ Kil expression in strain contain pBAD24- λ kil was induced with L-Arabinose when OD₆₀₀ approaching 0.08. Lxc expression in strain LZ1931 was induced with IPTG when OD₆₀₀ approached 0.1.

Single-Cell Infection Assay

Decision-making examination

The protocol was adapted from previous work¹²⁸. An overnight of LZ1915 was diluted for 100-fold in LBM and grown to OD₆₀₀ ~0.4, then CaCl₂ was added to 5 mM.

For the infections on Lxc-overexpressed cells IPTG was added at a final concentration of 0.2 mM in the cell culture (LZ1937) when OD₆₀₀ approaching 0.1. Purified P1LZ1914 phages were mixed with the cell to reach an MOI of 0.1-7, followed by incubation for 30 min at 30°C to trigger both phage adsorption and viral DNA injection. One microliter of the sample was placed on 1 mm 1.5% LB agarose pad resting on a small coverslip (18 x 18 mm, Fisher Scientific). After 1-2 min, a large coverslip (24 x 50 mm, Fisher Scientific) was gently overlaid and the sample was imaged under the microscope at 30°C.

To localize all phages surrounding the cells, a series of 7 z-axis images at spacing of 300 nm were taken through the CFP channel using a 500 ms exposure for each. Cells were imaged at multiple stage positions (typically 16) in each experiment. During the time-lapse movie, the sample was imaged in phase contrast (100 ms exposure for cell recognition), YFP (300 ms exposure for phage C1-mVenus expression), and CFP (100 ms exposure for lytic reporter signal) channels at time intervals of 5 min until cell fate was visible (3 hours in total).

DNA injection on SeqA-mKate2 strain

The protocol was adapted from previous work¹²⁸. An overnight of LZ1387 was diluted for 100-fold in LBM and grown to OD₆₀₀ ~0.4, then CaCl₂ was added to 5 mM. Purified P1LZ1914 phages were mixed with the cell to reach an MOI of 2, followed by incubation for 30 min at 30°C to trigger both phage adsorption and viral DNA injection. One microliter of the sample was placed on 1 mm 1.5% PBS agarose pad resting on a small coverslip (18 x 18 mm, Fisher Scientific). After 1-2 min, a large coverslip (24 x 50

mm, Fisher Scientific) was gently overlaid and the sample was imaged under the microscope at 30°C.

Cell images were taken at 24 stage positions in phase contrast (100 ms exposure for cell recognition), the CFP (500 ms exposure for fluorescent phages) and Far Red (100 ms exposure for SeqA-mKate2 foci) channels with 5 z-stacks at spacing of 300 nm.

DNA injection into TetR-mNeonGreen strain

An overnight of LZ2001 was diluted for 100-fold in EZ rich defined medium with 0.2% glucose and 10mM MgSO₄. For long cell with λ Kil induction, the overnight of LZ2001 with pBAD33-*λkil* was diluted for 100-fold in EZ rich defined medium with 30% LB and 10mM MgSO₄. Add L-Arabinose with final concentration of 0.05 % when OD₆₀₀ approaching 0.08. Grow the cell until OD₆₀₀ ~0.4, then CaCl₂ was added to 5 mM. Purified P1LZ1914 phages were mixed with the cell to reach an MOI of 2, followed by incubation for 30 min at 30°C to trigger both phage adsorption and viral DNA injection. One microliter of the sample was placed on 1 mm 1.5% agarose pad (PBS for cell imaging, EZ rich with 0.2% Glucose for time-lapse movie) resting on a small coverslip (18 x 18 mm, Fisher Scientific). After 1-2 min, a large coverslip (24 x 50 mm, Fisher Scientific) was gently overlaid and the sample was imaged under the microscope at 30°C.

A series of 7 z-axis images at spacing of 300 nm were taken through the CFP channel using a 500 ms exposure for fluorescent phages and the Green2#FISH channel using a 300 ms exposure for TetR-mNeonGreen labeled DNA foci. Cells were imaged at multiple stage positions (typically 16) in each experiment. During the time-lapse movie,

the sample was imaged in phase contrast (100 ms exposure for cell recognition) and Green2#FISH (300 ms exposure for DNA behavior) channels at time intervals of 5 min until cell fate was visible (3 hours in total).

RNA FISH

Different probes were synthesized to target different phage transcripts (3' TEG-Amino, Biosearch Technologies). Probes targeting *cI*, *coi* and *lxc* were designed following previous study²³⁵, labeled with Cy5 (GE Healthcare #PA15101), TAMRA (Biosearch Technologies, #SMF-1001-5) and Alexa Fluor 488 (ThermoFisher, #A20000), respectively (Fig. III.6A and B). Probes are listed Table III.4.

To perform RNA FISH on infection samples, the overnight host cell was diluted 100-fold into 65 ml of fresh LBM and grown at 37°C until OD₆₀₀ ~0.4. For the infections on Lxc-overexpressed cells IPTG was added at a final concentration of 0.2 mM in the cell culture (LZ1938) when OD₆₀₀ approaching 0.1. Then CaCl₂ was added to 5 mM. After that, 750 µL aliquot of cells was separated as a negative control without phages. The rest of cell culture was mixed with the purified P1LZ1856 to get MOI of 0.2, 1 or 5 and incubated the mixture at 30°C (0 min). At each time point (10, 20, 30, 40, 50, 60, 80, 100 min) during incubation, aliquot 750 µL of the mixture to a new 15 mL centrifuge tube with 830 µL of 37% formaldehyde. This tube was left to shake on a nutator for 30 min, and then centrifuged at 400 × g for 8 min to pellet the cells. Details of fixation, permeabilization, and hybridization are detailed in the previous studies^{135,235}. Briefly, after fixation, the cells were washed three times with 1× PBS. Subsequently, the cells were permeabilized by resuspension in 70% ethanol for 2 h at room temperature and

centrifuged to collect the cells. The pellet was then resuspended in wash solution (40% formamide, 2× SSC) and incubated for 5 min at room temperature, and pelleted again, ready for hybridization. The cells were then resuspended in 25 μL hybridization solution (40% formamide, 2× SSC, 1 mg mL^{-1} *E. coli* tRNA, 2 mM ribonucleoside-vanadyl complex, and 0.2 mg mL^{-1} BSA) with each set of probes reaching a final concentration of 1 μM . The samples were then incubated in a 30 °C water bath overnight. The next day, the cells were washed three times using wash solution by incubating the cell pellet for 30 min in a 30 °C water bath. After the final wash, the cells were resuspended in wash solution + 10 $\mu\text{g mL}^{-1}$ DAPI and incubated for 10 min at room temperature. This suspension was then pelleted and resuspended in 2× SSC. The sample was then ready for imaging.

Pipette 2 μL of the cell suspension onto the center of a 24 × 50 mm coverslip. Lay the 1.5% PBS agarose pad slowly on top of the cell suspension droplet with the razor blade. Cover the pad with an 18 × 18 mm coverslip. Under the microscope, images were taken in phase-contrast (100 ms), Cy5 (700 ms, *cI*), Cy3 (1 s, *coi*), GFP (2 s, *lxc*), and DAPI (30 ms, DAPI) channels at different stage positions. The average *cI* and *coi* mRNA level by qRT-PCR and smFISH is compared figure III.14.

Table III.4 smFISH RNA probes.

| Probe name | Sequence (5' to 3') |
|------------|-----------------------|
| P1-coi-1 | GTATTACGAAACGGCGGC |
| P1-coi-2 | AAATAGTGAATCCAAAGT |
| P1-coi-3 | ACAACGCTGAAGACACAT |
| P1-coi-4 | CATTTCTTCTGAGCCGC |
| P1-coi-5 | TAAGGTTTCCCTGTTTGC |
| P1-coi-6 | TAGCTGTAATGCCGTTGT |
| P1-coi-7 | GTGTAAGATGAGCAATGT |
| P1-coi-8 | TCTAACAACATTGCGCTG |
| P1-coi-9 | ATGATCCATGCTGGGGTA |
| P1-coi-10 | CTGACCTACTGTTTCACC |
| P1-coi-11 | CAACACAGAGCCTGAAGC |
| P1-coi-12 | TTATGCCTCACTGTATTG |
| P1-coi-13 | GGTGAATGAAAGCCATA |
| P1-coi-14 | TCTAACGTCGTCGATGGT |
| P1-coi-15 | ATAAAGCGTTAGAGCAAT |
| P1-coi-16 | GTTTCGGCGGGGTCTACA |
| P1-coi-17 | AATGGCGCGGGCAGCGTC |
| P1-coi-18 | TCTTTGAGTAGTGTTTCAG |
| P1-coi-19 | CGGTA CTCTGATTGGAT |
| P1-coi-20 | CAGGTCGTCTTGGGTGAT |
| P1-coi-21 | TTGTGTCAGTGAGATCAT |
| P1-coi-22 | GTGGCCATGAGATATTCG |
| P1-coi-23 | TTGTGAGTCTGGCTGGTT |
| P1-c1-1 | GGATTACACTGGGAGTTGTT |
| P1-c1-2 | TTGACATGGCCAACA ACTCA |
| P1-c1-3 | ATTTATCATTGATCCTCCTC |
| P1-c1-4 | TACAGTTGTTCCCGTAGAC |
| P1-c1-5 | AAGAGATCCCTGAAGCTGAC |
| P1-c1-6 | GCGTGCAACAGCTTTTTTTA |
| P1-c1-7 | AACCGGGCGAACAGGACGAC |
| P1-c1-8 | GTTTCTTTGAACGGCAGAAC |
| P1-c1-9 | AATTT CAGCCTGAATGCTGT |
| P1-c1-10 | GCGCCATTAATGTCCATTTA |
| P1-c1-11 | TGGGATATTGAGATCTGGGT |

Table III.4 Continued.

| | |
|-----------|----------------------|
| P1-c1-12 | GCGAAGGATGTTAGGTACAG |
| P1-c1-13 | AAGTCGTAACCTTACGCACA |
| P1-c1-14 | GTCATATTGACGCTGTTAC |
| P1-c1-15 | TCAGATGAATAATGCGGCCA |
| P1-c1-16 | TGGATGCGAATGTCCTTATC |
| P1-c1-17 | TTCGCACTGTGCTCATTGAT |
| P1-c1-18 | TTGCTTCCAGGTTCTCTATG |
| P1-c1-19 | TACTGCTTCATTAGCTCTTT |
| P1-c1-20 | TACGGAATTTTTCATCCTCC |
| P1-c1-21 | TTTCGCTAAAGCCGTGTACG |
| P1-c1-22 | ATGTAATGGACGCGCAGCAT |
| P1-c1-23 | ATTGTAGTTAGGGCTACTGG |
| P1-c1-24 | GGTAACTAACTGATTTGCCA |
| P1-c1-25 | AAACACGCAACATAGCGGCA |
| P1-c1-26 | CTCGGAGAGTTTCATCGCAG |
| P1-c1-27 | TCACCGTTGATGATGATTCC |
| P1-c1-28 | GGCTAAATTTTGCTTTCTCA |
| P1-c1-29 | CGCAGATGATCGGTTCTATA |
| P1-c1-30 | CGATATATTTTGGCCTGCGG |
| P1-c1-31 | TACATTTTCAATATCTGCCA |
| P1-c1-32 | TTTTCTCTTCGCGAGTGATG |
| P1-c1-33 | AACTGATGCGGCTGATTTGA |
| P1-c1-34 | TTCTTAGTTTTGCGGCTGCG |
| P1-c1-35 | TTCGGGGTTGTCGTTTACTG |
| P1-lxc-1 | CCAAGGCTTCAACTTCCA |
| P1-lxc-2 | CAAGTTTTCTCTCCAGCC |
| P1-lxc-3 | CCCATGCTTTACTGTGTA |
| P1-lxc-4 | TCTTGTAATGCTCGTAGC |
| P1-lxc-5 | GCACCTCAACGTTATGCT |
| P1-lxc-6 | AGCTTTACTTCCCCCTTC |
| P1-lxc-7 | TTTCCCGTCCGGACGGTA |
| P1-lxc-8 | TTGAAATCGACGACCGTC |
| P1-lxc-9 | CCTGGGGAACACTGTTTG |
| P1-lxc-10 | TTCGAATGCCCGGTCACG |
| P1-lxc-11 | ATGATGATCTGCTCCCAT |

Table III.4 Continued.

| | |
|-----------|--------------------|
| P1-lxc-12 | CGCATTGAGAAGCAATGC |
| P1-lxc-13 | GGTGAGCAAACAGCCATA |
| P1-lxc-14 | TCGTGCTTCTTTGAGCGA |
| P1-lxc-15 | GTGGCACTATCACTATCT |
| P1-lxc-16 | AGCCCGTTAGAGCCAGAA |
| P1-lxc-17 | TTAGCAACAAAGCGCCGC |
| P1-lxc-18 | TCCATTTTAAACCAGATC |
| P1-lxc-19 | CCGTTTCTACTTCGGAAA |
| P1-lxc-20 | GCTTTCAACACAGCCAGT |
| P1-lxc-21 | TTATCAAAACACTGTGGG |
| P1-lxc-22 | TTCTTGAATGAAGGCTCC |
| P1-lxc-23 | CTAATAATCTCAAGCAAT |
| P1-lxc-24 | AGAGTTCAACCTCCGATG |
| P1-lxc-25 | GCCAGTTTAAACTGTATG |

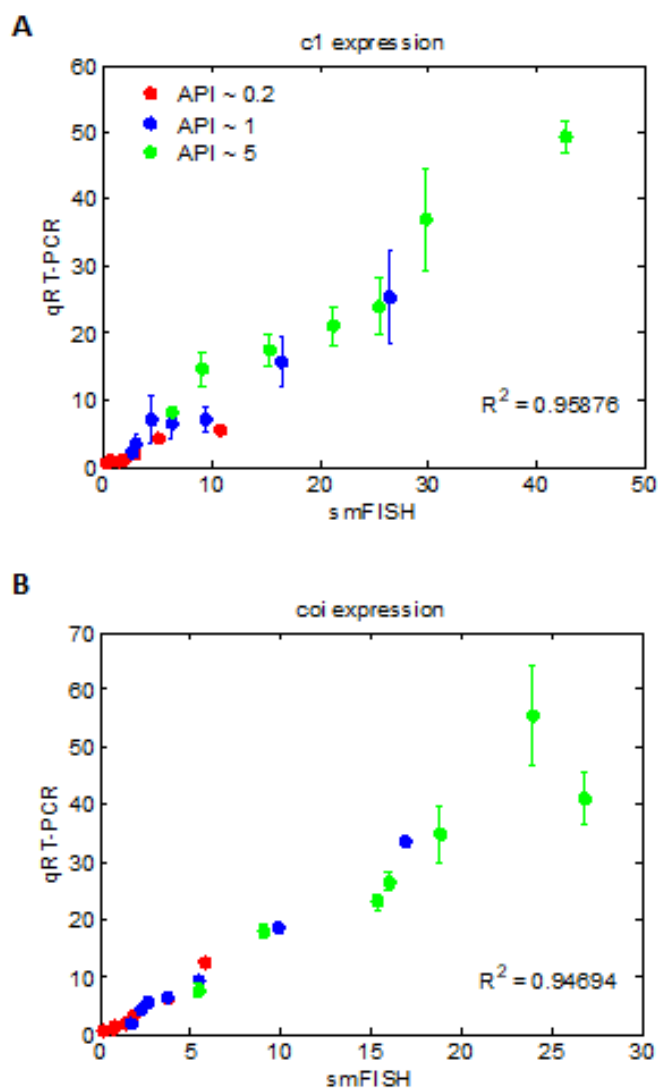


Figure III.14 Comparison of average *c1* and *coi* mRNA level by qRT-PCR and smFISH.

For smFISH, only the infected cells that with *c1* or *coi* fluorescent signal were analyzed, and the average mRNA numbers at different time points for different phages were shown. For qRT-PCR, the average mRNA numbers were calculated using *ihfB* gene expression as a reference, and further normalized to the number obtained at 0 min. The correlation coefficients are around 0.96 and 0.95 for *c1* (A) and *coi* (B), respectively, indicating good agreement between smFISH and qRT-PCR data. Error bar denotes the standard error of the mean.

DNA FISH

For DNA FISH for P1 DNA replication detection, probes were produced by PCR amplifying ~3 Kb of P1 DNA (dnafish-P1-for and dnafish-P1-rev primer pair listed in Table S2), using a phage lysate as the template, followed by treatment of the purified PCR product with a PromoFluor500-dUTP nick translation kit (PromoCell) to generate DNA-PromoFluor500 fragments ranging from 100 to 500 bp.

To perform DNA FISH on infection samples, the overnight host cell was diluted 100-fold into 50 mL of fresh LBM and grown at 37 °C until OD₆₀₀ ~0.4. Then CaCl₂ was added to 5 mM. After that, 5 mL aliquot of cells was separated as a negative control without phages and mixed with 550 µL of 37% formaldehyde for fixation. The rest of cell culture was mixed with the purified P1LZ1856 to reach MOI of 0.2, followed by incubation at 30°C. At each time point (30, 40, 50 and 60 min) during incubation, transfer 5 mL of the mixture to a 15 mL centrifuge tube with 550 µL of 37% formaldehyde. This tube was left to shake on a nutator for 30 min, and then centrifuged at 4,000 × g for 3 min to pellet the cells.

Details of fixation, permeabilization, and hybridization steps are detailed in a previous study²⁴³. Briefly, the fixed cells were washed with 1 mL of ice-cold 1× PBS three times and resuspended in 1 mL of GTE solution (50 mM glucose, 20 mM Tris-HCl [pH 7.5], 10 mM EDTA). For the control sample, three separate 500 µL aliquots of the cell suspension were then mixed with 10 µL of 0.01 µg µL⁻¹ lysozyme solution and incubated at room temperature for 2, 4, and 6 min followed by three washes with GTE, pelleting the cells via centrifugation at 10,000 × g for 30 s. The cells were then

resuspended in ~150 μL of GTE. For each control sample, 1 μL of the cells was deposited onto a PBS agarose pad and imaged. The lysozyme treatment time yielding ~90-95% intact cells (~1-5% lysed cells) represents the optimal treatment time for the samples. The actual time point samples, from the initial GTE wash, were then processed as the control was, using the optimal lysozyme time. For each time point, 10 μL of cells were deposited onto poly-L-lysine-coated large coverslips (24 \times 50 mm), then covered with a smaller, normal, coverslip (22 \times 22 mm). The coverslips were then immersed in 1 \times PBS and the smaller coverslip was removed, leaving only the sample coverslip. The cells were then dehydrated by immersing the coverslip in increasing concentrations of ethanol (70, 90, then 100%). Samples were then ready for hybridization. For each sample, approximately 160 μg of the probe mixture was combined with 10 μL of hybridization solution (50% formamide, 10% dextran sulfate, 50 mM $\text{NaPO}_4/\text{pH } 7$, 2 \times SSC). The dsDNA probes were denatured at 75 $^\circ\text{C}$ in a thermocycler, then placed on ice. Ten microliters of the denatured probe mixture were then deposited onto the center of the sample on the coverslip and overlaid with a small coverslip (22 \times 22 mm). The small coverslip was then sealed with nail polish, forming a sample chamber. The chambers were incubated at 80 $^\circ\text{C}$ for 5 min to denature the cellular DNA, and then placed on Kimwipes over ice for 5 min. The chambers were then incubated in a 37 $^\circ\text{C}$ incubator overnight to complete hybridization. The next day, the chambers were immersed in 2 \times SSC until the smaller coverslip dislodged. The remaining coverslips were soaked in wash solution (2 \times SSC, 50% formamide) for 20 min at 37 $^\circ\text{C}$ twice. The coverslips were then washed with a series of increasing SSC concentration washes (1, 2, then 4 \times), each

for 5 min at room temperature. A DAPI solution was then made by mixing 1 μL of 10 mg mL^{-1} DAPI with 1 mL of 4 \times SSC. For each sample, 500 μL of the DAPI solution was added over the sample, covering it, and incubated for 5 min at room temperature. After drying the coverslip, 10 μL of 2 \times SSC was added over the sample and overlaid with a small coverslip (22 \times 22 mm). The samples were then imaged.

Under the microscope, images were taken in phase-contrast (100 ms), GFP (300 ms), and DAPI (30 ms) channels at different stage positions.

qPCR

The overnight host cell was diluted 100-fold into fresh LBM and grown at 37 $^{\circ}\text{C}$. During cell growth, methanol was kept at -20 $^{\circ}\text{C}$ for cell fixation. When cell culture reached $\text{OD}_{600} \sim 0.4$, CaCl_2 was added to a final concentration of 5 mM. We then transferred 2 mL of cells to a 50 mL centrifuge tube and mixed it with 2 mL ice-cold methanol as the negative control sample. The rest of cell culture was mixed with the purified P1LZ1856 to get $\text{MOI} \sim 1$ and incubated at 30 $^{\circ}\text{C}$ (0 min). For given time point (0, 10, 20, 30, 40, 50, 60, 70 and 80 min), 2 mL of the reaction was aliquoted in to 50 mL tubes and vortexed for 10 s then centrifuged at 4000 \times g for 3 min. After removing the supernatant, we resuspended the cell pellet with 2 mL fresh ice-cold LB solution, added 2 mL ice-cold methanol and vortexed it for another 10 s. The mixture was centrifuged at 4000 \times g for 3 min. After removing the supernatant, the cell pellet was kept at -20 $^{\circ}\text{C}$ until ready for DNA extraction using UltraClean Microbial DNA Isolation Kit (MO BIO Laboratories #12224-50). The DNAs were then diluted and used for qPCR with primers targeting the phage DNA. The *E. coli* DNA number was used as a reference

using primers targeting the *dxs* gene²⁴⁴. Amplification was done using SYBR Green PCR master mix (Applied Biosystems, 4309155) with 250 nM of each primer (Table 3.2).

Data Analysis

Analysis of time-lapse movies

Movie images were analyzed firstly using the model created by deep learning with TensorFlow for the automatic cell recognition (collaboration with the lab of Anxiao Jiang, Department of Computer Science & Engineering, Texas A&M University) and then manually check using the program Schnitzcell²⁴⁵ (gift of Michael Elowitz, California Institute of Technology), in order to generate cellular index. The numbers of phages attached on the cell surface, as well as distances between phages on the cells of MOI = 2 and cell lengths were measured manually using the supporting tools of NIS element program. Cell fates and DNA behavior for each infected cell was recorded as well. All subsequent data analysis was performed in MATLAB.

Calculation of infected cells proportion and $MOI_{infected}$ in smFISH experiments

We used bulk MOI (total phage/total cell) as the average rate of success or the expected rate of occurrences in Poisson distribution calculation. Then, the proportion of infected cells over total cells equaled the cumulative probability $P(X \geq 1)$, where X indicated the number of occurrences. $MOI_{infected}$ was the quotient of bulk MOI over $P(X \geq 1)$.

Failed infections

We observed that, in some cases, adsorbed phages were seen on the cell surface, but the cell grew normally with neither lysis nor lysogeny detected, similar to phage

lambda infection ¹²⁹. These events were defined as “failed infections.” In our experiments, the rate of failed infection was defined as the number of failed infections divided by total number of infected cells with MOI = 1. In the decision-making reporter system, the failed infection rate was 16.6% (99 of 596). In the SeqA-FP DNA visualization system, the failed infection rate was 21.6% (19 of 88). In the *tetO*/TetR-FP system, the failed infection frequency was 21.5% (31 of 144). A possible explanation for this phenomenon is the failure of the adsorbed phage to inject its DNA into the cell.

“Dark” infections

Similar to phage lambda infection, a fraction of the cells exhibited dark infections: cells without any observed infecting phages on the cell surface, exhibiting lysis or lysogeny. With careful treatment of the sample, the dark infection rate was ~20% (120 cells with no phage attached at 0 min showed mVenus signal, compared to 596 cells with MOI = 1), testing in the decision-making reporter system. The calculation is based on the assumption that dark infections were mainly MOI = 1 events. We hypothesize that these dark infections are mainly due to the phages falling off after injecting their DNA into the host cell. Another possibility is that some cells may divide into two daughter cells during the 30 min incubation, resulting in an infected daughter cell without an observed infecting phage. Similarly, in the SeqA-FP DNA visualization system, the dark infection rate was 15.9 % (14 cells at MOI = 0 showing DNA signal, compared to 88 cells with MOI = 1) and in the *tetO*/TetR-FP system, the dark infection rate was 22.9% (33 cells at MOI = 0 showing DNA signal, compared to 144 cells with MOI = 1).

Analysis of DNA number and RNA number

Microscope images of the DNA injection in SeqA-FP or *tetO*/TetR-PF system and RNA FISH experiments were processed for cell recognition as described above. Then, the number of viral DNA was analyzed via the procedure reported in ²³⁵. Basically, fluorescent spots were first identified from the stacks of fluorescence images, using the Spätzcells program²³⁵. Then, the false-positive spots, corresponding to the unspecific binding of probes to nontarget RNA, were discarded through the comparison with negative control. After that, the spot intensity corresponding to a single mRNA molecule is identified by examining the single spot intensities in a low-expression sample (20 min), where individual mRNAs are spatially separable. Finally, the one-mRNA intensity value is used to convert the total spot intensity in cells from other samples to the number of target mRNA molecules.

Calculation of predicted intracellular DNA number due to failed and dark infection

Assume that the frequencies of phage failed and dark infections for MOI = 1 are a and b respectively, and the frequencies of failed or dark infection for an infected cell is a^n and b^n , where n is the number of failed or dark phages. Here we only consider $n = 1$ since the frequencies are low when $n > 1$. Thus, there will be four situations: No failed × No dark, No failed × One dark, One failed × One dark and One failed × No dark. The predicted number of injected DNA is:

for MOI = 1,

$$(1 - a) \times (1 - b) + 2 \times (1 - a) \times b + a \times b$$

for MOI = 2,

$$2 \times (1 - a)^2 \times (1 - b) + 3 \times (1 - a)^2 \times b + 2 \times 2 \times (1 - a) \times a \times b + 2 \times (1 - a) \times a \times (1 - b)$$

for MOI = 3,

$$3 \times (1 - a)^3 \times (1 - b) + 4 \times (1 - a)^3 \times b + 3 \times 3 \times (1 - a)^2 \times a \times b + 2 \times 3 \times (1 - a)^2 \times a \times (1 - b)$$

for MOI = 4,

$$4 \times (1 - a)^4 \times (1 - b) + 5 \times (1 - a)^4 \times b + 4 \times 4 \times (1 - a)^3 \times a \times b + 3 \times 4 \times (1 - a)^3 \times a \times (1 - b)$$

for MOI = 5,

$$5 \times (1 - a)^5 \times (1 - b) + 6 \times (1 - a)^5 \times b + 5 \times 5 \times (1 - a)^4 \times a \times b + 4 \times 5 \times (1 - a)^4 \times a \times (1 - b)$$

From our measurements, we found in SeqA-FP system, $a = 21.6\%$ and $b = 15.9\%$. Therefore, the sum probabilities of these four situations were 1, 0.95, 0.88, 0.79 and 0.70, for MOI from 1 to 5 respectively. The predictions of DNA number for were 0.94, 1.72, 2.38, 2.89 and 3.22, compared with the quantified data (1.07, 1.70, 2.40, 2.57 and 3.80) using Spätzcells²³⁵. In *tetO*/TetR-FP system, $a = 21.5\%$ and $b = 22.9\%$. Therefore, the sum probabilities of these four situations were 1, 0.95, 0.88, 0.80 and 0.71, for MOI from 1 to 4 respectively. The predictions of DNA number for were 1.01, 1.79, 2.45 and 3.21, compared with the quantified data (0.93, 1.55, 2.28 and 3.30) using Spätzcells.

CHAPTER IV
STUDYING THE PARAMETERS THAT INFLUENCE LYSIS-LYSOGENY
DECISIONS OF BACTERIOPHAGE P1

Introduction

If we want to control the fates of living cells, typically, we will modify their genomic information or change the growth environment. However, when examined at the single-cell level, though cells are from the same clonal population and subject to an identical growth condition, the cellular decision-making often appears “noisy”²⁴⁶⁻²⁵¹. This biological noise has been reported in various organisms with different levels of complexity, including viruses, bacteria, yeast, lower metazoans and mammals²⁵²⁻²⁵⁴. Considering that intercellular reactions usually happen between low copies of certain molecules (e.g., DNAs), the noise is unavoidable and the nongenetic diversity should be common in the cellular world. Noise becomes significant when individual cells are unable to adapt to changing environments. For instance, the co-existence of normal growing and growth-arrested but stress-resistant subpopulations may optimize their survival in the face of the fluctuating and frequently stressful environment: they are able to grow in the absence of stress with no metabolic burden of generating products useful for stress resistance and can also sustain in the presence of stress. Thus, it is necessary to investigate how noise arises and how it can contribute to the decision outcomes. Temperate phages, one of the simplest biological systems display lysis or lysogeny after infecting the host bacterium, are used to study underlying mechanisms of cellular

decision-making. Many factors have been shown to contribute to the noisy phenotypes of phage decisions, such as stochastic gene expression that underlies every biochemical reaction²⁵⁵⁻²⁶⁰, the heterogeneous bacterial cytoplasm in which the decision-making happens^{206,261-265} and the variability in the timing of infection²⁶⁶⁻²⁶⁸. On the other hand, recent studies with higher resolution and careful quantification of cell-to-cell variations explained away some though not all cell-fate heterogeneity, arguing for the growing need for quantitative methods to be applied. For example, during phage λ infections, the number of infecting phages, or the MOI, was the first factor known to affect the lysis-lysogeny decision-making. The probability of lysogeny increased as the bulk MOI increased and followed the Poisson distribution of $N \geq 2$, suggesting that it required two or more phages on average to lysogenize a cell²²⁹. Another deterministic factor of λ decision-making was found to be the cell volume²⁶⁹. The group of infecting bacteria with small volumes exhibited a much higher probability of lysogeny compared to the group with large volumes. Furthermore, with fluorescent phage labeling and live-cell imaging techniques, the decision process followed by phage λ infection was studied in more detail. The data suggested that a choice between lysis and lysogeny was initially made at the level of individual phages. The final cell fate was “voted” by all infecting phages and a lysogenic cell fate required the unanimous voting¹²⁹. By considering the decision-making at the single-phage level, it reduced the noise compared to the single-cell and population levels. Overall, high resolution studies allow more detailed understanding of phage λ infection and decision-making process. The failure in characterizing the deterministic factors may render the decision-making as noisy as it was assumed. It is

possible that, if one can identify all the deterministic factors, a cell outcome can be accurately predicted²⁶⁹.

In the previous chapter, we have demonstrated that, different from λ , there is a constant probability for a P1 infected cell undergoes the lysogenic development regardless of MOIs. Furthermore, instead of making individual decision, co-infecting P1 phages make an ensemble decision. However, factors that bias the choice of lysis or lysogeny for a single cell is still obscure. Does it indicate that there is reduced level of noisiness during P1 infection? If not MOI, what does P1 “utilize” to sense the environmental conditions and make corresponding responses? In order to answer these questions, here we explored more details during P1 infection and correlated the consequent changes of the lysogenic response to the variations of certain parameters. Bulk assays revealed that cell growth state influenced P1 decision-making and single-cell studies showed that the different cellular lengths in the same population biased the outcome of each infected cell. Furthermore, by monitoring viral DNA behaviors in bacteria cytoplasm, we observed distinctive DNA replication patterns in lytic and lysogenic cells. Finally, the co-infection of P1 virions with different lysogenization capabilities gave us some insights in phage interactions during decision-making processes.

Results

The Growth State of Host Cells Influences P1 Decision-Making

We first deduced different lysogenic outcomes in host cells with different growth states upon P1 infection. To test this hypothesis, we performed bulk experiments in *E.*

coli cells in different growth phases. Higher probabilities of lysogeny were exhibited in the cells in stationary phase compared with the cells in exponential phase (Fig. IV.1). These data indicate that cell state can bias the decision-making process, causing certain cellular fates to be more frequently chosen.

As the cell size is directly correlated with growth states in the bacterium²⁷⁰⁻²⁷², we further analyzed the single-cell infection data from Chapter III to characterize the effect of cell size on P1 decision-making. As shown in Fig. IV.2, the mean length of infected cells (l , as a metric for both cell age and volume) that enter the lysogenic pathway is significantly shorter than the ones undergoing lytic growth. It suggests that the cellular length can influence the outcome of each infection event and contribute to the cell-fate heterogeneity.

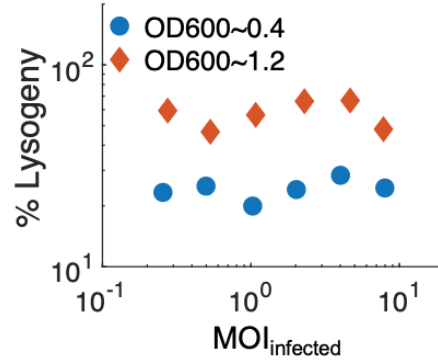


Figure IV.1 The probability of lysogeny at different growth states.

Cells in stationary phase (orange diamond) exhibit higher probabilities of lysogeny than cells in exponential phase (blue circle). The probability of lysogeny and MOI_{infected} are both calculated based on the number of infected cells.

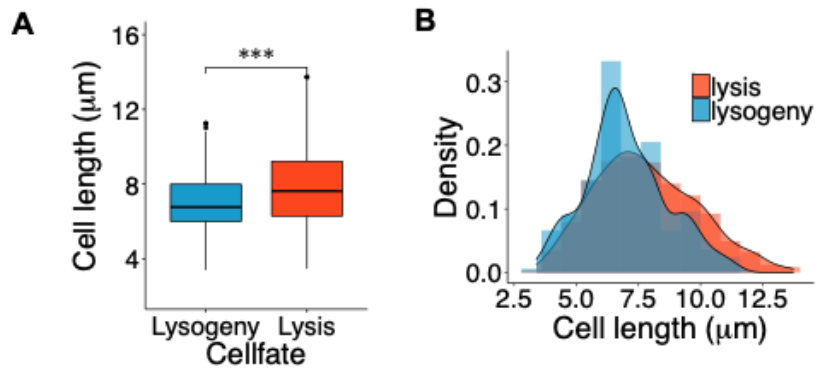


Figure IV.2 The length of cells entering the lytic or lysogenic pathway.

(A) The mean length of cells resulting in lytic growth is significantly larger than the mean length of lysogenic cells. The values of cell length are recorded at 0 min in the infection movies. p-value = 3.282e-07. ***p < 0.001 as determined by a Wilcoxon rank sum test. (B) Histogram and density plots of the probability distribution of the cell length.

To explore the mechanism of how the cell length influences P1 decision-making, we examined the correlations between l and different post-infection parameters. Of note, as the viral DNA copy number increased dramatically around 30 min after the phage infection (Fig. III.5) at which time the decision probably had been made, we performed our tests at this time point, unless otherwise stated. We found that the probability of lysogeny and cell lysis time decreased with l (Fig. IV.3A and Fig. IV.4C), while the levels of DNA replication and lytic gene expression increased with l (Fig. IV.4 A and B). At the beginning of P1 infection, the late gene activator (Lpa)¹¹⁷ can be expressed until C1 repressor activity reaches a certain threshold to shut it down. Thus, we hypothesized that in longer cells, C1 activity increased relatively slower such that Lpa had a higher chance to accumulate, stimulating lytic growth. We first used the free C1 concentration, $(C1-Coi)/l$, to represent the C1 activity and assumed its negative correlation with cell length. However, smFISH data showed that $(c1-coi)/l$ did not change with the cell length (Fig. IV.3B). This suggested that there would be other components that work together to regulate C1 inhibition activity.

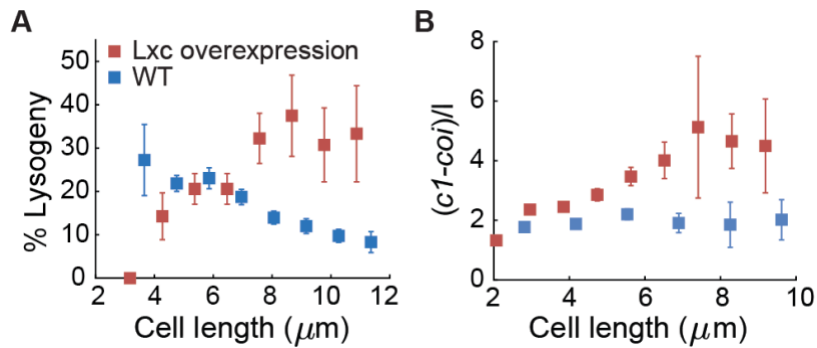


Figure IV.3 Cell size acts as a deterministic factor of P1 decision-making. (A) The probability of lysogeny decreases with cell size (blue). However, with overexpressed *Lxc*, the probability of lysogeny increases with cell size (red). Error bars denote counting error. (B) In WT host, the free *c1* concentration does not change over cell length, however, it increases with cell size in the cell with overexpressed *Lxc*, by using smFISH at bulk MOI around 0.2. Error bars denote standard error of the mean.

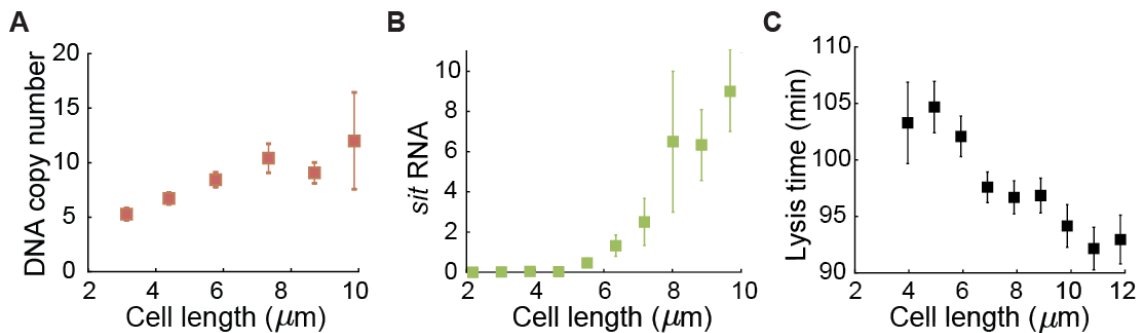


Figure IV.4 Different infection characteristics as a function of cell length. (A) DNA copy number and (B) lytic gene *sit* expression increase with cell size, detected by DNA FISH and smFISH, respectively. Data are collected at 30 min after phage infection. (C) Lysis time decreases with cell size based on the data from the decision-making reporter system. In all plots, error bars denote standard error of the mean.

Again, given the regulation function of Lxc on both C1 repression activity and Coi anti-repression ability, we took Lxc into consideration. We hypothesized that Lxc concentration decreased with cell length. If free C1 concentration was a constant, the C1 inhibition activity, $[(C1-Coi) \times Lxc]/l$, would be lower in longer cells. To test this model, we first examined the relationship between the free C1 concentration and cell fate when Lxc differences were removed. When overexpressing Lxc, it became a constant and smFISH data showed the increased $(cI-coi)/l$ with cell length (Fig. IV.3B). As expected, the probability of lysogeny also increased with cell length in the Lxc-overexpressed cell (Fig. IV.3A). Next, we directly quantified *lxc* mRNA levels as a function of cell length. Contrary to our hypothesis, neither *lxc* concentration nor $[(cI-coi) \times lxc]/l$ decreased in longer cells (Fig. IV. 5A and B). Further, we found that, in each MOI group, shorter cells exhibited a higher probability to be lysogenized. However, the cell length effect was averaged out when examining all cells within different MOI groups (Fig. IV.6B), corresponding to the comparable mean cellular lengths (Fig. IV.6A). In summary, these data suggested that cell length was a deterministic factor of P1 decision-making in which Lxc played an important role, but the mechanism could not be explained by the simple model only counting for the expression of C1, Coi and Lxc.

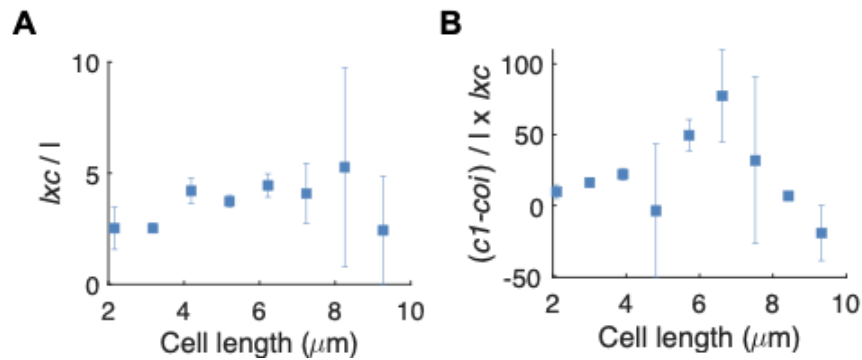


Figure IV.5 The role of Lxc in cell length effect on P1 decision-making.

(A) The concentration of lxc, lxc/l, does not change in cells with different lengths, tested using smFISH. (B) The level of $[(c1-coi) \times lxc]/l$ is plotted as a function of cell length. Error bars denote standard error of the mean.

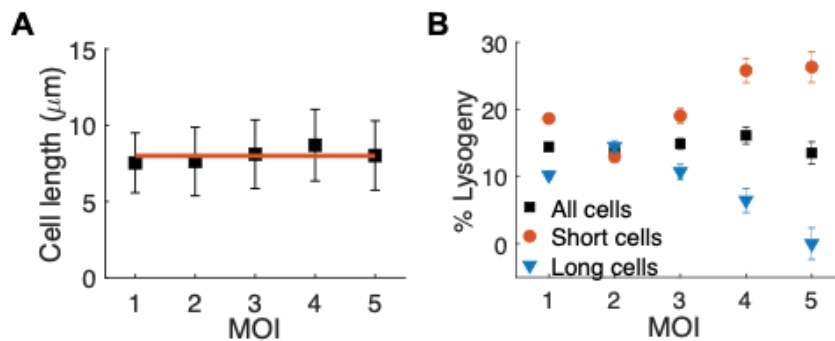


Figure IV.6 Consider both cell length and MOI on P1 lysogenization.

(A) Mean cell lengths at different MOIs. Red line shows the mean length of all infected cells at 0 min of the infection movies (8.00 μm). (B) The percentage of cells undergoing lysogeny as a function of MOI. Red square: all cells. Blue triangle: long cells (length \geq population mean). Green square: short cells (length $<$ population mean).

Moreover, the decreased probability of lysogeny in filamentous cells (Fig. III.11) might rely on this cell-size effect or a totally different decision-making mechanism given the MOI-dependent lysogenic response. In normal-sized cells, we did not find obvious correlations between the distance of phages and the level of phage individuality, as co-infecting phages exhibiting individual and non-individual behaviors have comparable distances (Fig. III.9B). This indicates a possible threshold value of the phage distance to make individual decisions. It is likely that in the normal-sized bacterial host, on which the distance of co-infecting phages is under the threshold, the cell with larger size has a higher chance of entering lysogenic pathway; when the cell length is large enough to allow an above-threshold distance between the phages infecting the same cell, the *trans* regulation or the intracellular phage communication is blocked and the final cell fate depends on the individual phage decisions and probably phage voting.

The Replication of Viral DNAs Shows Distinctive Patterns in Lytic and Lysogenic Cells

DNA replication is essential for life, and the variation of gene copy number due to DNA replication can exhibit intense effects on the downstream cell phenotype. Thus, it is of great interest to examine how DNA replication is associated with phage decision-making between lysis and lysogeny. To obtain a spatiotemporal picture of how DNA replication of phage P1 leads to different cell outcomes, we used the P1*tetO* system (Fig. IV.7) to follow DNA replication along with cell fate. Basically, a 120×*tetO* sequence was inserted in the phage DNA. Upon infecting the host cell constitutively expressing TetR-mNeonGreen, all injected and replicated viral DNAs are labeled at *tetO* sites by fluorescent TetR proteins (see more details in Chapter III). Based on this DNA

visualization system, we found that phage DNA replication exhibits distinct patterns in cells with alternative outcomes. In lytic cells (Fig. IV.7A and B), the injected P1 DNA first replicated into big blobs, and separated into smaller blobs, possibly by the *par* system⁹⁸, then the cell was lysed with new progeny particles. In lysogenic cells (Fig. IV.7C), the injected DNA slightly replicated, then separated into small foci. These small foci were distributed into daughter cells. Similar patterns were also found during the infection of unlabeled phages tested in fixed bacterial cells (Fig. IV.7, right).

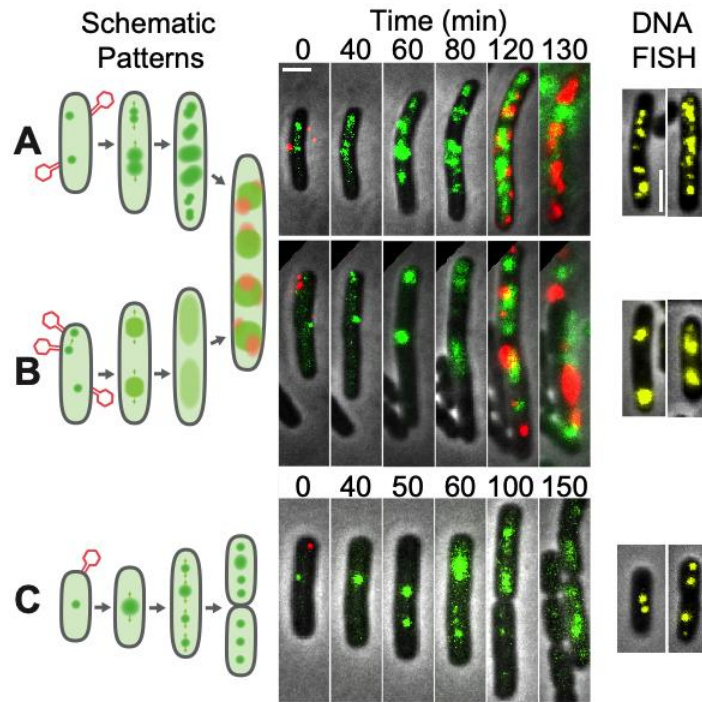


Figure IV.7 Replication patterns of viral DNAs during P1 infection.

(A) A lytic cell at MOI = 2 (red dots at 0 min). Two injected DNA (small green foci at 0 min) replicates into different sizes (40 min), further replicate and separate into four clusters (60 min) and more clusters (80, 120 min). (B) A lytic cell at MOI = 3. Two close DNAs merge (40 min). The merged DNA and another DNA replicate into two big foci (60 min), spread out (80 min) and then separate into more clusters (120 min). Finally, the cell lyses with new progeny particles (red, at 130 min). (C) A lysogenic cell at MOI = 1. The injected DNA replicates into a big focus (40 min) which is separated into two foci (50 min). DNA further replicates (60 min) and distributes into daughter cells (100, 150 min). The DNA replication pattern agrees well with DNA FISH data (yellow) on the right. Scale bar = 2 μ m.

We next got more insight about P1 DNA replication and movements using the SeqA-mKate2 DNA visualization system. The contraction of phage tail is important for P1 DNA injection⁸⁰ and it is nearly impossible for this conformational change to happen if the environment is too restrictive, such as on a 1.5% agarose gel used in the previous single-cell infection assays¹²⁸. Therefore, to capture the whole process of DNA injection and intracellular movements under the microscope, we modified the infection condition to be more flexible by lowering the agarose concentration to 0.2% (see more details in Methods). Through this system, we currently found that some P1 DNAs moved discernibly in the cell cytoplasm while the other phage DNAs preferred to stay still (Fig. IV.8). There was no relationship between infection positions and moving motions, though needed further demonstration. For phage λ , the injected DNA molecule also moved via two distinct modes, localized motion and motion spanning the whole cell²⁰⁶. However, one or the other mode was preferred depending on where the phage DNA was injected into the cell. When entering within the quarter to mid-cell region, phage DNA motions were more likely to span the whole cell; on the other hand, when the entry point was within the quarter-cell to polar region, the phage DNA tended to exhibit more localized motions.

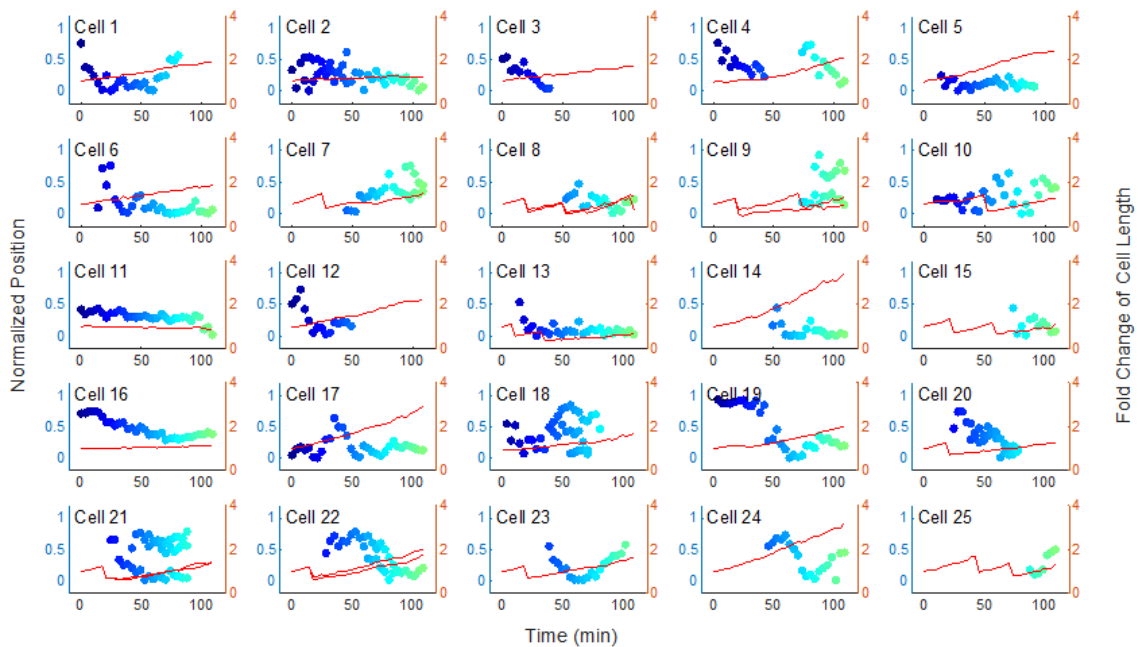


Figure IV.8 Monitoring phage DNA movement during P1 infection.

DNA locations in 25 infected cells are tracked during phage infection using SeqA-mKate2 system. The location of viral DNA is normalized to cell length with 0 and 1 representing the mid-cell and the polar region, respectively. 0 min indicates the start of infection movie. Dots evince the data of phage DNA locations in the host cell during imaging process. To present the data clearly, dots at different time points are separated by different colors. Fluorescently labeled phage DNAs appear at different time points along the detection. Some of the phage DNAs exhibit more movement than the others and the motion of movement has no correlation with infection sites. The replicated daughter DNAs can stay together or get separate. Fold changes of cell length are also plotted over time for each infected cell and daughter cell (red line). The dramatic drop of cell length indicates cell division.

Further, infected cells could be grouped into two major types based on DNA intensities. As shown in Fig. IV.9, in both groups, DNA intensities were doubled in 15-30 min after phage DNA was transmitted into the host cell. However, in later times, DNA intensities keep unchanged in one group of infected cells while reduced in the other. It has been shown that P1 encodes a DNA methyltransferase (Dmt) from a C1-controlled promoter¹², which can complement the defect in *dam* mutants of *E. coli*^{273,274}. One possible explanation of the decreased DNA intensity is that C1 fails to inhibit lytic gene expression, thereby the cell enters lytic lifecycle and Dmt proteins are expressed to methylate GATC sites on host chromosome. The increased number of binding sites dilutes SeqA-mKate2 from viral DNA. On the other hand, the unchanged DNA intensity indicates an efficient C1 repression, thereby the infected cell undergoes lysogenic development. Of note, it is hard to track the whole cell infection cycle using our current system. Since the 0.2% agarose gel dried quickly, cells growth halted when it was dehydrated and final outcomes could not be observed. Infection experiments were also tried in microfluidics chambers, where cells can survive longer. However, I did not observe lysogeny due to unknown reasons. More optimization will be necessary in the future studies.

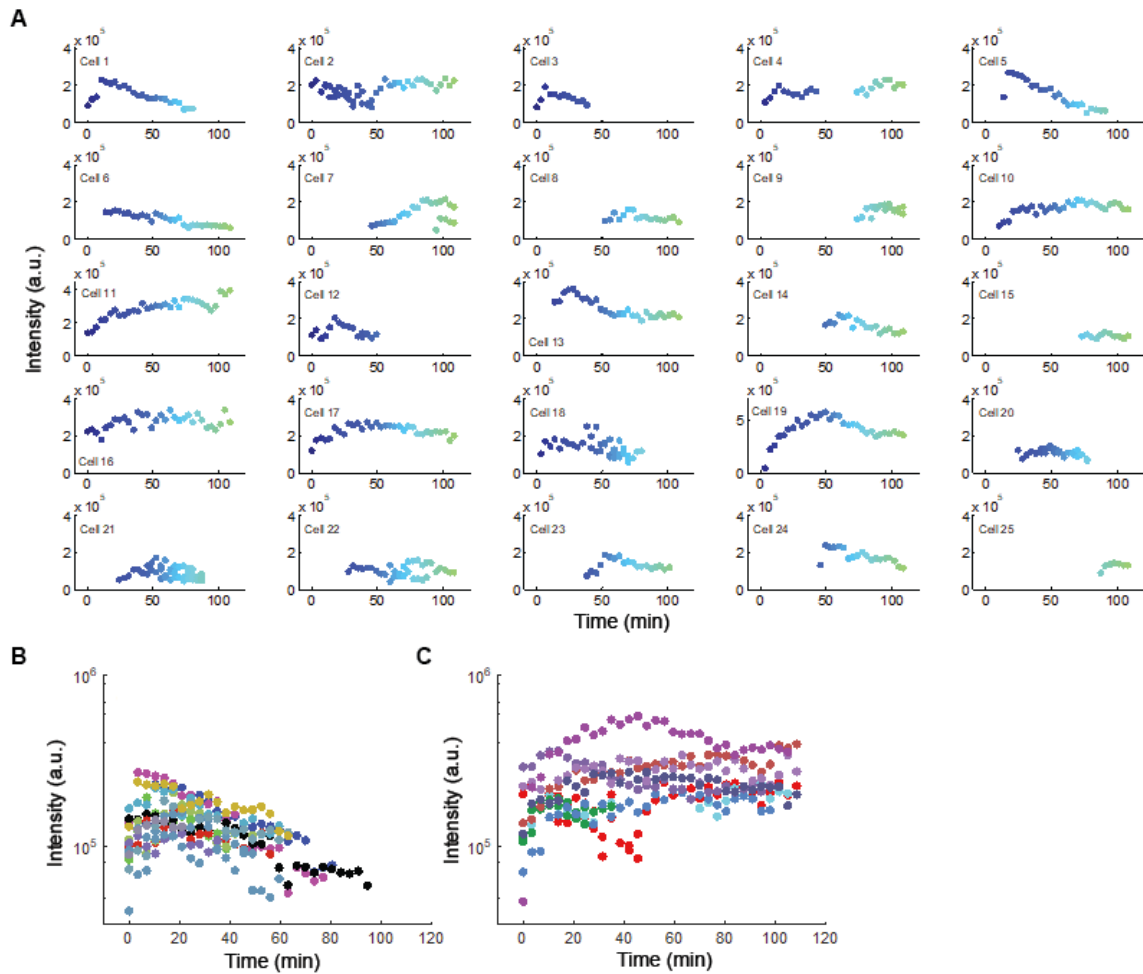


Figure IV.9 DNA replication over time after phage infection.

(A) DNA replications are analyzed in the same 25 infected cells in Fig. IV.8. 0 min indicates the start of infection movie. Dots evince intensities of the fluorescently labeled phage DNA in the host cell during imaging process. To present the data clearly, dots at different time points are separated by different colors. (B-C) These cells are categorized into two groups based on the DNA intensity. Each color represents the data of a single cell and the data of all cells are aligned with the timing that the DNA first appears inside the host cell. The intensities of the initial injected phage DNAs are comparable in these two groups and doubled at 15-30 min after DNA injection. However, in later times, viral DNA intensities do not change in one group (C) of infected cells while reduced in the other (B), suggesting distinct rates of DNA replication, probably corresponding to different phage decisions.

Mixed Infection from Phages with Different Lysogenization Capabilities

To understand how the interaction between co-infecting phages contribute to the final cell-fate decision, we constructed two sets of P1 phages (Fig. IV.10). For the phage 1 (CFP phage): we introduced gp23-mTurquoise2 fusion on the P1 capsid to identify infecting virions, in combination with *cI* transcriptional labeling with *mVenus* to evince gene expression and lysogenic pathway. Similarly, we made phage 2 (mCherry phage) with gp23-mCherry and *cI-mKO2*. In addition, we introduced the lytic reporter plasmid in the host cells to indicate lytic growth. There are some shortcomings of the current constructed system for mixed infection. First, since the lytic signal is generated from a reporter plasmid, it is impossible to differentiate the origin of the late gene activator or indicate the decision made by each infecting phage. Second, when tested in separate experiments, phage 1 and phage 2 exhibited different probabilities of lysogeny, though both showed MOI-independent manners (Fig. IV.12). This might be because different FPs had different effect on C1 expression or stability. From a different perspective, they can be seen as phages with distinct C1 repression activities and lysogenization capabilities. In addition, the localizations of the phage adsorbing on the cell surface and the dark infection rates were comparable for both phages; while phage 1 showed lower frequency of failed infection than phage 2 (Fig. IV.11 and Table IV.1). Finally, fluorescent proteins used for *cI* labeling have different maturation times^{275,276} (t_{50} is 5 min for mVenus and 1-2 hrs for mKO2 at 30°C), resulting in difficulties to determine the expression of C1-mKO2, especially at the beginning of phage infection. It is possible

that some of the mKO2 expression was lost in the lytic cells, which might be the reason of the higher failed infection rate of phage 2.

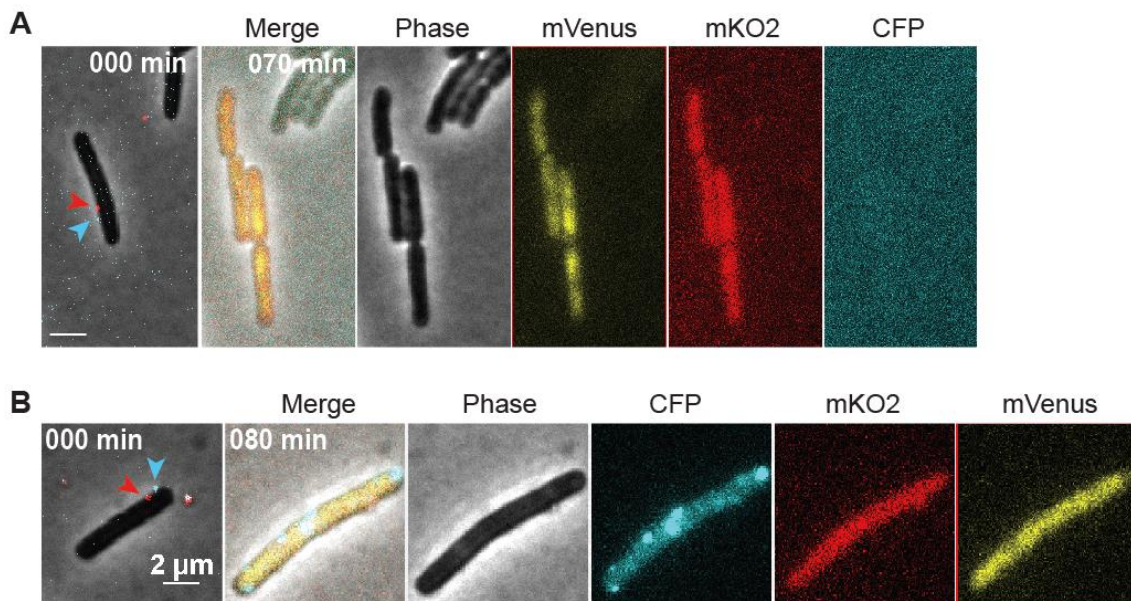


Figure IV.10 Representative images of the co-infection system.

Cells are infected with a CFP phage (blue arrow) and a mCherry phage (red arrow). (A) A lysogenic cell expresses both C1-mVenus and C1-mKO2 from different phages at 70 min. The host cell has divided twice. (B) An infected cell enters the lytic pathway. It expresses both C1-mVenus and C1-mKO2 at 80 min. The lytic signal (CFP) is induced from the lytic reporter plasmid. Scale bar = 2 μm.

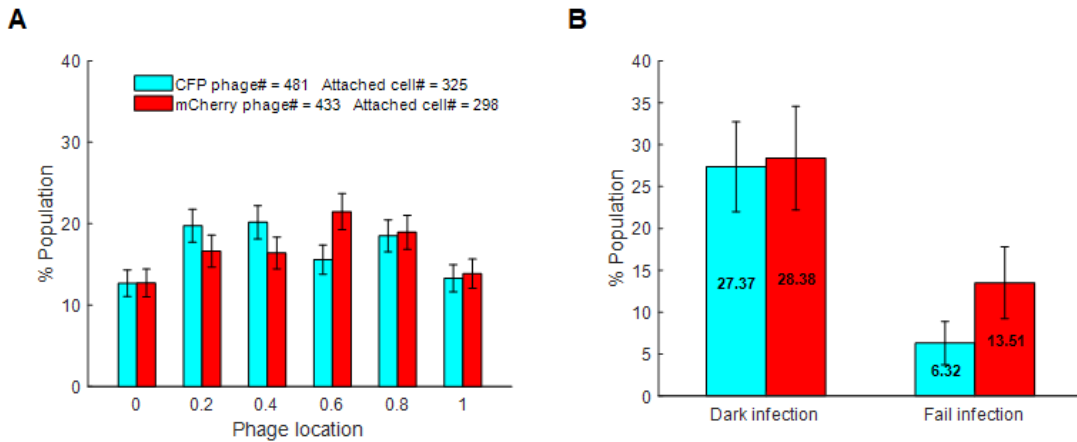


Figure IV.11 The localization and infection rate of CFP and mCherry phages. (A) Both phages show uniform distribution on host cell surface. Phage location is normalized to cell length where 0 represents mid-cell and 1 represents cell poles. (B) Both phages exhibit similar dark infection rate while mCherry phage has higher failed infection rate than CFP phage.

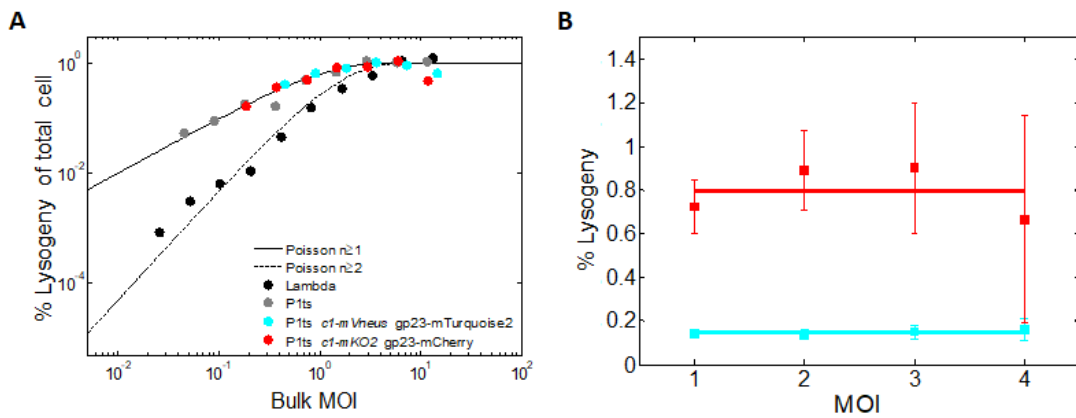


Figure IV.12 CFP and mCherry phages show different probabilities of lysogeny. (A) The probability of lysogeny is tested at the bulk level. Possibilities of lysogeny for P1 with different *cl* labeling as a function of bulk MOI (total phage/total cell), follow the theoretical prediction of Poisson distribution of $N \geq 1$. Whereas lysogenic response of phage λ follows the theoretical prediction of Poisson distribution of $N \geq 2$. Data are shifted with the maximum % lysogeny of 100%. (B) The probability of lysogeny is tested at the single-cell level. The mCherry phage shows overall higher probability to lysogenize the host cell than the CFP phage, although both exhibit MOI-independent manner.

Table IV.1 Probabilities of lysogeny over infected cells for WT, CFP and mCherry phages tested separately in bulk assays.

| | | | | | | | |
|---------|-----------|-------|-------|-------|-------|-------|-------|
| WT | API | 4.29 | 2.49 | 1.28 | 0.74 | 0.37 | 0.19 |
| | %Lysogeny | 30.07 | 31.28 | 43.03 | 37.20 | 45.14 | 26.81 |
| CFP | API | 12.09 | 6.36 | 3.96 | 2.13 | 1.11 | 0.56 |
| | %Lysogeny | 2.17 | 2.50 | 3.42 | 3.06 | 3.22 | 3.14 |
| mCherry | API | 4.77 | 3.77 | 2.03 | 1.03 | 0.52 | 0.26 |
| | %Lysogeny | 14.72 | 13.30 | 18.99 | 15.18 | 17.72 | 14.61 |

With these concerns in mind, we could first briefly look at the correlation between C1 expressions and cell outcomes. During the mixed infection (Fig. IV.13), around two third of cells, infected by both phages (CFP and mCherry), only exhibited one type of C1 signal (pure expression), indicating that the repressor produced from one phage quickly inhibit the expression of genes on the others, which reaffirmed the observation of non-individual decisions of P1 in normal-sized cells (Chapter III). Moreover, cells with C1-mVenus domination have higher chance to enter the lytic pathway; whereas cells with C1-mKO2 domination have higher chance to be lysogenized. By far, it is hard to make any conclusive statements and I believe that an improved co-infection system can allow us to reveal more interesting findings between phage interactions and final cell outcomes.

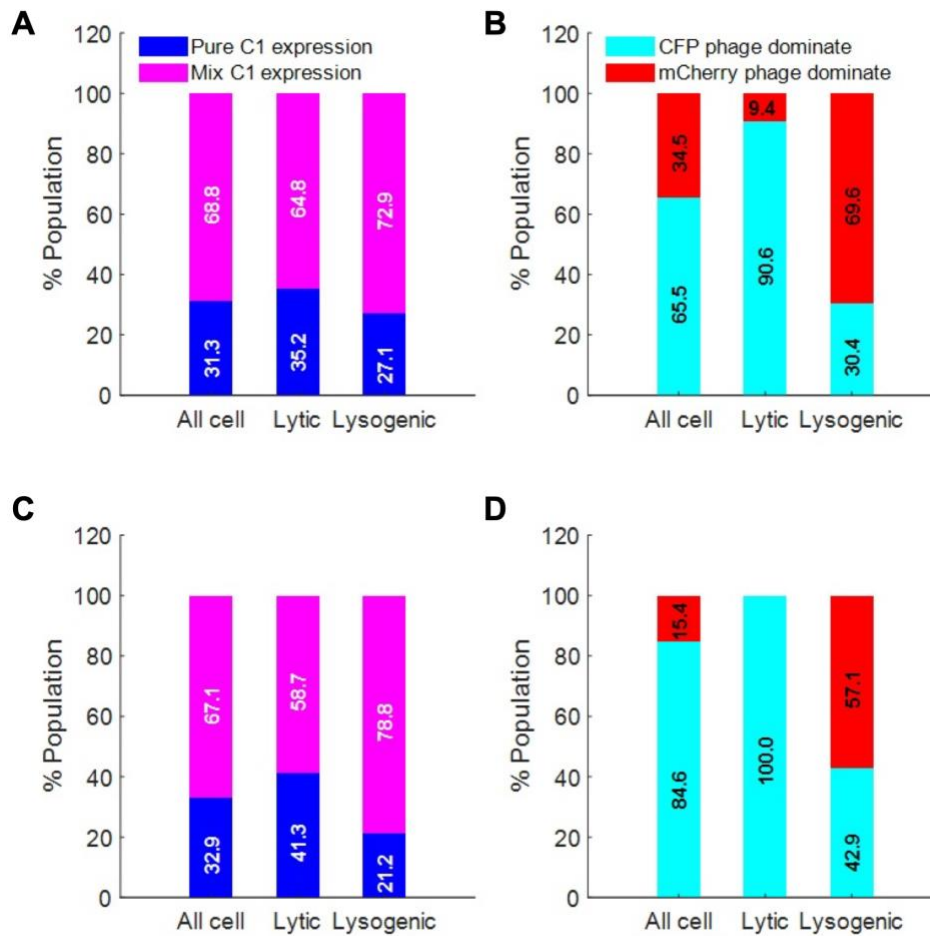


Figure IV.13 A quantitative analysis of C1 expression in infected cells adsorbed by different phages.

(A) In all mixed infection events, the majority of the cells exhibit single phage C1 signal. This pure C1 expression pattern dominates in both lytic and lysogenic cells. (B) Cells with single C1-mVenus (CFP phage) expression have higher chance of ending up with lytic pathway; whereas cells with single C1-mKO2 (mCherry phage) expression have higher chance to be lysogenized. C1 expression in cells with one CFP and one mCherry phage attached are shown here as well (C and D).

Discussion

Decision-making is a ubiquitous and essential process among all life forms. Our research investigates the mechanisms of noisy phenotypes during cellular decision-making with the purpose to make accurate predictions of or even control cell-fate outcomes. In recent years, some studies began to elucidate the origins of the heterogeneity of cell fate. In the parallel, measurements of cellular parameters with higher-resolution techniques unveiled more variables that had a deterministic effect on cell fate, which explained away some of the observed cell-fate heterogeneity. In our previous work, we have shown that $P1$ and λ serve as “opposite” paradigms in the spectrum of stochastic lysis-lysogeny decision-making, in terms of the sensitivities towards the number of infecting phages. Here, we further examined certain pre- and post-infection parameters of $P1$ at single-cell/single-virus level, in order to have a more advanced and complementary understanding on the noisy decisions of temperate phages.

In particular, we first demonstrated that the growth state of the host cell influenced cellular outcome and cells in stationary phase exhibited higher probabilities of lysogeny compared with the cells in exponential phase. Besides environmental nutrient conditions, bacterial growth phase also reflects the cell size, growth rate and metabolic state (such as ATP level)^{277,278} of the host cell. For cells growing faster, there will be more intracellular machinery available for DNA replication and protein synthesis, representing a higher level of productivity. Our data indicate that cell growth state hence host productivity can bias the decision-making process, causing certain cellular fates to be more frequently chosen. Specifically, when $P1$ infecting a group of

bacteria cells, there will be a fixed number of infected cells that undergo lysogenic growth^{56,130}, as we demonstrate previously. Therefore, lysing the host with higher potency to produce progeny phages and lysogenizing the cell with less productivity is an optimal solution to propagate its genomic information. Considering the presence of heterogeneous growth rates within bacterial populations during infection to mammalian systems²⁷⁹ and the positive correlation between bacteria growth rate and antibiotic lethality²⁸⁰⁻²⁸³, it would be rewarding to investigate how phage can detect cellular states and make final decisions.

Cells from different growth phases can vary in enormous ways, especially inherent gene expression²⁸⁴⁻²⁸⁶. A few single-cell techniques, including smFISH, immunofluorescence and fluorescent labeling of target proteins have been used to characterize distinct gene expression in lytic and lysogenic cells. To get a more comprehensive expression profile with higher dimensions, one can consider performing single-cell sequencing in decision-making studies. Single-cell sequencing methods analyze mRNA transcripts from lots of individual cells simultaneously while able to retain transcripts' cell origin. One of them is called Drop-seq²⁸⁷⁻²⁹⁰, a strategy based on the use of microfluidics for quickly profiling thousands of individual cells by encapsulating them in tiny aqueous droplets with different barcodes. The barcodes have oligo-dT oligos attached on the surface of microparticles (beads), allowing to capture the RNA that comes from each cell that is co-encapsulated. Therefore, a foundation of this method is to generate droplets contains one cell and one bead. Through engineering both microfluidic device and beads, a similar method called 10X Genomics Chromium^{291,292}

shows a 90% of the droplets contain one bead and only one cell, where the reverse transcription reactions are also subjected. An another method, called SPLiT-seq (split-pool ligation-based transcriptome sequencing), relies on the cells themselves as compartments to partition single cells²⁹³ rather than using droplets and specific instruments. In SPLiT-seq, cDNA is generated with an in-cell reverse transcription reaction and individual transcriptomes are labeled by four rounds of combinatorial barcoding which is enough to uniquely label over one million cells. In addition, it is possible to do other things with single cell sequencing platforms, such as quantifying proteins. One related method is called CITE-seq²⁹⁴, in which oligonucleotide-labeled antibodies are used to incorporate cellular protein and transcriptome measurements into single-cell readouts. The antibodies are similar with the ones used for flow cytometry analysis, but instead of a fluorophore or an isotope, it is conjugated a DNA barcode. The DNA barcode constitutes a terminal PCR handle sequence, a unique barcode specifically for each antibody and a polyA tail to bind with beads. Moreover, some advanced studies also integrate single-cell sequencing with live-cell imaging in the same individual cell^{295,296}. By far, these methods were developed and mainly used for eukaryotic cell analysis. Considering that the diverse bacterial cell walls and membranes often interfere with the cell lysis or permeabilization step, a recent technique, based on SPLiT-seq (microSPLiT-seq), was designed to perform single-cell RNA sequencing for bacterial cells, through including an additional step to remove cell walls, as well as optimizing the fixation and permeabilization steps for a higher level of RNA enrichment²⁹⁷. Proper

applications of these techniques in cellular decision-making will help us disclose more details in cell-to-cell variations and their correlations with cell-fate heterogeneity.

Methods

Bulk Lysogenization Assay

We measured the probability of lysogeny upon infection of *E. coli* cells at different growth phases as a function of the MOI. An overnight culture of host strain (MG1655) was diluted for 100-fold into LB with 10 mM MgSO₄ and 5mM CaCl₂ and grown at 37°C with 275 r.p.m. shaking. Once OD600 is around 0.4 and 1.2, transfer 1.5 mL of cell sample to a 2 mL tube and chill at 4°C for 10 min. Then, 100 μL of the cell was added to 100 μL of phage solutions with different concentrations. After a 30 min-incubation at 30°C, we transferred 20 μL of the mixture into 980 μL ice-cold LB and SM buffer to stop the adsorption process. Aliquots in LB media were plated on LBCM plates and incubated overnight at 30°C. Lysogen concentrations were determined by counting the number of CM^R colonies. To examine the concentration of free phages or the phages that were not adsorbed to host cells, we centrifuged the aliquots of phage-cell mixture in SM buffer at max speed for 2 min and titrated the supernatant on MG1655. Total phage and bacteria concentrations were measured using plate assays as well. Bulk MOI = total phage/total cell. The probability of lysogeny of all cells or of the infected cells (determined from the bulk MOI using the Poisson distribution with cumulative probability ≥ 1) was plotted as a function of the MOI on a log-log scale. MOI_{infected} is calculated by (total phages – nonadsorbed phage)/total cell.

RNA FISH

smFISH experiment to test gene *sit* expression followed the same protocol described in Chapter III (Fig. IV.14). Probes are listed Table IV.2.

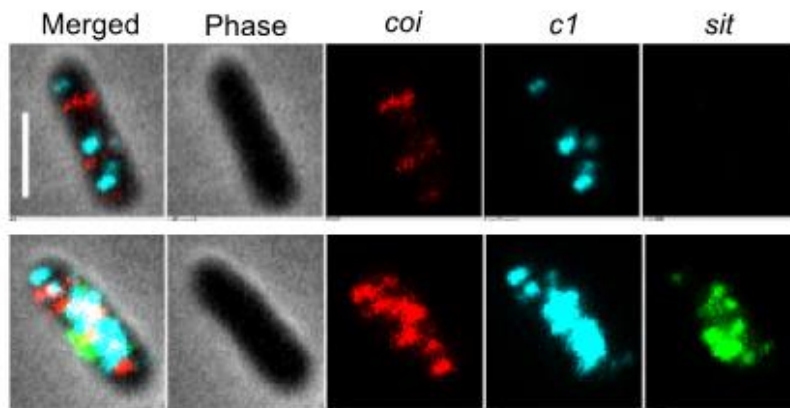


Figure IV.14 Representative images showing mRNA expression. Test *c1*, *coi* and late gene *sit* expression at 30 min (top) and 60 min (bottom) after infection. Cyan: *c1*; Red: *coi*; Green *sit*. Scale bar = 2 μ m.

Table IV.2 smFISH RNA probes.

| Probe name | Sequence (5' to 3') |
|------------|-----------------------|
| P1-sit-1 | GACTTTCTGGCACCATTAAG |
| P1-sit-2 | TCATTGCCACGAATCACATC |
| P1-sit-3 | AAACCTTTTCTACGGCTGTT |
| P1-sit-4 | ACATCGGCACTATTTTGTGA |
| P1-sit-5 | GTTTTTGGGTGTTAACCTGA |
| P1-sit-6 | TGCTCCTGAAGTTCCTGAAC |
| P1-sit-7 | TGATCAAGGGCGCTGAGAAT |
| P1-sit-8 | AATAGTTTGGACAGCAAGCC |
| P1-sit-9 | AGCTTTTTTCAGCATGCCAC |
| P1-sit-10 | CGTAGCATTCCCTACAAGTTT |
| P1-sit-11 | GAGAGTCTTCTTACCACCAC |
| P1-sit-12 | AACCAAATCTCCGCCTTCAT |
| P1-sit-13 | TAACGCCCTTTACCAACTG |
| P1-sit-14 | CGCATCATAAATACCTCCAG |
| P1-sit-15 | CGCTTCTGTATCATTCCAAC |
| P1-sit-16 | GAATGATGGATCTTGTCCCTG |
| P1-sit-17 | ACGTATAAGCGGATTTTTGC |
| P1-sit-18 | CTGCTAATACCAGATACCAG |
| P1-sit-19 | AGTGATTTGAGAACCTCACC |
| P1-sit-20 | ATTGCCGATATCCTCAAATC |
| P1-sit-21 | TTCCGTCGAAAATGATTGCA |
| P1-sit-22 | TATCAATGGCCTGGGCAATA |
| P1-sit-23 | GTTTCTAAGTTGGTAATCCC |
| P1-sit-24 | GTGTCGCCAAGGTTAGAAAT |
| P1-sit-25 | GTGTCGCCAAGGTTAGAAAT |
| P1-sit-26 | AACAGCATCACCAATCTTTG |
| P1-sit-27 | ATGTATCGCTAAACCATGCT |
| P1-sit-28 | CAGCTTTTCAAGCAGCTTAT |
| P1-sit-29 | GTAAAGAAGTCCTTGATGGC |
| P1-sit-30 | AACCTGTTTCAGGTTATCGA |
| P1-sit-31 | GCACTATCAATTGCATCACT |
| P1-sit-32 | CCCTGGGTTCTGAATGAAAT |
| P1-sit-33 | CATCTAATGCTTTACCTGGT |
| P1-sit-34 | TTTTTAACGGCATCAACCGC |

Table IV.2 Continued.

| | |
|-----------|----------------------|
| P1-sit-35 | ATACAATCATTGCCGCAGGG |
| P1-sit-36 | CCGATCGGATTGGGTATTTT |
| P1-sit-37 | TGGAGTGATTTCTTTCGCAT |
| P1-sit-38 | GCTATTAACCGGAGCTTTTA |
| P1-sit-39 | TAGAATCAGACGTCTCCTGG |
| P1-sit-40 | CTGTTTGGCATCGGATTCAG |
| P1-sit-41 | TATCACGCGGGTAGCAATAT |
| P1-sit-42 | TTCTACGGCATTTCATTGA |
| P1-sit-43 | AATTTTCTGCAACGCGCTAT |
| P1-sit-44 | CCAGTGGTATTAAGCGACGA |
| P1-sit-45 | GCAGCTTTCTGAATGTCATT |
| P1-sit-46 | CCAAGACTTCCGACTTTTAC |
| P1-sit-47 | GAGATTTGCCTTACCTTCAG |
| P1-sit-48 | GCAAATACGGAGCCA ACTT |

Monitoring Phage DNA Movement and Replication

An overnight of LZ1387 was diluted for 100-fold in LBM and grown till $OD_{600} \sim 0.4$. Add $CaCl_2$ to a final concentration of 5 mM. Then, purified P1LZ1856 phages were mixed with the cell to reach an MOI around 1, followed by incubation for 5 min at RT to allow some adsorption. Load 1 μ L of the sample on 1 mm 0.2% LB agarose pad resting on a small coverslip (18 \times 18 mm, Fisher Scientific). After resting for 1 min, a large coverslip (24 \times 50 mm, Fisher Scientific) was gently overlaid and the sample was imaged under the microscope at 30 °C inversely. To make a 0.2% agarose pad, first melted 0.02 g of agarose powder in 10 mL LB medium, and then loaded 0.5 mL agarose solution on a small coverslip. Let the solution cool down a bit and overlay a big coverslip. If gently enough, the liquid solution would pave the whole area but not spread out from edge of the small coverslip. After 1 hr at room temperature, it became a semi-solidified agarose pad with 1 mm in width. When using it, gently removed the big coverslip with tweezers.

During the DNA injection movies, 5 z-stacks at spacing of 300 nm were taken in the DNA reporter channel throughout the whole movie to track the DNA focus. Cells were imaged were imaged at multiple stage positions (typically 12) in phase contrast (100 ms exposure for cell recognition) and Far Red (200 ms exposure for SeqA-mKate2 foci) channels at time intervals of 3 min for 2 hrs in total. The movies recorded the processes for the DNA injection as foci appeared in the infected cells.

Co-Infection Experiments

The construction of mCherry phages is followed the same protocols with CFP phages introduced in the materials and methods session in Chapter II.

Both phages (P1LZ1914 and P1LZ1941) were purified (the detailed protocol is described in Chapter II and III) then diluted to the same concentration and mixed together at a 1:1 ratio to generate the phage mixture for infection. For the purified CFP and mCherry phages, the titers are 4.7×10^{10} and 2.8×10^{10} pfu/mL, and labeling efficiencies (phages with both capsid labeling and viral DNA tested by DAPI labeling over the number of total phages) are 95.5% and 96.4%, respectively. Infection was done as previously described. Briefly, a 1 ml overnight culture of host LZ1915, grown at 37 °C (265 r.p.m. shaking) in LB, was diluted for 100-fold into LBM (50 μ L of overnight culture into 5 mL of LBM), and grown at 37 °C (265 r.p.m. shaking) until $OD_{600} \sim 0.4$. Once grown, 50 μ L of the phage mixture was then mixed with 50 μ L of MG1655 culture to reach an MOI around 1. After 30 min-incubation at 30°C, 1 μ L of the mixture was placed (pipette tips cut for wider opening) onto a 1.5% LB agarose pad setting on a small coverslip until visibly dry (~ 1 min), then covered by a large coverslip, and then moved to the microscope for time-lapse imaging, where the time=0 is set to the first time-lapse image taken.

To localize both CFP and mCherry phages surrounding the cells, a series of 7 z-axis images at spacing of 300 nm were taken through the CFP and mCherry channels using a 600 ms and 500 ms exposure for each. Cells were imaged at multiple stage positions (typically 16) in each experiment. During the time-lapse movie, the sample

was imaged in phase contrast (100 ms exposure for cell recognition), YFP (800 ms exposure for phage C1-mVenus expression), Orange (1.5 s exposure for phage C1-mKO2 expression), and CFP (100 ms exposure for lytic reporter signal) channels at time intervals of 5 min until cell fate was visible (3 hours in total).

Table IV.3 Phage Strains for Co-infection Experiments.

| Strain | Genotype | Titer (pfu/mL) | Labeling Efficiency % |
|------------------|--|----------------------|-----------------------|
| LZ1914 (CFP) | P1Cm, <i>cI</i> -100(ts) Δ <i>cin</i> , <i>cI</i> -mVenus-Kan ^R [pACYC177 PLlacO-1- <i>gene23</i> - | 4.7×10 ¹⁰ | 95.48 |
| LZ1941 (mCherry) | P1Cm, <i>cI</i> -100(ts) Δ <i>cin</i> , <i>cI</i> -mKO2-Kan ^R [pACYC177 <i>HindIII</i> -PLlacO-1- <i>gene23</i> (no | 2.8×10 ¹⁰ | 96.36 |

Linear-Tracking Analysis of Injected Phage DNA

Microscope images of the DNA injection were analyzed via a MATLAB-based software package called MicrobeTracker Suite²¹⁶. We first used MicrobeTracker program to outline the cells in each frame so that generates a cell index. Next, we utilized specific tools or supporting functions in the suite to determine the profile of signal along the cell, i.e., used the SpotFinder to detect the fluorescent foci inside cells and displayed the data as the cell length, the time of appearance for the fluorescent foci, the intensity of individual foci and their polarity of localization. In order to follow the infection event in the same cell overtime, parent and daughter cells are tracked by assigning cell index from each frame manually. All data were saved in comprehensive MATLAB format and processed by homemade MATLAB scripts to plot phage DNA movements and intensities as functions of time.

Analysis of Co-Infection Movies

Cell recognition in the phase-contrast channel was performed using the Schnitzcell (gift of Michael Elowitz, California Institute of Technology), with the purpose of generating cell indices. The numbers and positions of phages attached on the cell surface, as well as cell lengths were measured manually using the supporting tools of NIS element program. Cell fates and lysis times for each cell was recorded as well. All subsequent data analysis was performed in MATLAB.

In our experiments, the rate of failed infection was defined as the number of failed infections divided by total number of infected cells with $MOI = 1$. In the decision-making reporter system, the failed infection rate was 6.32% for CFP phage and 13.51 for

mCherry phage. Moreover, a fraction of the cells exhibited dark infections: cells without any observed infecting phages on the cell surface, exhibiting lysis or lysogeny. With careful treatment of the sample, the dark infection rate was 27.4% and 28.4% for CFP and mCherry phages respectively. The calculation is based on the assumption that dark infections were mainly MOI = 1 events. Of note, both failed and dark infection rates of these two phages were tested from separate single-cell infection assays.

CHAPTER V

SUMMARY AND CONCLUSION

In our work, we developed innovative tools to study the phage P1 lifecycle, from adsorption to lysis-lysogeny decision, at the single cell/virus and subcellular levels. The goal is to elucidate the hidden, detailed mechanisms that occur during P1 infection. Our findings complement the knowledge from paradigmatic phage λ and further unveil the diversified functions acquired by these two phages. Further, we hope the methods and discoveries from prokaryotic virus studies can be applied to varied cell types and benefit the understanding of phage-related antibiotic resistance development.

The Spatial Distribution of Phage P1 During Infection

Given complex spatial organization inside bacteria, we investigated the adsorption localization of phage P1 on the *E. coli* cell surface, and its influence on the subsequent DNA injection and lysis-lysogeny cell fate. In order to examine the spatial distribution of P1, we constructed fluorescent virions, and found that P1 showed no preference for binding to different cellular locations. Interestingly, the success rate of DNA injection was high and similar at different adsorption locations. The lysis-lysogeny decision-making was also independent of the spatial distribution of the phage adsorption. Based on our results, P1 has the ability to adsorb all over the cell surface with high injection rate, which guarantee the success of P1 infection and the progeny production. In contrast, several lines of research demonstrated that phage λ preferred to adsorb to the

cell poles and failed infection at cell poles was relatively lower. These different spatial behaviors of P1 and λ might reflect different infection strategies.

MOI-Independent Lysogenization

During infection of bacteria cells, P1 can make decisions to kill the cell and produce new phages (lysis) or maintain as a low copy plasmid and replicate autonomously (lysogeny). It has been reported that the probability of P1 lysogeny is independent of MOI tested at the bulk level. To investigate the underlying mechanisms, we combined multiple tools to target the relationship of the expression of viral regulatory proteins with cell outcomes. We found that the repression activity of lytic genes is a deterministic factor for P1 decisions. Interactions between three phage-encoded proteins controlled the repression activity of each phage which was remained in a constant level. Moreover, the limited space of the normal-sized *E. coli* cell allowed the communication between co-infecting phages, through moving to the same intracellular locations or sharing regulatory proteins. It suggested that all phages infecting the same host made an ensemble decision. Together with constant repression activity, P1 decision-making was MOI-independent. Finally, by increasing the distance between infecting phages, we achieved a higher level of individuality in P1 behaviors which imposed an MOI-dependent lysogenic response. Our work establishes a highly precise and quantitative framework to describe P1 lysogeny establishment. This system plays an important role in disseminating antibiotic resistance by P1-like plasmids, and provides a complementary in its features to the paradigmatic model λ .

To further examine the strategies acquired by different viruses that benefit their host survival, we can construct computational models to simulate the spreading processes of phage-carried antibiotic resistance during the infection. For example, the model can simulate spreading rate and stabilities of the antibiotic marker on phage backbones, as well as host population dynamics, by altering the input parameters including recognition receptors, prophage forms as autonomous plasmids or integrated DNA, and different lysogenization strategies that are dependent or independent of MOI. Corresponding bench studies can focus on testing the interaction of co-infecting phages, i.e. P1 and λ , in various conditions, different in ion concentrations, host compositions, infection timings and stress conditions.

More Deterministic Factors for P1 Decision-Making

If not virus-to-microbe cell ratio, phage P1 could sense other environmental factors to make decisions to achieve a high efficiency of genomic propagation. The role of host growth state in P1 decision-making process was investigated. It showed that host cells in the stationary phase had higher probabilities to enter the lysogenic pathway upon P1 infection. The ability to detect cellular states and make final decisions is important to survive in complex and fluctuated intracellular and environmental conditions.

Additionally, cell length is highly correlated with cell state and growth rate. When infecting bacteria from a clonal population, longer cells exhibited reduced probability of lysogenization. Moreover, heterogeneous growth rates within bacterial populations during infection has been demonstrated from *in vivo* studies²⁷⁹. Therefore, it would be

interesting and ideal to explore the implications of lytic-lysogenic switch inside human-associated systems.

We further plan to obtain a spatiotemporal quantitative picture of P1 DNA replication linking to different cell fates. In particular, we expect to understand how many different DNA replication patterns exist in lytic and lysogenic cells, which DNA replication clusters lead to the final cell fate, which DNA copy establishes as the lysogen, and how the physical separation of the co-infecting phages affects its replication and thereby its lysis-lysogeny decision. In this work, we revealed distinct patterns of DNA replication existing in lytic and lysogenic cells through the P1*tetO* system. Furthermore, using the SeqA system, two types of infected cells were indicated based on the DNA replication rate. Future studies can also focus on the P1 partitioning system. Since P1 encodes a plasmid partition system, ParB/*parS*, with its locus physically linked to the replication origin, it will be interesting to find out how this partition system plays a role in DNA replication in both lytic and lysogenic cells.

Finally, our mixed infection experiments of two P1 phages with different lysogenization capabilities indicated the repressed function of one phage on the other. The repressed function could be raised in various aspects such as DNA replication and gene expression. A combination of live-cell imaging and single-cell sequencing techniques would be recommended for the cell state and mixed infection studies.

REFERENCES

- 1 Brown-Jaque, M., Calero-Caceres, W. & Muniesa, M. Transfer of antibiotic-resistance genes via phage-related mobile elements. *Plasmid* **79**, 1-7, doi:10.1016/j.plasmid.2015.01.001 (2015).
- 2 De Martino, B., Kumaran, D., Seymour, B. & Dolan, R. J. Frames, biases, and rational decision-making in the human brain. *Science* **313**, 684-687, doi:10.1126/science.1128356 (2006).
- 3 Lennox, E. S. Transduction of linked genetic characters of the host by bacteriophage P1. *Virology* **1**, 190-206 (1955).
- 4 Moore, S. D. Assembling new Escherichia coli strains by transduction using phage P1. *Methods Mol Biol* **765**, 155-169, doi:10.1007/978-1-61779-197-0_10 (2011).
- 5 Li, X. T., Thomason, L. C., Sawitzke, J. A., Costantino, N. & Court, D. L. Positive and negative selection using the tetA-sacB cassette: recombineering and P1 transduction in Escherichia coli. *Nucleic Acids Res* **41**, e204, doi:10.1093/nar/gkt1075 (2013).
- 6 Saragliadis, A., Trunk, T. & Leo, J. C. Producing Gene Deletions in Escherichia coli by P1 Transduction with Excisable Antibiotic Resistance Cassettes. *J Vis Exp*, doi:10.3791/58267 (2018).

- 7 Boyd, E. F., Davis, B. M. & Hochhut, B. Bacteriophage-bacteriophage interactions in the evolution of pathogenic bacteria. *Trends Microbiol* **9**, 137-144, doi:10.1016/s0966-842x(01)01960-6 (2001).
- 8 Stevens, R. H., Zhang, H., Sedgley, C., Bergman, A. & Manda, A. R. The prevalence and impact of lysogeny among oral isolates of *Enterococcus faecalis*. *J Oral Microbiol* **11**, 1643207, doi:10.1080/20002297.2019.1643207 (2019).
- 9 Rabiey, M. *et al.* Phage biocontrol to combat *Pseudomonas syringae* pathogens causing disease in cherry. *Microb Biotechnol* **13**, 1428-1445, doi:10.1111/1751-7915.13585 (2020).
- 10 Desvaux, M. *et al.* Pathogenicity Factors of Genomic Islands in Intestinal and Extraintestinal *Escherichia coli*. *Front Microbiol* **11**, 2065, doi:10.3389/fmicb.2020.02065 (2020).
- 11 Balcazar, J. L. Bacteriophages as vehicles for antibiotic resistance genes in the environment. *PLoS Pathog* **10**, e1004219, doi:10.1371/journal.ppat.1004219 (2014).
- 12 Lobocka, M. B. *et al.* Genome of bacteriophage P1. *J Bacteriol* **186**, 7032-7068, doi:10.1128/JB.186.21.7032-7068.2004 (2004).
- 13 Blattner, F. R. *et al.* The complete genome sequence of *Escherichia coli* K-12. *Science* **277**, 1453-1462, doi:10.1126/science.277.5331.1453 (1997).
- 14 Walker, D. H., Jr. & Anderson, T. F. Morphological variants of coliphage P1. *J Virol* **5**, 765-782, doi:10.1128/JVI.5.6.765-782.1970 (1970).

- 15 Ikeda, H. & Tomizawa, J. I. Transducing fragments in generalized transduction by phage P1. 3. Studies with small phage particles. *J Mol Biol* **14**, 120-129 (1965).
- 16 Walker, J. T., Iida, S. & Walker, D. H., Jr. Permutation of the DNA in small-headed virions of coliphage P1. *Mol Gen Genet* **167**, 341-344 (1979).
- 17 Piya, D., Vara, L., Russell, W. K., Young, R. & Gill, J. J. The multicomponent antirestriction system of phage P1 is linked to capsid morphogenesis. *Mol Microbiol* **105**, 399-412, doi:10.1111/mmi.13705 (2017).
- 18 Iida, S., Hiestand-Nauer, R., Sandmeier, H., Lehnherr, H. & Arber, W. Accessory genes in the darA operon of bacteriophage P1 affect antirestriction function, generalized transduction, head morphogenesis, and host cell lysis. *Virology* **251**, 49-58, doi:10.1006/viro.1998.9405 (1998).
- 19 Calendar, R., Calendar, R. L. & Abedon, S. T. *The Bacteriophages*. (Oxford University Press, USA, 2006).
- 20 Iida, S., Meyer, J., Kennedy, K. E. & Arber, W. A site-specific, conservative recombination system carried by bacteriophage P1. Mapping the recombinase gene cin and the cross-over sites cix for the inversion of the C segment. *EMBO J* **1**, 1445-1453 (1982).
- 21 Hiestand-Nauer, R. & Iida, S. Sequence of the site-specific recombinase gene cin and of its substrates serving in the inversion of the C segment of bacteriophage P1. *EMBO J* **2**, 1733-1740 (1983).

- 22 Iida, S. *et al.* The bacteriophage P1 site-specific recombinase cin: recombination events and DNA recognition sequences. *Cold Spring Harb Symp Quant Biol* **49**, 769-777 (1984).
- 23 Haffter, P. & Bickle, T. A. Purification and DNA-binding properties of FIS and Cin, two proteins required for the bacteriophage P1 site-specific recombination system, cin. *J Mol Biol* **198**, 579-587 (1987).
- 24 Iida, S. & Hiestand-Nauer, R. Localized conversion at the crossover sequences in the site-specific DNA inversion system of bacteriophage P1. *Cell* **45**, 71-79, doi:10.1016/0092-8674(86)90539-8 (1986).
- 25 Iida, S. & Hiestand-Nauer, R. Role of the central dinucleotide at the crossover sites for the selection of quasi sites in DNA inversion mediated by the site-specific Cin recombinase of phage P1. *Mol Gen Genet* **208**, 464-468, doi:10.1007/BF00328140 (1987).
- 26 Kostrewa, D. *et al.* Three-dimensional structure of the E. coli DNA-binding protein FIS. *Nature* **349**, 178-180, doi:10.1038/349178a0 (1991).
- 27 Hubner, P. & Arber, W. Mutational analysis of a prokaryotic recombinational enhancer element with two functions. *EMBO J* **8**, 577-585 (1989).
- 28 Hubner, P., Haffter, P., Iida, S. & Arber, W. Bent DNA is needed for recombinational enhancer activity in the site-specific recombination system Cin of bacteriophage P1. The role of FIS protein. *J Mol Biol* **205**, 493-500, doi:10.1016/0022-2836(89)90220-9 (1989).

- 29 Huber, H. E., Iida, S., Arber, W. & Bickle, T. A. Site-specific DNA inversion is enhanced by a DNA sequence element in cis. *Proc Natl Acad Sci U S A* **82**, 3776-3780, doi:10.1073/pnas.82.11.3776 (1985).
- 30 Huber, H. E., Iida, S. & Bickle, T. A. Expression of the bacteriophage P1 cin recombinase gene from its own and heterologous promoters. *Gene* **34**, 63-72, doi:10.1016/0378-1119(85)90295-1 (1985).
- 31 Ali Azam, T., Iwata, A., Nishimura, A., Ueda, S. & Ishihama, A. Growth phase-dependent variation in protein composition of the Escherichia coli nucleoid. *J Bacteriol* **181**, 6361-6370, doi:10.1128/JB.181.20.6361-6370.1999 (1999).
- 32 Kamp, D., Kahmann, R., Zipser, D., Broker, T. R. & Chow, L. T. Inversion of the G DNA segment of phage Mu controls phage infectivity. *Nature* **271**, 577-580, doi:10.1038/271577a0 (1978).
- 33 Plasterk, R. H. & van de Putte, P. The invertible P-DNA segment in the chromosome of Escherichia coli. *EMBO J* **4**, 237-242 (1985).
- 34 Iida, S. *et al.* The Min DNA inversion enzyme of plasmid p15B of Escherichia coli 15T-: a new member of the Din family of site-specific recombinases. *Mol Microbiol* **4**, 991-997, doi:10.1111/j.1365-2958.1990.tb00671.x (1990).
- 35 Sandmeier, H., Iida, S. & Arber, W. DNA inversion regions Min of plasmid p15B and Cin of bacteriophage P1: evolution of bacteriophage tail fiber genes. *J Bacteriol* **174**, 3936-3944, doi:10.1128/jb.174.12.3936-3944.1992 (1992).
- 36 Sandmeier, H., Iida, S., Hubner, P., Hiestand-Nauer, R. & Arber, W. Gene organization in the multiple DNA inversion region min of plasmid p15B of E.coli

- 15T-: assemblage of a variable gene. *Nucleic Acids Res* **19**, 5831-5838, doi:10.1093/nar/19.21.5831 (1991).
- 37 Nguyen, H. A. *et al.* DNA inversion in the tail fiber gene alters the host range specificity of carotovoricin Er, a phage-tail-like bacteriocin of phytopathogenic *Erwinia carotovora* subsp. *carotovora* Er. *J Bacteriol* **183**, 6274-6281, doi:10.1128/JB.183.21.6274-6281.2001 (2001).
- 38 Silverman, M., Zieg, J., Hilmen, M. & Simon, M. Phase variation in *Salmonella*: genetic analysis of a recombinational switch. *Proc Natl Acad Sci U S A* **76**, 391-395, doi:10.1073/pnas.76.1.391 (1979).
- 39 Sandmeier, H. Acquisition and rearrangement of sequence motifs in the evolution of bacteriophage tail fibres. *Mol Microbiol* **12**, 343-350, doi:10.1111/j.1365-2958.1994.tb01023.x (1994).
- 40 Xue, Q. & Egan, J. B. DNA sequence of tail fiber genes of coliphage 186 and evidence for a common ancestor shared by dsDNA phage fiber genes. *Virology* **212**, 128-133, doi:10.1006/viro.1995.1461 (1995).
- 41 Sandulache, R., Prehm, P. & Kamp, D. Cell wall receptor for bacteriophage Mu G(+). *J Bacteriol* **160**, 299-303 (1984).
- 42 Bertani, G. Studies on lysogenesis. I. The mode of phage liberation by lysogenic *Escherichia coli*. *J Bacteriol* **62**, 293-300 (1951).
- 43 Luria, S. E., Adams, J. N. & Ting, R. C. Transduction of lactose-utilizing ability among strains of *E. coli* and *S. dysenteriae* and the properties of the transducing

- phage particles. *Virology* **12**, 348-390, doi:10.1016/0042-6822(60)90161-6 (1960).
- 44 Franklin, N. C. Mutation in gal U gene of E. coli blocks phage P1 infection. *Virology* **38**, 189-191 (1969).
- 45 Crawford, J. T. & Goldberg, E. B. The function of tail fibers in triggering baseplate expansion of bacteriophage T4. *J Mol Biol* **139**, 679-690 (1980).
- 46 Fermin, G., Mazumdar-Leighton, S. & Tennant, P. in *Viruses* (eds Paula Tennant, Gustavo Fermin, & Jerome E. Foster) 217-244 (Academic Press, 2018).
- 47 Garcia, L. R. & Molineux, I. J. Transcription-independent DNA translocation of bacteriophage T7 DNA into Escherichia coli. *J Bacteriol* **178**, 6921-6929, doi:10.1128/jb.178.23.6921-6929.1996 (1996).
- 48 Struthers-Schlinke, J. S., Robins, W. P., Kemp, P. & Molineux, I. J. The internal head protein Gp16 controls DNA ejection from the bacteriophage T7 virion. *J Mol Biol* **301**, 35-45, doi:10.1006/jmbi.2000.3940 (2000).
- 49 Iida, S., Streiff, M. B., Bickle, T. A. & Arber, W. Two DNA antirestriction systems of bacteriophage P1, darA, and darB: characterization of darA- phages. *Virology* **157**, 156-166 (1987).
- 50 Liu, J., Chen, C. Y., Shiomi, D., Niki, H. & Margolin, W. Visualization of bacteriophage P1 infection by cryo-electron tomography of tiny Escherichia coli. *Virology* **417**, 304-311, doi:10.1016/j.virol.2011.06.005 (2011).

- 51 Hofer, B., Ruge, M. & Dreiseikelmann, B. The superinfection exclusion gene (sieA) of bacteriophage P22: identification and overexpression of the gene and localization of the gene product. *J Bacteriol* **177**, 3080-3086, doi:10.1128/jb.177.11.3080-3086.1995 (1995).
- 52 Lu, M. J. & Henning, U. Superinfection exclusion by T-even-type coliphages. *Trends Microbiol* **2**, 137-139, doi:10.1016/0966-842x(94)90601-7 (1994).
- 53 Devlin, B. H., Baumstark, B. R. & Scott, J. R. Superimmunity: characterization of a new gene in the immunity region of P1. *Virology* **120**, 360-375, doi:10.1016/0042-6822(82)90037-x (1982).
- 54 Kliem, M. & Dreiseikelmann, B. The superimmunity gene sim of bacteriophage P1 causes superinfection exclusion. *Virology* **171**, 350-355, doi:10.1016/0042-6822(89)90602-8 (1989).
- 55 Sternberg, N., Sauer, B., Hoess, R. & Abremski, K. Bacteriophage P1 cre gene and its regulatory region. Evidence for multiple promoters and for regulation by DNA methylation. *J Mol Biol* **187**, 197-212, doi:10.1016/0022-2836(86)90228-7 (1986).
- 56 Rosner, J. L. Formation, induction, and curing of bacteriophage P1 lysogens. *Virology* **48**, 679-689 (1972).
- 57 Zabrovitz, S., Segev, N. & Cohen, G. Growth of bacteriophage P1 in recombination-deficient hosts of Escherichia coli. *Virology* **80**, 233-248, doi:10.1016/s0042-6822(77)80001-9 (1977).
- 58 Smith, G. General recombination. *Lambda II*, 175-209 (1983).

- 59 Amundsen, S. K., Taylor, A. F., Chaudhury, A. M. & Smith, G. R. recD: the
gene for an essential third subunit of exonuclease V. *Proc Natl Acad Sci U S A*
83, 5558-5562, doi:10.1073/pnas.83.15.5558 (1986).
- 60 Smith, G. R. How RecBCD enzyme and Chi promote DNA break repair and
recombination: a molecular biologist's view. *Microbiol Mol Biol Rev* **76**, 217-
228, doi:10.1128/MMBR.05026-11 (2012).
- 61 Singleton, M. R., Dillingham, M. S., Gaudier, M., Kowalczykowski, S. C. &
Wigley, D. B. Crystal structure of RecBCD enzyme reveals a machine for
processing DNA breaks. *Nature* **432**, 187-193, doi:10.1038/nature02988 (2004).
- 62 Spies, M. & Kowalczykowski, S. Homologous recombination by RecBCD and
RecF pathways. *The Bacterial Chromosome* **3** (2004).
- 63 Sakaki, Y. Inactivation of the ATP-dependent DNase of Escherichia coli after
infection with double-stranded DNA phages. *J Virol* **14**, 1611-1612,
doi:10.1128/JVI.14.6.1611-1612.1974 (1974).
- 64 Bachi, B. & Arber, W. Physical mapping of BglII, BamHI, EcoRI, HindIII and
PstI restriction fragments of bacteriophage P1 DNA. *Mol Gen Genet* **153**, 311-
324, doi:10.1007/BF00431596 (1977).
- 65 Sternberg, N. & Coulby, J. Recognition and cleavage of the bacteriophage P1
packaging site (pac). II. Functional limits of pac and location of pac cleavage
termini. *J Mol Biol* **194**, 469-479, doi:10.1016/0022-2836(87)90675-9 (1987).

- 66 Sternberg, N. & Coulby, J. Recognition and cleavage of the bacteriophage P1 packaging site (pac). I. Differential processing of the cleaved ends in vivo. *J Mol Biol* **194**, 453-468, doi:10.1016/0022-2836(87)90674-7 (1987).
- 67 Heinrich, J., Velleman, M. & Schuster, H. The tripartite immunity system of phages P1 and P7. *FEMS Microbiol Rev* **17**, 121-126, doi:10.1111/j.1574-6976.1995.tb00193.x (1995).
- 68 Heinzl, T., Lurz, R., Dobrinski, B., Velleman, M. & Schuster, H. C1 repressor-mediated DNA looping is involved in C1 autoregulation of bacteriophage P1. *J Biol Chem* **269**, 31885-31890 (1994).
- 69 Biere, A. L., Citron, M. & Schuster, H. Transcriptional control via translational repression by c4 antisense RNA of bacteriophages P1 and P7. *Genes Dev* **6**, 2409-2416, doi:10.1101/gad.6.12a.2409 (1992).
- 70 Heisig, A., Riedel, H. D., Dobrinski, B., Lurz, R. & Schuster, H. Organization of the immunity region immI of bacteriophage P1 and synthesis of the P1 antirepressor. *J Mol Biol* **209**, 525-538 (1989).
- 71 Yun, T. & Vapnek, D. Electron microscopic analysis of bacteriophages P1, P1Cm, and P7. Determination of genome sizes, sequence homology, and location of antibiotic-resistance determinants. *Virology* **77**, 376-385 (1977).
- 72 Citron, M. & Schuster, H. The c4 repressors of bacteriophages P1 and P7 are antisense RNAs. *Cell* **62**, 591-598 (1990).

- 73 Sternberg, N. A characterization of bacteriophage P1 DNA fragments cloned in a lambda vector. *Virology* **96**, 129-142, doi:10.1016/0042-6822(79)90179-x (1979).
- 74 Velleman, M., Heirich, M., Gunther, A. & Schuster, H. A bacteriophage P1-encoded modulator protein affects the P1 c1 repression system. *J Biol Chem* **265**, 18511-18517 (1990).
- 75 Schaefer, T. S. & Hays, J. B. The bof gene of bacteriophage P1: DNA sequence and evidence for roles in regulation of phage c1 and ref genes. *J Bacteriol* **172**, 3269-3277 (1990).
- 76 Johnson, B. F. Suppression of the lexC (ssbA) mutation of Escherichia coli by a mutant of bacteriophage P1. *Mol Gen Genet* **186**, 122-126 (1982).
- 77 Touati-Schwartz, D. A new pleiotropic bacteriophage P1 mutation, bof, affecting c1 repression activity, the expression of plasmid incompatibility and the expression of certain constitutive prophage genes. *Mol Gen Genet* **174**, 189-202 (1979).
- 78 Velleman, M., Heinzl, T. & Schuster, H. The Bof protein of bacteriophage P1 exerts its modulating function by formation of a ternary complex with operator DNA and C1 repressor. *J Biol Chem* **267**, 12174-12181 (1992).
- 79 Prentki, P., Chandler, M. & Caro, L. Replication of prophage P1 during the cell cycle of Escherichia coli. *Mol Gen Genet* **152**, 71-76 (1977).
- 80 Yarmolinsky, M. B. & Sternberg, N. in *The Bacteriophages* (ed R. Calendar) Ch. 291-438, 291-438 (Plenum Press, 1988).

- 81 Park, K., Han, E., Paulsson, J. & Chattoraj, D. K. Origin pairing ('handcuffing') as a mode of negative control of P1 plasmid copy number. *EMBO J* **20**, 7323-7332, doi:10.1093/emboj/20.24.7323 (2001).
- 82 Abeles, A. L. & Austin, S. J. P1 plasmid replication requires methylated DNA. *EMBO J* **6**, 3185-3189 (1987).
- 83 Abeles, A., Brendler, T. & Austin, S. Evidence of two levels of control of P1 oriR and host oriC replication origins by DNA adenine methylation. *J Bacteriol* **175**, 7801-7807, doi:10.1128/jb.175.24.7801-7807.1993 (1993).
- 84 Brendler, T., Abeles, A. & Austin, S. A protein that binds to the P1 origin core and the oriC 13mer region in a methylation-specific fashion is the product of the host seqA gene. *EMBO J* **14**, 4083-4089 (1995).
- 85 Brendler, T. & Austin, S. Binding of SeqA protein to DNA requires interaction between two or more complexes bound to separate hemimethylated GATC sequences. *EMBO J* **18**, 2304-2310, doi:10.1093/emboj/18.8.2304 (1999).
- 86 Chattoraj, D. K. Control of plasmid DNA replication by iterons: no longer paradoxical. *Mol Microbiol* **37**, 467-476 (2000).
- 87 Wickner, S., Skowyra, D., Hoskins, J. & McKenney, K. DnaJ, DnaK, and GrpE heat shock proteins are required in oriP1 DNA replication solely at the RepA monomerization step. *Proc Natl Acad Sci U S A* **89**, 10345-10349, doi:10.1073/pnas.89.21.10345 (1992).

- 88 Sozhamannan, S. & Chattoraj, D. K. Heat shock proteins DnaJ, DnaK, and GrpE stimulate P1 plasmid replication by promoting initiator binding to the origin. *J Bacteriol* **175**, 3546-3555, doi:10.1128/jb.175.11.3546-3555.1993 (1993).
- 89 Skowrya, D. & Wickner, S. The interplay of the GrpE heat shock protein and Mg²⁺ in RepA monomerization by DnaJ and DnaK. *J Biol Chem* **268**, 25296-25301 (1993).
- 90 DasGupta, S., Mukhopadhyay, G., Papp, P. P., Lewis, M. S. & Chattoraj, D. K. Activation of DNA binding by the monomeric form of the P1 replication initiator RepA by heat shock proteins DnaJ and DnaK. *J Mol Biol* **232**, 23-34, doi:10.1006/jmbi.1993.1367 (1993).
- 91 Wickner, S., Hoskins, J. & McKenney, K. Monomerization of RepA dimers by heat shock proteins activates binding to DNA replication origin. *Proc Natl Acad Sci U S A* **88**, 7903-7907 (1991).
- 92 Manen, D., Upegui-Gonzalez, L. C. & Caro, L. Monomers and dimers of the RepA protein in plasmid pSC101 replication: domains in RepA. *Proc Natl Acad Sci U S A* **89**, 8923-8927 (1992).
- 93 Komori, H. *et al.* Crystal structure of a prokaryotic replication initiator protein bound to DNA at 2.6 Å resolution. *EMBO J* **18**, 4597-4607, doi:10.1093/emboj/18.17.4597 (1999).
- 94 Mukhopadhyay, G., Sozhamannan, S. & Chattoraj, D. K. Relaxation of replication control in chaperone-independent initiator mutants of plasmid P1. *EMBO J* **13**, 2089-2096 (1994).

- 95 Das, N. & Chattoraj, D. K. Origin pairing ('handcuffing') and unpairing in the control of P1 plasmid replication. *Mol Microbiol* **54**, 836-849, doi:10.1111/j.1365-2958.2004.04322.x (2004).
- 96 Mukhopadhyay, S. & Chattoraj, D. K. Replication-induced transcription of an autorepressed gene: the replication initiator gene of plasmid P1. *Proc Natl Acad Sci U S A* **97**, 7142-7147, doi:10.1073/pnas.130189497 (2000).
- 97 Treptow, N., Rosenfeld, R. & Yarmolinsky, M. Partition of nonreplicating DNA by the par system of bacteriophage P1. *J Bacteriol* **176**, 1782-1786, doi:10.1128/jb.176.6.1782-1786.1994 (1994).
- 98 Abeles, A. L., Friedman, S. A. & Austin, S. J. Partition of unit-copy miniplasmids to daughter cells. III. The DNA sequence and functional organization of the P1 partition region. *J Mol Biol* **185**, 261-272, doi:10.1016/0022-2836(85)90402-4 (1985).
- 99 Fung, E., Bouet, J. Y. & Funnell, B. E. Probing the ATP-binding site of P1 ParA: partition and repression have different requirements for ATP binding and hydrolysis. *EMBO J* **20**, 4901-4911, doi:10.1093/emboj/20.17.4901 (2001).
- 100 Davey, M. J. & Funnell, B. E. Modulation of the P1 plasmid partition protein ParA by ATP, ADP, and P1 ParB. *J Biol Chem* **272**, 15286-15292, doi:10.1074/jbc.272.24.15286 (1997).
- 101 Funnell, B. E. The P1 plasmid partition complex at parS. The influence of Escherichia coli integration host factor and of substrate topology. *J Biol Chem* **266**, 14328-14337 (1991).

- 102 Bouet, J. Y. & Funnell, B. E. P1 ParA interacts with the P1 partition complex at parS and an ATP-ADP switch controls ParA activities. *EMBO J* **18**, 1415-1424, doi:10.1093/emboj/18.5.1415 (1999).
- 103 Davis, M. A., Martin, K. A. & Austin, S. J. Biochemical activities of the parA partition protein of the P1 plasmid. *Mol Microbiol* **6**, 1141-1147, doi:10.1111/j.1365-2958.1992.tb01552.x (1992).
- 104 Radnedge, L., Davis, M. A. & Austin, S. J. P1 and P7 plasmid partition: ParB protein bound to its partition site makes a separate discriminator contact with the DNA that determines species specificity. *EMBO J* **15**, 1155-1162 (1996).
- 105 Surtees, J. A. & Funnell, B. E. The DNA binding domains of P1 ParB and the architecture of the P1 plasmid partition complex. *J Biol Chem* **276**, 12385-12394, doi:10.1074/jbc.M009370200 (2001).
- 106 Rodionov, O., Lobočka, M. & Yarmolinsky, M. Silencing of genes flanking the P1 plasmid centromere. *Science* **283**, 546-549, doi:10.1126/science.283.5401.546 (1999).
- 107 Williams, D. R., Macartney, D. P. & Thomas, C. M. The partitioning activity of the RK2 central control region requires only incC, korB and KorB-binding site O(B)3 but other KorB-binding sites form destabilizing complexes in the absence of O(B)3. *Microbiology (Reading)* **144** (Pt 12), 3369-3378, doi:10.1099/00221287-144-12-3369 (1998).

- 108 Ravin, N. V., Rech, J. & Lane, D. Mapping of functional domains in F plasmid partition proteins reveals a bipartite SopB-recognition domain in SopA. *J Mol Biol* **329**, 875-889, doi:10.1016/s0022-2836(03)00525-4 (2003).
- 109 Grigoriev, P. S. & Lobočka, M. B. Determinants of segregational stability of the linear plasmid-prophage N15 of Escherichia coli. *Mol Microbiol* **42**, 355-368, doi:10.1046/j.1365-2958.2001.02632.x (2001).
- 110 Oppenheim, A. B., Kobilier, O., Stavans, J., Court, D. L. & Adhya, S. Switches in bacteriophage lambda development. *Annu Rev Genet* **39**, 409-429, doi:10.1146/annurev.genet.39.073003.113656 (2005).
- 111 Kutter, E. *et al.* Evolution of T4-related phages. *Virus Genes* **11**, 285-297, doi:10.1007/BF01728666 (1995).
- 112 Chiang, L. W. & Howe, M. M. Mutational analysis of a C-dependent late promoter of bacteriophage Mu. *Genetics* **135**, 619-629 (1993).
- 113 Artsimovitch, I., Murakami, K., Ishihama, A. & Howe, M. M. Transcription activation by the bacteriophage Mu Mor protein requires the C-terminal regions of both alpha and sigma70 subunits of Escherichia coli RNA polymerase. *J Biol Chem* **271**, 32343-32348, doi:10.1074/jbc.271.50.32343 (1996).
- 114 Wood, L. F., Tszine, N. Y. & Christie, G. E. Activation of P2 late transcription by P2 Ogr protein requires a discrete contact site on the C terminus of the alpha subunit of Escherichia coli RNA polymerase. *J Mol Biol* **274**, 1-7, doi:10.1006/jmbi.1997.1390 (1997).

- 115 Ghisotti, D. *et al.* Multiple regulatory mechanisms controlling phage-plasmid P4 propagation. *FEMS Microbiol Rev* **17**, 127-134, doi:10.1111/j.1574-6976.1995.tb00194.x (1995).
- 116 Lehnherr, H., Velleman, M., Guidolin, A. & Arber, W. Bacteriophage P1 gene 10 is expressed from a promoter-operator sequence controlled by C1 and Bof proteins. *J Bacteriol* **174**, 6138-6144, doi:10.1128/jb.174.19.6138-6144.1992 (1992).
- 117 Lehnherr, H., Guidolin, A. & Arber, W. Bacteriophage P1 gene 10 encodes a trans-activating factor required for late gene expression. *J Bacteriol* **173**, 6438-6445, doi:10.1128/jb.173.20.6438-6445.1991 (1991).
- 118 Lehnherr, H., Guidolin, A. & Arber, W. Mutational analysis of the bacteriophage P1 late promoter sequence Ps. *J Mol Biol* **228**, 101-107, doi:10.1016/0022-2836(92)90494-5 (1992).
- 119 Hansen, A. M., Lehnherr, H., Wang, X., Mobley, V. & Jin, D. J. Escherichia coli SspA is a transcription activator for bacteriophage P1 late genes. *Mol Microbiol* **48**, 1621-1631, doi:10.1046/j.1365-2958.2003.03533.x (2003).
- 120 Ishihama, A. & Saitoh, T. Subunits of RNA polymerase in function and structure. IX. Regulation of RNA polymerase activity by stringent starvation protein (SSP). *J Mol Biol* **129**, 517-530, doi:10.1016/0022-2836(79)90466-2 (1979).
- 121 Williams, M. D., Fuchs, J. A. & Flickinger, M. C. Null mutation in the stringent starvation protein of Escherichia coli disrupts lytic development of bacteriophage P1. *Gene* **109**, 21-30, doi:10.1016/0378-1119(91)90584-x (1991).

- 122 Cohen, G. Electron microscopy study of early lytic replication forms of bacteriophage P1 DNA. *Virology* **131**, 159-170, doi:10.1016/0042-6822(83)90542-1 (1983).
- 123 Skorupski, K., Pierce, J. C., Sauer, B. & Sternberg, N. Bacteriophage P1 genes involved in the recognition and cleavage of the phage packaging site (pac). *J Mol Biol* **223**, 977-989, doi:10.1016/0022-2836(92)90256-j (1992).
- 124 Walker, J. T. & Walker, D. H., Jr. Structural proteins of coliphage P1. *Prog Clin Biol Res* **64**, 69-77 (1981).
- 125 Kaiser, D. & Dworkin, M. Gene transfer to myxobacterium by Escherichia coli phage P1. *Science* **187**, 653-654, doi:10.1126/science.803710 (1975).
- 126 Downard, J. S. Tn5-mediated transposition of plasmid DNA after transduction to Myxococcus xanthus. *J Bacteriol* **170**, 4939-4941, doi:10.1128/jb.170.10.4939-4941.1988 (1988).
- 127 Rothenberg, E. *et al.* Single-virus tracking reveals a spatial receptor-dependent search mechanism. *Biophys J* **100**, 2875-2882, doi:10.1016/j.bpj.2011.05.014 (2011).
- 128 Zhang, K., Young, R. & Zeng, L. Bacteriophage P1 does not show spatial preference when infecting Escherichia coli. *Virology* **542**, 1-7, doi:10.1016/j.virol.2019.12.012 (2020).
- 129 Zeng, L. *et al.* Decision making at a subcellular level determines the outcome of bacteriophage infection. *Cell* **141**, 682-691, doi:10.1016/j.cell.2010.03.034 (2010).

- 130 Bertani, G. & Nice, S. J. Studies on lysogenesis. II. The effect of temperature on the lysogenization of *Shigella dysenteriae* with phage P1. *J Bacteriol* **67**, 202-209 (1954).
- 131 Trinh, J. T., Shao, Q., Guan, J. & Zeng, L. Emerging heterogeneous compartments by viruses in single bacterial cells. *Nat Commun* **11**, 3813, doi:10.1038/s41467-020-17515-8 (2020).
- 132 Trinh, J. T., Szekely, T., Shao, Q., Balazsi, G. & Zeng, L. Cell fate decisions emerge as phages cooperate or compete inside their host. *Nat Commun* **8**, 14341, doi:10.1038/ncomms14341 (2017).
- 133 Cortes, M. G., Trinh, J. T., Zeng, L. & Balazsi, G. Late-Arriving Signals Contribute Less to Cell-Fate Decisions. *Biophys J* **113**, 2110-2120, doi:10.1016/j.bpj.2017.09.012 (2017).
- 134 Shao, Q. *et al.* Lysis-lysogeny coexistence: prophage integration during lytic development. *Microbiologyopen* **6**, doi:10.1002/mbo3.395 (2017).
- 135 Shao, Q. *et al.* Coupling of DNA Replication and Negative Feedback Controls Gene Expression for Cell-Fate Decisions. *iScience* **6**, 1-12, doi:10.1016/j.isci.2018.07.006 (2018).
- 136 van der Pligt, J. in *International Encyclopedia of the Social & Behavioral Sciences* (eds Neil J. Smelser & Paul B. Baltes) 3309-3315 (Pergamon, 2001).
- 137 Starcke, K. & Brand, M. Decision making under stress: a selective review. *Neurosci Biobehav Rev* **36**, 1228-1248, doi:10.1016/j.neubiorev.2012.02.003 (2012).

- 138 Lovejoy, D. A. & Barsyte, D. *Sex, stress and reproductive success*. (Wiley-Blackwell, 2011).
- 139 Tversky, A. & Kahneman, D. The framing of decisions and the psychology of choice. *Science* **211**, 453-458, doi:10.1126/science.7455683 (1981).
- 140 Groman, S. M. *et al.* Orbitofrontal Circuits Control Multiple Reinforcement-Learning Processes. *Neuron* **103**, 734-746 e733, doi:10.1016/j.neuron.2019.05.042 (2019).
- 141 Maier, B. Competence and Transformation in *Bacillus subtilis*. *Curr Issues Mol Biol* **37**, 57-76, doi:10.21775/cimb.037.057 (2020).
- 142 Schultz, D., Wolynes, P. G., Ben Jacob, E. & Onuchic, J. N. Deciding fate in adverse times: sporulation and competence in *Bacillus subtilis*. *Proc Natl Acad Sci U S A* **106**, 21027-21034, doi:10.1073/pnas.0912185106 (2009).
- 143 van Sinderen, D. *et al.* comK encodes the competence transcription factor, the key regulatory protein for competence development in *Bacillus subtilis*. *Mol Microbiol* **15**, 455-462, doi:10.1111/j.1365-2958.1995.tb02259.x (1995).
- 144 Hamoen, L. W., Venema, G. & Kuipers, O. P. Controlling competence in *Bacillus subtilis*: shared use of regulators. *Microbiology (Reading)* **149**, 9-17, doi:10.1099/mic.0.26003-0 (2003).
- 145 Heurtier, V. *et al.* The molecular logic of Nanog-induced self-renewal in mouse embryonic stem cells. *Nat Commun* **10**, 1109, doi:10.1038/s41467-019-09041-z (2019).

- 146 Kalmar, T. *et al.* Regulated fluctuations in nanog expression mediate cell fate decisions in embryonic stem cells. *PLoS Biol* **7**, e1000149, doi:10.1371/journal.pbio.1000149 (2009).
- 147 Jeter, C. R., Yang, T., Wang, J., Chao, H. P. & Tang, D. G. Concise Review: NANOG in Cancer Stem Cells and Tumor Development: An Update and Outstanding Questions. *Stem Cells* **33**, 2381-2390, doi:10.1002/stem.2007 (2015).
- 148 Gawlik-Rzemieniewska, N. & Bednarek, I. The role of NANOG transcriptional factor in the development of malignant phenotype of cancer cells. *Cancer Biol Ther* **17**, 1-10, doi:10.1080/15384047.2015.1121348 (2016).
- 149 Rakonjac, J., Bennett, N. J., Spagnuolo, J., Gagic, D. & Russel, M. Filamentous bacteriophage: biology, phage display and nanotechnology applications. *Curr Issues Mol Biol* **13**, 51-76 (2011).
- 150 Wei, Q. *et al.* Global regulation of gene expression by OxyR in an important human opportunistic pathogen. *Nucleic Acids Res* **40**, 4320-4333, doi:10.1093/nar/gks017 (2012).
- 151 Li, Y. *et al.* Excisionase in Pf filamentous prophage controls lysis-lysogeny decision-making in *Pseudomonas aeruginosa*. *Mol Microbiol* **111**, 495-513, doi:10.1111/mmi.14170 (2019).
- 152 Secor, P. R. *et al.* Pf Bacteriophage and Their Impact on *Pseudomonas* Virulence, Mammalian Immunity, and Chronic Infections. *Front Immunol* **11**, 244, doi:10.3389/fimmu.2020.00244 (2020).

- 153 Sweere, J. M. *et al.* Bacteriophage trigger antiviral immunity and prevent clearance of bacterial infection. *Science* **363**, doi:10.1126/science.aat9691 (2019).
- 154 Secor, P. R. *et al.* Filamentous Bacteriophage Produced by *Pseudomonas aeruginosa* Alters the Inflammatory Response and Promotes Noninvasive Infection In Vivo. *Infect Immun* **85**, doi:10.1128/IAI.00648-16 (2017).
- 155 Bujak, K., Decewicz, P., Kaminski, J. & Radlinska, M. Identification, Characterization, and Genomic Analysis of Novel *Serratia* Temperate Phages from a Gold Mine. *Int J Mol Sci* **21**, doi:10.3390/ijms21186709 (2020).
- 156 Canchaya, C., Proux, C., Fournous, G., Bruttin, A. & Brussow, H. Prophage genomics. *Microbiol Mol Biol Rev* **67**, 238-276, table of contents, doi:10.1128/mnbr.67.2.238-276.2003 (2003).
- 157 Casjens, S. Prophages and bacterial genomics: what have we learned so far? *Mol Microbiol* **49**, 277-300, doi:10.1046/j.1365-2958.2003.03580.x (2003).
- 158 Keen, E. C. & Dantas, G. Close Encounters of Three Kinds: Bacteriophages, Commensal Bacteria, and Host Immunity. *Trends Microbiol* **26**, 943-954, doi:10.1016/j.tim.2018.05.009 (2018).
- 159 Miller-Ensminger, T. *et al.* Bacteriophages of the Urinary Microbiome. *J Bacteriol* **200**, doi:10.1128/JB.00738-17 (2018).
- 160 Paul, J. H. Prophages in marine bacteria: dangerous molecular time bombs or the key to survival in the seas? *ISME J* **2**, 579-589, doi:10.1038/ismej.2008.35 (2008).

- 161 Menouni, R., Hutinet, G., Petit, M. A. & Ansaldi, M. Bacterial genome remodeling through bacteriophage recombination. *FEMS Microbiol Lett* **362**, 1-10, doi:10.1093/femsle/fnu022 (2015).
- 162 Feiner, R. *et al.* A new perspective on lysogeny: prophages as active regulatory switches of bacteria. *Nat Rev Microbiol* **13**, 641-650, doi:10.1038/nrmicro3527 (2015).
- 163 Hargreaves, K. R., Kropinski, A. M. & Clokie, M. R. Bacteriophage behavioral ecology: How phages alter their bacterial host's habits. *Bacteriophage* **4**, e29866, doi:10.4161/bact.29866 (2014).
- 164 Davies, E. V., Winstanley, C., Fothergill, J. L. & James, C. E. The role of temperate bacteriophages in bacterial infection. *FEMS Microbiol Lett* **363**, fnw015, doi:10.1093/femsle/fnw015 (2016).
- 165 Gama, J. A. *et al.* Temperate bacterial viruses as double-edged swords in bacterial warfare. *PLoS One* **8**, e59043, doi:10.1371/journal.pone.0059043 (2013).
- 166 Nanda, A. M., Thormann, K. & Frunzke, J. Impact of spontaneous prophage induction on the fitness of bacterial populations and host-microbe interactions. *J Bacteriol* **197**, 410-419, doi:10.1128/JB.02230-14 (2015).
- 167 Brussow, H., Canchaya, C. & Hardt, W. D. Phages and the evolution of bacterial pathogens: from genomic rearrangements to lysogenic conversion. *Microbiol Mol Biol Rev* **68**, 560-602, table of contents, doi:10.1128/MMBR.68.3.560-602.2004 (2004).

- 168 Billard-Pomares, T. *et al.* Characterization of a P1-like bacteriophage carrying an SHV-2 extended-spectrum beta-lactamase from an Escherichia coli strain. *Antimicrob Agents Chemother* **58**, 6550-6557, doi:10.1128/AAC.03183-14 (2014).
- 169 Shin, J. & Ko, K. S. A Plasmid Bearing the bla(CTX-M-15) Gene and Phage P1-Like Sequences from a Sequence Type 11 Klebsiella pneumoniae Isolate. *Antimicrob Agents Chemother* **59**, 6608-6610, doi:10.1128/AAC.00265-15 (2015).
- 170 Li, R., Xie, M., Lv, J., Wai-Chi Chan, E. & Chen, S. Complete genetic analysis of plasmids carrying mcr-1 and other resistance genes in an Escherichia coli isolate of animal origin. *J Antimicrob Chemother* **72**, 696-699, doi:10.1093/jac/dkw509 (2017).
- 171 Venturini, C. *et al.* Diversity of P1 phage-like elements in multidrug resistant Escherichia coli. *Sci Rep* **9**, 18861, doi:10.1038/s41598-019-54895-4 (2019).
- 172 Kamal, S. M. *et al.* A recently isolated human commensal Escherichia coli ST10 clone member mediates enhanced thermotolerance and tetrathionate respiration on a P1 phage-derived IncY plasmid. *Mol Microbiol*, doi:10.1111/mmi.14614 (2020).
- 173 Kondo, E. & Mitsuhashi, S. Drug resistance of enteric bacteria. VI. Introduction of bacteriophage P1CM into Salmonella typhi and formation of PldCM and F-CM elements. *J Bacteriol* **91**, 1787-1794, doi:10.1128/JB.91.5.1787-1794.1966 (1966).

- 174 Okada, M. & Watanabe, T. Transduction with phage P1 in *Salmonella typhimurium*. *Nature* **218**, 185-187, doi:10.1038/218185a0 (1968).
- 175 Ornellas, E. P. & Stocker, B. A. Relation of lipopolysaccharide character to P1 sensitivity in *Salmonella typhimurium*. *Virology* **60**, 491-502, doi:10.1016/0042-6822(74)90343-2 (1974).
- 176 Murooka, Y. & Harada, T. Expansion of the host range of coliphage P1 and gene transfer from enteric bacteria to other gram-negative bacteria. *Appl Environ Microbiol* **38**, 754-757, doi:10.1128/AEM.38.4.754-757.1979 (1979).
- 177 Amati, P. Abortive infection of *Pseudomonas aeruginosa* and *Serratia marcescens* with coliphage P1. *J Bacteriol* **83**, 433-434, doi:10.1128/JB.83.2.433-434.1962 (1962).
- 178 Streiff, M. B., Iida, S. & Bickle, T. A. Expression and proteolytic processing of the *darA* antirestriction gene product of bacteriophage P1. *Virology* **157**, 167-171, doi:10.1016/0042-6822(87)90325-4 (1987).
- 179 Humbelin, M. *et al.* Type III DNA restriction and modification systems EcoP1 and EcoP15. Nucleotide sequence of the EcoP1 operon, the EcoP15 mod gene and some EcoP1 mod mutants. *J Mol Biol* **200**, 23-29, doi:10.1016/0022-2836(88)90330-0 (1988).
- 180 Hadi, S. M., Bachi, B., Iida, S. & Bickle, T. A. DNA restriction--modification enzymes of phage P1 and plasmid p15B. Subunit functions and structural homologies. *J Mol Biol* **165**, 19-34, doi:10.1016/s0022-2836(83)80240-x (1983).

- 181 Iida, S. *et al.* DNA restriction--modification genes of phage P1 and plasmid
p15B. Structure and in vitro transcription. *J Mol Biol* **165**, 1-18,
doi:10.1016/s0022-2836(83)80239-3 (1983).
- 182 Ikeda, H. & Tomizawa, J. Prophage P1, and extrachromosomal replication unit.
Cold Spring Harb Symp Quant Biol **33**, 791-798 (1968).
- 183 Lehnherr, H., Maguin, E., Jafri, S. & Yarmolinsky, M. B. Plasmid addiction
genes of bacteriophage P1: doc, which causes cell death on curing of prophage,
and phd, which prevents host death when prophage is retained. *J Mol Biol* **233**,
414-428, doi:10.1006/jmbi.1993.1521 (1993).
- 184 Gazit, E. & Sauer, R. T. The Doc toxin and Phd antidote proteins of the
bacteriophage P1 plasmid addiction system form a heterotrimeric complex. *J Biol*
Chem **274**, 16813-16818, doi:10.1074/jbc.274.24.16813 (1999).
- 185 El Haddad, L., Harb, C. P., Gebara, M. A., Stibich, M. A. & Chemaly, R. F. A
Systematic and Critical Review of Bacteriophage Therapy Against Multidrug-
resistant ESKAPE Organisms in Humans. *Clin Infect Dis* **69**, 167-178,
doi:10.1093/cid/ciy947 (2019).
- 186 Gordillo Altamirano, F. L. & Barr, J. J. Phage Therapy in the Postantibiotic Era.
Clin Microbiol Rev **32**, doi:10.1128/CMR.00066-18 (2019).
- 187 Manrique, P. *et al.* Healthy human gut phageome. *Proc Natl Acad Sci U S A* **113**,
10400-10405, doi:10.1073/pnas.1601060113 (2016).
- 188 Bollyky, P. L. & Secor, P. R. The Innate Sense of Bacteriophages. *Cell Host*
Microbe **25**, 177-179, doi:10.1016/j.chom.2019.01.020 (2019).

- 189 Argov, T. *et al.* Coordination of cohabiting phage elements supports bacteria-phage cooperation. *Nat Commun* **10**, 5288, doi:10.1038/s41467-019-13296-x (2019).
- 190 Pasechnek, A. *et al.* Active Lysogeny in *Listeria Monocytogenes* Is a Bacteria-Phage Adaptive Response in the Mammalian Environment. *Cell Rep* **32**, 107956, doi:10.1016/j.celrep.2020.107956 (2020).
- 191 Claverys, J. P., Prudhomme, M. & Martin, B. Induction of competence regulons as a general response to stress in gram-positive bacteria. *Annu Rev Microbiol* **60**, 451-475, doi:10.1146/annurev.micro.60.080805.142139 (2006).
- 192 Berka, R. M. *et al.* Microarray analysis of the *Bacillus subtilis* K-state: genome-wide expression changes dependent on ComK. *Mol Microbiol* **43**, 1331-1345, doi:10.1046/j.1365-2958.2002.02833.x (2002).
- 193 Elkon, K. B. *et al.* Tumor necrosis factor alpha plays a central role in immune-mediated clearance of adenoviral vectors. *Proc Natl Acad Sci U S A* **94**, 9814-9819, doi:10.1073/pnas.94.18.9814 (1997).
- 194 Chyuan, I. T. *et al.* Tumor necrosis factor-alpha blockage therapy impairs hepatitis B viral clearance and enhances T-cell exhaustion in a mouse model. *Cell Mol Immunol* **12**, 317-325, doi:10.1038/cmi.2015.01 (2015).
- 195 Chyuan, I. T. & Hsu, P. N. Tumor necrosis factor: The key to hepatitis B viral clearance. *Cell Mol Immunol* **15**, 731-733, doi:10.1038/cmi.2017.139 (2018).
- 196 Schooley, R. T. *et al.* Development and Use of Personalized Bacteriophage-Based Therapeutic Cocktails To Treat a Patient with a Disseminated Resistant

- Acinetobacter baumannii Infection. *Antimicrob Agents Chemother* **61**,
doi:10.1128/AAC.00954-17 (2017).
- 197 Chan, B. K. *et al.* Phage treatment of an aortic graft infected with *Pseudomonas aeruginosa*. *Evol Med Public Health* **2018**, 60-66, doi:10.1093/emph/eoy005 (2018).
- 198 Dedrick, R. M. *et al.* Engineered bacteriophages for treatment of a patient with a disseminated drug-resistant *Mycobacterium abscessus*. *Nat Med* **25**, 730-733, doi:10.1038/s41591-019-0437-z (2019).
- 199 Chen, Y. *et al.* Specific Integration of Temperate Phage Decreases the Pathogenicity of Host Bacteria. *Front Cell Infect Microbiol* **10**, 14, doi:10.3389/fcimb.2020.00014 (2020).
- 200 Walker, J. T. & Walker, D. H., Jr. Coliphage P1 morphogenesis: analysis of mutants by electron microscopy. *J Virol* **45**, 1118-1139 (1983).
- 201 Surovtsev, I. V. & Jacobs-Wagner, C. Subcellular Organization: A Critical Feature of Bacterial Cell Replication. *Cell* **172**, 1271-1293, doi:10.1016/j.cell.2018.01.014 (2018).
- 202 Fei, J. & Sharma, C. M. RNA Localization in Bacteria. *Microbiol Spectr* **6**, doi:10.1128/microbiolspec.RWR-0024-2018 (2018).
- 203 Edgar, R. *et al.* Bacteriophage infection is targeted to cellular poles. *Mol Microbiol* **68**, 1107-1116, doi:10.1111/j.1365-2958.2008.06205.x (2008).

- 204 Bakshi, S., Choi, H. & Weisshaar, J. C. The spatial biology of transcription and translation in rapidly growing *Escherichia coli*. *Front Microbiol* **6**, 636, doi:10.3389/fmicb.2015.00636 (2015).
- 205 Ghosh, A. S. & Young, K. D. Helical disposition of proteins and lipopolysaccharide in the outer membrane of *Escherichia coli*. *J Bacteriol* **187**, 1913-1922, doi:10.1128/JB.187.6.1913-1922.2005 (2005).
- 206 Shao, Q., Hawkins, A. & Zeng, L. Phage DNA dynamics in cells with different fates. *Biophys J* **108**, 2048-2060, doi:10.1016/j.bpj.2015.03.027 (2015).
- 207 Iida, S. Bacteriophage P1 carries two related sets of genes determining its host range in the invertible C segment of its genome. *Virology* **134**, 421-434 (1984).
- 208 Huang, K. C. & Ramamurthi, K. S. Macromolecules that prefer their membranes curvy. *Mol Microbiol* **76**, 822-832, doi:10.1111/j.1365-2958.2010.07168.x (2010).
- 209 Shapiro, L., McAdams, H. H. & Losick, R. Why and how bacteria localize proteins. *Science* **326**, 1225-1228, doi:10.1126/science.1175685 (2009).
- 210 Koler, M., Peretz, E., Aditya, C., Shimizu, T. S. & Vaknin, A. Long-term positioning and polar preference of chemoreceptor clusters in *E. coli*. *Nat Commun* **9**, 4444, doi:10.1038/s41467-018-06835-5 (2018).
- 211 Taniguchi, S., Kasho, K., Ozaki, S. & Katayama, T. *Escherichia coli* CrfC Protein, a Nucleoid Partition Factor, Localizes to Nucleoid Poles via the Activities of Specific Nucleoid-Associated Proteins. *Front Microbiol* **10**, 72, doi:10.3389/fmicb.2019.00072 (2019).

- 212 Sternberg, N. Bacteriophage P1 cloning system for the isolation, amplification, and recovery of DNA fragments as large as 100 kilobase pairs. *Proc Natl Acad Sci U S A* **87**, 103-107 (1990).
- 213 Gibbs, K. A. *et al.* Complex spatial distribution and dynamics of an abundant *Escherichia coli* outer membrane protein, LamB. *Mol Microbiol* **53**, 1771-1783, doi:10.1111/j.1365-2958.2004.04242.x (2004).
- 214 Datsenko, K. A. & Wanner, B. L. One-step inactivation of chromosomal genes in *Escherichia coli* K-12 using PCR products. *Proc Natl Acad Sci U S A* **97**, 6640-6645, doi:10.1073/pnas.120163297 (2000).
- 215 Mise, K. & Arber, W. Plaque-forming transducing bacteriophage P1 derivatives and their behaviour in lysogenic conditions. *Virology* **69**, 191-205 (1976).
- 216 Sliusarenko, O., Heinritz, J., Emonet, T. & Jacobs-Wagner, C. High-throughput, subpixel precision analysis of bacterial morphogenesis and intracellular spatio-temporal dynamics. *Mol Microbiol* **80**, 612-627, doi:10.1111/j.1365-2958.2011.07579.x (2011).
- 217 Yang, L. *et al.* Characterization of a P1-like bacteriophage carrying CTX-M-27 in *Salmonella* spp. resistant to third generation cephalosporins isolated from pork in China. *Sci Rep* **7**, 40710, doi:10.1038/srep40710 (2017).
- 218 Brown-Jaque, M. *et al.* Antibiotic resistance genes in phage particles isolated from human faeces and induced from clinical bacterial isolates. *Int J Antimicrob Agents* **51**, 434-442, doi:10.1016/j.ijantimicag.2017.11.014 (2018).

- 219 Brown-Jaque, M. *et al.* Detection of Bacteriophage Particles Containing Antibiotic Resistance Genes in the Sputum of Cystic Fibrosis Patients. *Front Microbiol* **9**, 856, doi:10.3389/fmicb.2018.00856 (2018).
- 220 Hendrickx, A. P. A. *et al.* Plasmid diversity among genetically related *Klebsiella pneumoniae* blaKPC-2 and blaKPC-3 isolates collected in the Dutch national surveillance. *Sci Rep* **10**, 16778, doi:10.1038/s41598-020-73440-2 (2020).
- 221 Eliason, J. L. & Sternberg, N. Characterization of the binding sites of c1 repressor of bacteriophage P1. Evidence for multiple asymmetric sites. *J Mol Biol* **198**, 281-293 (1987).
- 222 Osborne, F. A., Stovall, S. R. & Baumstark, B. R. The c1 genes of P1 and P7. *Nucleic Acids Res* **17**, 7671-7680, doi:10.1093/nar/17.19.7671 (1989).
- 223 Baumstark, B. R., Stovall, S. R. & Bralley, P. The ImmC region of phage P1 codes for a gene whose product promotes lytic growth. *Virology* **179**, 217-227, doi:10.1016/0042-6822(90)90291-x (1990).
- 224 Heinzl, T., Velleman, M. & Schuster, H. The c1 repressor inactivator protein coi of bacteriophage P1. Cloning and expression of coi and its interference with c1 repressor function. *J Biol Chem* **265**, 17928-17934 (1990).
- 225 Heinzl, T., Velleman, M. & Schuster, H. C1 repressor of phage P1 is inactivated by noncovalent binding of P1 Coi protein. *J Biol Chem* **267**, 4183-4188 (1992).
- 226 Dreiseikelmann, B., Velleman, M. & Schuster, H. The c1 repressor of bacteriophage P1. Isolation and characterization of the repressor protein. *J Biol Chem* **263**, 1391-1397 (1988).

- 227 Citron, M. & Schuster, H. The c4 repressor of bacteriophage P1 is a processed 77
base antisense RNA. *Nucleic Acids Res* **20**, 3085-3090,
doi:10.1093/nar/20.12.3085 (1992).
- 228 Heinrich, J., Citron, M., Gunther, A. & Schuster, H. Second-site suppressors of
the bacteriophage P1 virs mutant reveal the interdependence of the c4, icd, and
ant genes in the P1 immI operon. *J Bacteriol* **176**, 4931-4936,
doi:10.1128/jb.176.16.4931-4936.1994 (1994).
- 229 Kourilsky, P. Lysogenization by bacteriophage lambda. I. Multiple infection and
the lysogenic response. *Mol Gen Genet* **122**, 183-195, doi:10.1007/BF00435190
(1973).
- 230 Kourilsky, P. & Knapp, A. Lysogenization by bacteriophage lambda. III.
Multiplicity dependent phenomena occurring upon infection by lambda.
Biochimie **56**, 1517-1523 (1974).
- 231 Silpe, J. E. & Bassler, B. L. Phage-Encoded LuxR-Type Receptors Responsive to
Host-Produced Bacterial Quorum-Sensing Autoinducers. *mBio* **10**,
doi:10.1128/mBio.00638-19 (2019).
- 232 Silpe, J. E. & Bassler, B. L. A Host-Produced Quorum-Sensing Autoinducer
Controls a Phage Lysis-Lysogeny Decision. *Cell* **176**, 268-280 e213,
doi:10.1016/j.cell.2018.10.059 (2019).
- 233 Erez, Z. *et al.* Communication between viruses guides lysis-lysogeny decisions.
Nature **541**, 488-493, doi:10.1038/nature21049 (2017).

- 234 Stokar-Avihail, A., Tal, N., Erez, Z., Lopatina, A. & Sorek, R. Widespread Utilization of Peptide Communication in Phages Infecting Soil and Pathogenic Bacteria. *Cell Host Microbe* **25**, 746-755 e745, doi:10.1016/j.chom.2019.03.017 (2019).
- 235 Skinner, S. O., Sepulveda, L. A., Xu, H. & Golding, I. Measuring mRNA copy number in individual Escherichia coli cells using single-molecule fluorescent in situ hybridization. *Nat Protoc* **8**, 1100-1113, doi:10.1038/nprot.2013.066 (2013).
- 236 Lau, I. F. *et al.* Spatial and temporal organization of replicating Escherichia coli chromosomes. *Mol Microbiol* **49**, 731-743, doi:10.1046/j.1365-2958.2003.03640.x (2003).
- 237 Greer, H. The kil gene of bacteriophage lambda. *Virology* **66**, 589-604, doi:10.1016/0042-6822(75)90231-7 (1975).
- 238 Haeusser, D. P. *et al.* The Kil peptide of bacteriophage lambda blocks Escherichia coli cytokinesis via ZipA-dependent inhibition of FtsZ assembly. *PLoS Genet* **10**, e1004217, doi:10.1371/journal.pgen.1004217 (2014).
- 239 Romantsov, T. *et al.* Cardiolipin promotes polar localization of osmosensory transporter ProP in Escherichia coli. *Mol Microbiol* **64**, 1455-1465, doi:10.1111/j.1365-2958.2007.05727.x (2007).
- 240 Shao, Q., Trinh, J. T. & Zeng, L. High-resolution studies of lysis-lysogeny decision-making in bacteriophage lambda. *J Biol Chem* **294**, 3343-3349, doi:10.1074/jbc.TM118.003209 (2019).

- 241 Bryant, J. A., Sellars, L. E., Busby, S. J. & Lee, D. J. Chromosome position effects on gene expression in Escherichia coli K-12. *Nucleic Acids Res* **42**, 11383-11392, doi:10.1093/nar/gku828 (2014).
- 242 Neidhardt, F. C., Bloch, P. L. & Smith, D. F. Culture medium for enterobacteria. *J Bacteriol* **119**, 736-747, doi:10.1128/JB.119.3.736-747.1974 (1974).
- 243 Bates, D. & Kleckner, N. Chromosome and replisome dynamics in E. coli: loss of sister cohesion triggers global chromosome movement and mediates chromosome segregation. *Cell* **121**, 899-911, doi:10.1016/j.cell.2005.04.013 (2005).
- 244 Lee, C., Kim, J., Shin, S. G. & Hwang, S. Absolute and relative QPCR quantification of plasmid copy number in Escherichia coli. *J Biotechnol* **123**, 273-280, doi:10.1016/j.jbiotec.2005.11.014 (2006).
- 245 Young, J. W. *et al.* Measuring single-cell gene expression dynamics in bacteria using fluorescence time-lapse microscopy. *Nat Protoc* **7**, 80-88, doi:10.1038/nprot.2011.432 (2011).
- 246 Lord, N. D. *et al.* Stochastic antagonism between two proteins governs a bacterial cell fate switch. *Science* **366**, 116-120, doi:10.1126/science.aaw4506 (2019).
- 247 Locke, J. C., Young, J. W., Fontes, M., Hernandez Jimenez, M. J. & Elowitz, M. B. Stochastic pulse regulation in bacterial stress response. *Science* **334**, 366-369, doi:10.1126/science.1208144 (2011).

- 248 Spencer, S. L., Gaudet, S., Albeck, J. G., Burke, J. M. & Sorger, P. K. Non-genetic origins of cell-to-cell variability in TRAIL-induced apoptosis. *Nature* **459**, 428-432, doi:10.1038/nature08012 (2009).
- 249 Singh, A. & Weinberger, L. S. Stochastic gene expression as a molecular switch for viral latency. *Curr Opin Microbiol* **12**, 460-466, doi:10.1016/j.mib.2009.06.016 (2009).
- 250 Chang, H. H., Hemberg, M., Barahona, M., Ingber, D. E. & Huang, S. Transcriptome-wide noise controls lineage choice in mammalian progenitor cells. *Nature* **453**, 544-547, doi:10.1038/nature06965 (2008).
- 251 Maamar, H., Raj, A. & Dubnau, D. Noise in gene expression determines cell fate in *Bacillus subtilis*. *Science* **317**, 526-529, doi:10.1126/science.1140818 (2007).
- 252 Losick, R. & Desplan, C. Stochasticity and cell fate. *Science* **320**, 65-68, doi:10.1126/science.1147888 (2008).
- 253 Altschuler, S. J. & Wu, L. F. Cellular heterogeneity: do differences make a difference? *Cell* **141**, 559-563, doi:10.1016/j.cell.2010.04.033 (2010).
- 254 Balazsi, G., van Oudenaarden, A. & Collins, J. J. Cellular decision making and biological noise: from microbes to mammals. *Cell* **144**, 910-925, doi:10.1016/j.cell.2011.01.030 (2011).
- 255 Elowitz, M. B., Levine, A. J., Siggia, E. D. & Swain, P. S. Stochastic gene expression in a single cell. *Science* **297**, 1183-1186, doi:10.1126/science.1070919 (2002).

- 256 Carey, J. N. *et al.* Regulated Stochasticity in a Bacterial Signaling Network Permits Tolerance to a Rapid Environmental Change. *Cell* **173**, 196-207 e114, doi:10.1016/j.cell.2018.02.005 (2018).
- 257 Chavali, A. K., Wong, V. C. & Miller-Jensen, K. Distinct promoter activation mechanisms modulate noise-driven HIV gene expression. *Sci Rep* **5**, 17661, doi:10.1038/srep17661 (2015).
- 258 Cai, L., Friedman, N. & Xie, X. S. Stochastic protein expression in individual cells at the single molecule level. *Nature* **440**, 358-362, doi:10.1038/nature04599 (2006).
- 259 Weinberger, L. S., Burnett, J. C., Toettcher, J. E., Arkin, A. P. & Schaffer, D. V. Stochastic gene expression in a lentiviral positive-feedback loop: HIV-1 Tat fluctuations drive phenotypic diversity. *Cell* **122**, 169-182, doi:10.1016/j.cell.2005.06.006 (2005).
- 260 Ozbudak, E. M., Thattai, M., Kurtser, I., Grossman, A. D. & van Oudenaarden, A. Regulation of noise in the expression of a single gene. *Nat Genet* **31**, 69-73, doi:10.1038/ng869 (2002).
- 261 Hansen, M. M. *et al.* Macromolecular crowding creates heterogeneous environments of gene expression in picolitre droplets. *Nat Nanotechnol* **11**, 191-197, doi:10.1038/nnano.2015.243 (2016).
- 262 Nevo-Dinur, K., Nussbaum-Shochat, A., Ben-Yehuda, S. & Amster-Choder, O. Translation-independent localization of mRNA in *E. coli*. *Science* **331**, 1081-1084, doi:10.1126/science.1195691 (2011).

- 263 Forrest, K. M. & Gavis, E. R. Live imaging of endogenous RNA reveals a diffusion and entrapment mechanism for nanos mRNA localization in *Drosophila*. *Curr Biol* **13**, 1159-1168, doi:10.1016/s0960-9822(03)00451-2 (2003).
- 264 van Zon, J. S., Morelli, M. J., Tanase-Nicola, S. & ten Wolde, P. R. Diffusion of transcription factors can drastically enhance the noise in gene expression. *Biophys J* **91**, 4350-4367, doi:10.1529/biophysj.106.086157 (2006).
- 265 Dix, J. A. & Verkman, A. S. Crowding effects on diffusion in solutions and cells. *Annu Rev Biophys* **37**, 247-263, doi:10.1146/annurev.biophys.37.032807.125824 (2008).
- 266 Van Valen, D. *et al.* A single-molecule Hershey-Chase experiment. *Curr Biol* **22**, 1339-1343, doi:10.1016/j.cub.2012.05.023 (2012).
- 267 Shao, Y. & Wang, I. N. Bacteriophage adsorption rate and optimal lysis time. *Genetics* **180**, 471-482, doi:10.1534/genetics.108.090100 (2008).
- 268 Grayson, P., Han, L., Winther, T. & Phillips, R. Real-time observations of single bacteriophage lambda DNA ejections in vitro. *Proc Natl Acad Sci U S A* **104**, 14652-14657, doi:10.1073/pnas.0703274104 (2007).
- 269 St-Pierre, F. & Endy, D. Determination of cell fate selection during phage lambda infection. *Proc Natl Acad Sci U S A* **105**, 20705-20710, doi:10.1073/pnas.0808831105 (2008).
- 270 Donachie, W. D. Relationship between cell size and time of initiation of DNA replication. *Nature* **219**, 1077-1079, doi:10.1038/2191077a0 (1968).

- 271 Zaritsky, A., Woldringh, C. L., Helmstetter, C. E. & Grover, N. B. Dimensional rearrangement of Escherichia coli B/r cells during a nutritional shift-down. *J Gen Microbiol* **139**, 2711-2714, doi:10.1099/00221287-139-11-2711 (1993).
- 272 Grover, N. B. & Woldringh, C. L. Dimensional regulation of cell-cycle events in Escherichia coli during steady-state growth. *Microbiology (Reading)* **147**, 171-181, doi:10.1099/00221287-147-1-171 (2001).
- 273 Citron, M., Velleman, M. & Schuster, H. Three additional operators, Op21, Op68, and Op88, of bacteriophage P1. Evidence for control of the P1 dam methylase by Op68. *J Biol Chem* **264**, 3611-3617 (1989).
- 274 Coulby, J. N. & Sternberg, N. L. Characterization of the phage P1 dam gene. *Gene* **74**, 191, doi:10.1016/0378-1119(88)90284-3 (1988).
- 275 Balleza, E., Kim, J. M. & Cluzel, P. Systematic characterization of maturation time of fluorescent proteins in living cells. *Nat Methods* **15**, 47-51, doi:10.1038/nmeth.4509 (2018).
- 276 Shaner, N. C., Steinbach, P. A. & Tsien, R. Y. A guide to choosing fluorescent proteins. *Nat Methods* **2**, 905-909, doi:10.1038/nmeth819 (2005).
- 277 Bjorklund, M. Cell size homeostasis: Metabolic control of growth and cell division. *Biochim Biophys Acta Mol Cell Res* **1866**, 409-417, doi:10.1016/j.bbamcr.2018.10.002 (2019).
- 278 Westfall, C. S. & Levin, P. A. Comprehensive analysis of central carbon metabolism illuminates connections between nutrient availability, growth rate,

- and cell morphology in *Escherichia coli*. *PLoS Genet* **14**, e1007205, doi:10.1371/journal.pgen.1007205 (2018).
- 279 Haugan, M. S., Charbon, G., Frimodt-Moller, N. & Lobner-Olesen, A. Chromosome replication as a measure of bacterial growth rate during *Escherichia coli* infection in the mouse peritonitis model. *Sci Rep* **8**, 14961, doi:10.1038/s41598-018-33264-7 (2018).
- 280 Greulich, P., Scott, M., Evans, M. R. & Allen, R. J. Growth-dependent bacterial susceptibility to ribosome-targeting antibiotics. *Mol Syst Biol* **11**, 796, doi:10.15252/msb.20145949 (2015).
- 281 Lee, A. J. *et al.* Robust, linear correlations between growth rates and beta-lactam-mediated lysis rates. *Proc Natl Acad Sci U S A* **115**, 4069-4074, doi:10.1073/pnas.1719504115 (2018).
- 282 Zampieri, M., Zimmermann, M., Claassen, M. & Sauer, U. Nontargeted Metabolomics Reveals the Multilevel Response to Antibiotic Perturbations. *Cell Rep* **19**, 1214-1228, doi:10.1016/j.celrep.2017.04.002 (2017).
- 283 Lopatkin, A. J. *et al.* Bacterial metabolic state more accurately predicts antibiotic lethality than growth rate. *Nat Microbiol* **4**, 2109-2117, doi:10.1038/s41564-019-0536-0 (2019).
- 284 O'Donnell, M., Langston, L. & Stillman, B. Principles and concepts of DNA replication in bacteria, archaea, and eukarya. *Cold Spring Harb Perspect Biol* **5**, doi:10.1101/cshperspect.a010108 (2013).

- 285 Sobetzko, P., Travers, A. & Muskhelishvili, G. Gene order and chromosome dynamics coordinate spatiotemporal gene expression during the bacterial growth cycle. *Proc Natl Acad Sci U S A* **109**, E42-50, doi:10.1073/pnas.1108229109 (2012).
- 286 Grunenfelder, B. *et al.* Proteomic analysis of the bacterial cell cycle. *Proc Natl Acad Sci U S A* **98**, 4681-4686, doi:10.1073/pnas.071538098 (2001).
- 287 Zilionis, R. *et al.* Single-cell barcoding and sequencing using droplet microfluidics. *Nat Protoc* **12**, 44-73, doi:10.1038/nprot.2016.154 (2017).
- 288 Klein, A. M. *et al.* Droplet barcoding for single-cell transcriptomics applied to embryonic stem cells. *Cell* **161**, 1187-1201, doi:10.1016/j.cell.2015.04.044 (2015).
- 289 Macosko, E. Z. *et al.* Highly Parallel Genome-wide Expression Profiling of Individual Cells Using Nanoliter Droplets. *Cell* **161**, 1202-1214, doi:10.1016/j.cell.2015.05.002 (2015).
- 290 Farrell, J. A. *et al.* Single-cell reconstruction of developmental trajectories during zebrafish embryogenesis. *Science* **360**, doi:10.1126/science.aar3131 (2018).
- 291 Zhang, X. *et al.* Comparative Analysis of Droplet-Based Ultra-High-Throughput Single-Cell RNA-Seq Systems. *Mol Cell* **73**, 130-142 e135, doi:10.1016/j.molcel.2018.10.020 (2019).
- 292 Zheng, G. X. *et al.* Massively parallel digital transcriptional profiling of single cells. *Nat Commun* **8**, 14049, doi:10.1038/ncomms14049 (2017).

- 293 Rosenberg, A. B. *et al.* Single-cell profiling of the developing mouse brain and spinal cord with split-pool barcoding. *Science* **360**, 176-182, doi:10.1126/science.aam8999 (2018).
- 294 Stoeckius, M. *et al.* Simultaneous epitope and transcriptome measurement in single cells. *Nat Methods* **14**, 865-868, doi:10.1038/nmeth.4380 (2017).
- 295 Lane, K. *et al.* Measuring Signaling and RNA-Seq in the Same Cell Links Gene Expression to Dynamic Patterns of NF-kappaB Activation. *Cell Syst* **4**, 458-469 e455, doi:10.1016/j.cels.2017.03.010 (2017).
- 296 Liu, Z. *et al.* Integrating single-cell RNA-seq and imaging with SCOPE-seq2. *Sci Rep* **10**, 19482, doi:10.1038/s41598-020-76599-w (2020).
- 297 Kuchina, A. *et al.* Microbial single-cell RNA sequencing by split-pool barcoding. *Science* **371**, doi:10.1126/science.aba5257 (2021).